

REPORT DOCUMENTATION PAGE					<i>Form Approved</i> OMB No. 0704-0188	
The public reporting burden for this collection of information is estimated to average 1 hour per response, including the time for reviewing instructions, searching existing data sources, gathering and maintaining the data needed, and completing and reviewing the collection of information. Send comments regarding this burden estimate or any other aspect of this collection of information, including suggestions for reducing the burden, to Department of Defense, Washington Headquarters Services, Directorate for Information Operations and Reports (0704-0188), 1215 Jefferson Davis Highway, Suite 1204, Arlington, VA 22202-4302. Respondents should be aware that notwithstanding any other provision of law, no person shall be subject to any penalty for failing to comply with a collection of information if it does not display a currently valid OMB control number. PLEASE DO NOT RETURN YOUR FORM TO THE ABOVE ADDRESS.						
1. REPORT DATE (DD-MM-YYYY) 20-04-2015		2. REPORT TYPE Final			3. DATES COVERED (From - To) 26-July-2011 to 25-January-2015	
4. TITLE AND SUBTITLE Device Performance and Reliability Improvements of AlGaIn/GaN/Si MOSFET Using Defect-Free Gate Recess and Laser Annealing				5a. CONTRACT NUMBER FA2386-11-1-4077		
				5b. GRANT NUMBER Grant AOARD-114077		
				5c. PROGRAM ELEMENT NUMBER 61102F		
6. AUTHOR(S) Prof. Robert Wallace				5d. PROJECT NUMBER		
				5e. TASK NUMBER		
				5f. WORK UNIT NUMBER		
7. PERFORMING ORGANIZATION NAME(S) AND ADDRESS(ES) University of Texas at Dallas 800 W Campbell Rd RL 10 Richardson TX 75080 United States					8. PERFORMING ORGANIZATION REPORT NUMBER N/A	
9. SPONSORING/MONITORING AGENCY NAME(S) AND ADDRESS(ES) AOARD PSC 706 APO AP 96338-5002					10. SPONSOR/MONITOR'S ACRONYM(S) AFRL/AFOSR/IOA(AOARD)	
					11. SPONSOR/MONITOR'S REPORT NUMBER(S) AOARD-114077	
12. DISTRIBUTION/AVAILABILITY STATEMENT Distribution Code A: Approved for public release, distribution is unlimited.						
13. SUPPLEMENTARY NOTES						
14. ABSTRACT AlGaIn/GaN high electron mobility transistors are promising for high frequency and high power application due to their unique properties. High-k dielectrics, such as Al ₂ O ₃ and HfO ₂ , are attractive materials which suppresses the gate leakage current of AlGaIn/GaN high electron mobility transistors. Since the interface quality of AlGaIn and high k dielectrics are critical to device performance, such as the threshold voltage and interface state density (Dit), it is therefore necessary to understand that the relationship between interface chemistry and device performance is fundamental for examining optimization strategies for device applications. Firstly, the impact of various chemical pretreatments on AlGaIn surface is studied. Then the interfaces formed upon atomic layer deposition (ALD) of Al ₂ O ₃ and HfO ₂ are investigated using <i>in situ</i> X-ray photoelectron spectroscopy (XPS). The impacts of ALD of Al ₂ O ₃ and HfO ₂ on native AlGaIn are studied by capacitance voltage characterization. The XPS and device results uncover a high density of interface states. <i>In situ</i> N ₂ forming gas and O ₂ plasma pretreatments prior to ALD as optimization strategies are investigated using <i>in situ</i> XPS, LEED and C-V characterizations.						
15. SUBJECT TERMS Nanotechnology, Power-efficient System-on-Chip, AlGaIn/GaN/Si						
16. SECURITY CLASSIFICATION OF:			17. LIMITATION OF ABSTRACT SAR	18. NUMBER OF PAGES 87	19a. NAME OF RESPONSIBLE PERSON Kenneth Caster, Ph.D.	
a. REPORT U	b. ABSTRACT U	c. THIS PAGE U			19b. TELEPHONE NUMBER (Include area code) +81-42-511-2000	

Annual Report for AOARD Grant FA2386-11-1-4077
“Interface studies of High-k/AlGa_N/Ga_N/Si for MOSFET Applications”

February 15, 2015

Name of Principal Investigators: Robert M. Wallace

E-mail address: rmwallace@utdallas.edu

Institution: University of Texas at Dallas

Mailing Address: 800 W. Campbell Road, RL10, Richardson, TX 75080

Phone: 972-883-6638

Fax: 972-883-5725

Period of Performance: 7/26/2011-1/25/2015

Abstract: AlGa_N/Ga_N high electron mobility transistors are promising for high frequency and high power application due to their unique properties. High-k dielectrics, such as Al₂O₃ and HfO₂, are attractive materials which suppresses the gate leakage current of AlGa_N/Ga_N high electron mobility transistors. Since the interface quality of AlGa_N and high k dielectrics are critical to the device performance, such as the threshold voltage and interface state density (D_{it}), it is therefore necessary to understand that the relationship between interface chemistry and device performance is fundamental for examining optimization strategies for device applications. Firstly, the impact of various chemical pretreatments on AlGa_N surface is studied. Then the interfaces formed upon atomic layer deposition (ALD) of Al₂O₃ and HfO₂ are investigated using *in situ* X-ray photoelectron spectroscopy (XPS). The impacts of ALD of Al₂O₃ and HfO₂ on native AlGa_N are studied by capacitance voltage characterization. The XPS and device results uncover a high density of interface states. *In situ* N₂ forming gas and O₂ plasma pretreatments prior to ALD as optimization strategies are investigated using *in situ* XPS, LEED and C-V characterizations.

This FINAL report summarizes the work accomplished at UT-Dallas under AOARD award FA2386-11-1-4077, "Device Performance and Reliability Improvements of AlGa_N/Ga_N/Si MOSFET Using Defect-Free Gate Recess and Laser Annealing". Under the USAF-Taiwan research program, the partner institution was National Chiao Tung University under the direction of Professor Albert Chin. The scope of work at UT-Dallas entailed basic research of the high-k dielectric/AlGa_N interface for MOSFET applications.

EXECUTIVE SUMMARY

CHAPTER 1: *In Situ Atomic Layer Deposition Half Cycle Study of Al₂O₃ Growth on AlGaN/GaN* - Initial and wet chemical treated AlGaN surfaces were investigated firstly using X-ray photoelectron spectroscopy (XPS). Then a detailed half cycle study of atomic layer deposition (ALD) of Al₂O₃ on AlGaN was studied. The work in this chapter is an important reference for later work. The ALD of Al₂O₃ on the native oxide and HF treated Al_{0.25}Ga_{0.75}N surface was studied using *in situ* XPS, after each individual “half cycle” of the ALD process. The Al₂O₃ growth rate initially is seen to be very low, indication of low reactivity between the TMA molecule and the AlGaN surface. We collaborated with Prof. Albert Chin to understand the device performance. The contents of this chapter are published in *Applied Physics Letters*, 101, 211604, (2012).

CHAPTER 2: *In Situ Atomic Layer Deposition Study of HfO₂ Growth on NH₄OH and Atomic Hydrogen Treated AlGaN* - HfO₂ is another important high k dielectric which also widely used as oxide layer in metal oxide semiconductor (AlGaN/GaN) high electron mobility transistors, the initial study for ALD of HfO₂ on AlGaN is discussed in this chapter. In this chapter, the focus is to optimize the nucleation and cleaning of AlGaN surface using an *in situ* atomic hydrogen pretreatment. The ALD of HfO₂ on the native oxide, NH₄OH and atomic hydrogen treated Al_{0.25}Ga_{0.75}N surface was studied using XPS. During the deposition process, minimal change in the chemical states of Ga and Al is detected, with no evidence of interfacial oxide generation. The initial HfO₂ growth rate on the native oxide Al_{0.25}Ga_{0.75}N surface is very low, however exposure of the Al_{0.25}Ga_{0.75}N surface to atomic hydrogen decreases the concentration of carbon and oxygen and enhances the HfO₂ growth rate. The contents of this chapter are published in *Journal of Applied Physics*, **113**, 244102 (2013).

CHAPTER 3: *A Comparative Study of Atomic Layer Deposition Of Al₂O₃ And HfO₂ on AlGaN/GaN* - In this chapter, the device performances and surface state types are investigated by capacitance voltage (C-V) and gate leakage measurements. The ALD of Al₂O₃ and HfO₂ on AlGaN/GaN were systematically studied. The band alignments of Al₂O₃/AlGaN and HfO₂/AlGaN were investigated using the *in situ* XPS. Band offsets of 1.8 and 1.1 eV were

observed for Al₂O₃/AlGa_{0.75}N and HfO₂/AlGa_{0.75}N, respectively. The Al₂O₃ and HfO₂ dielectric layers were found to reduce the leakage current as expected, but neither of them changes the density of surface states. The positive ionized surface donor states and average interface state density (D_{it}) below the conduction band edge. Prof. Albert Chin group prepared samples to evaluate the impact of high temperature annealing on high k/AlGa_{0.75}N/GaN structures.

CHAPTER 4: *Impact of N₂ and Forming Gas Plasma Exposure on the Growth and Interfacial Characteristics of Al₂O₃ on AlGa_{0.75}N* - In this chapter, the *in situ* N₂ plasma and forming gas plasma pretreatments are used to clean the surface and improve the nucleation. The interface and ALD of Al₂O₃ on the annealed, N₂ plasma and forming gas (N₂:H₂) exposed Al_{0.25}Ga_{0.75}N surface was studied using *in situ* XPS and low energy ion scattering spectroscopy (LEIS). Exposure of the Al_{0.25}Ga_{0.75}N surface to the plasma treatments is able to remove spurious carbon, and readily facilitate uniform ALD Al₂O₃ nucleation. The contents of this chapter are published in *Applied Physics Letters*, **103**, 2441604 (2013).

CHAPTER 5: *In Situ X-Ray Photoelectron Spectroscopy and Capacitance Voltage Characterization of Plasma Treatments for Al₂O₃/ AlGa_{0.75}N/ GaN* - As noted in Chapter 4, the *in situ* N₂ and forming gas plasma is effective for the removal of carbon contamination and improvement of the initial nucleation. In this chapter, we investigate the Al₂O₃/AlGa_{0.75}N/GaN metal-oxide-semiconductor structure pretreated by O₂ anneals, N₂ remote plasma and forming gas remote plasma prior to atomic layer deposition of Al₂O₃ using *in situ* XPS, LEED, and C-V measurements. Plasma pretreatments reduce the Ga-oxide/oxy-nitride formation and the interface state density, while inducing a threshold voltage instability. The contents of this chapter are published in *Applied Physics Letters*, **105**, 011602 (2014).

CHAPTER 6: *A Crystalline Oxide Passivation for Al₂O₃/ AlGa_{0.75}N/ GaN* - According to previous studies, neither ALD of Al₂O₃ nor HfO₂ could passivate the interface due to the AlGa_{0.75}N surface is stable. The high density of positive charges results in a large negative threshold voltage shift. In addition, the high D_{it} could not be passivated by the ALD. Although N₂ and forming gas plasma pretreatments are helpful for the removal of carbon contamination and initial nucleation of ALD, it is not effective for the decreasing of the interface state density. In this chapter, it is demonstrated that a crystalline oxide structure enable to passivate the surface. *In situ* XPS and

LEED are performed to study the formation of a crystalline oxide on the AlGa_N surface. The oxidation of the AlGa_N surface is prepared by annealing and remote N₂+O₂ plasma pretreatments resulting in a stable crystalline oxide. The impact of the oxide on the interface state density is studied by C-V measurements. It is found that a remote plasma exposure at 550 °C shows the smallest frequency dispersion. Crystalline oxide formation may provide a novel passivation method for high quality AlGa_N/Ga_N devices. The contents of this chapter are published in *Applied Physics Letters*, **105**, 141604 (2014).

CHAPTER 7: Very High I_{ON} and Low I_{OFF} Metal-Gate/High- κ /AlGa_N/Ga_N MOSFET with Excellent Reliability - As a part of the US-Taiwan collaboration, a gate-recessed AlGa_N/Ga_N MOSFET on a Si substrate is demonstrated to achieve a record best normalized transistor current (μC_{ox}) of 335 $\mu A/V^2$ (410 mA/mm at $L_G=5 \mu m$ & only $V_G=4 V$), high breakdown voltage (V_{BD}) of 970 V, I_{ON}/I_{OFF} of 9~10 orders of magnitude, small 75 mV/dec sub-threshold slope (SS), low on-resistance (R_{on}) of 17.0 Ω -mm, excellent reliability of only 40 mV ΔV_T after 175°C 1000 sec stress at $I_{D,max}$, good V_T uniformity of $\pm 0.35 V$, and a small $\Delta V_T/V_{BD}$ of only <0.04%. Such excellent device integrities are due to the small EOT by using high- κ gate dielectric, p⁺-Ga_N buffer, and AlN etching stop layer. This work was submitted for consideration at the 2014 IEEE International Electron Devices Meeting.

EXECUTIVE SUMMARY	iii
CHAPTER 1 In Situ Atomic Layer Deposition Half Cycle Study of Al ₂ O ₃ Growth on AlGa _N /Ga _N	1
1.1 Preface	1
1.2 Introduction	1
1.3 Experimental	2
1.3.1 <i>Ex Situ</i> Wet Chemical Pretreatments	2
1.3.2 <i>In Situ</i> ALD Half Cycle Setup	2
1.4 Results and Discussion	4
1.5 Conclusion	12
1.6 References	12
CHAPTER 2 In Situ Atomic Layer Deposition Study of HfO ₂ Growth on NH ₄ OH and Atomic Hydrogen Treated AlGa _N	14
2.1 Preface	14
2.2 Introduction	14
2.3 Experimental	15
2.4 Results and Discussion	17
2.5 Conclusion	24
2.6 References	24
CHAPTER 3 A Comparative Study of Atomic Layer Deposition of Al ₂ O ₃ and HfO ₂ on AlGa _N /Ga _N	27
3.1 Preface	27
3.2 Introduction	27
3.3 Experimental	28
3.4 Results and Discussion	29
3.5 Conclusion	37
3.6 References	37
CHAPTER 4 Impact of N ₂ and Forming Gas Plasma Exposure on the Growth and Interfacial Characteristics of Al ₂ O ₃ on AlGa _N	40
4.1 Preface	40
4.2 Introduction	40
4.3 Experimental	41

4.4	Results and Discussion	42
4.5	Conclusion	49
4.6	References	50
CHAPTER 5 In Situ X-Ray Photoelectron Spectroscopy and Capacitance Voltage Characterization of Plasma Treatments for Al ₂ O ₃ / AlGa _N / Ga _N		53
5.1	Preface.....	53
5.2	Introduction	53
5.3	Experimental	54
5.4	Results and Discussion	55
5.5	Conclusion.....	61
5.6	References	61
CHAPTER 6 A Crystalline Oxide Passivation for Al ₂ O ₃ / AlGa _N / Ga _N		64
6.1	Preface.....	64
6.2	Introduction	64
6.3	Experimental	65
6.4	Results and Discussion	66
6.5	Conclusion.....	75
6.6	References	76
CHAPTER 7 Very High I _{ON} and Low I _{OFF} Metal-Gate/High-κ/AlGa _N /Ga _N MOSFET with Excellent Reliability.....		78
7.1	Preface.....	78
7.2	Introduction.....	78
7.3	Device Fabrication	79
7.4	Results and Discussion	79
7.4.1	Interface & Buffer Leakage Effects.....	79
7.4.2	Uniformity, V _{BD} , & Reliability	80
7.5	Conclusions.....	81
7.6	References.....	81
List of Publications		84
List of Presentations.....		85

CHAPTER 1

In Situ Atomic Layer Deposition Half Cycle Study of Al₂O₃ Growth on AlGa_{0.25}N/GaN

1.1 Preface

In order to understand the initial AlGa_{0.25}N interface and remove native oxide and carbon contamination, initial and wet chemical treated AlGa_{0.25}N surfaces were investigated firstly using X-ray photoelectron spectroscopy (XPS). Then a detailed half cycle study of atomic layer deposition (ALD) of Al₂O₃ on AlGa_{0.25}N was studied. The work in this chapter is an important reference for later work. The ALD of Al₂O₃ on the native oxide and HF treated Al_{0.25}Ga_{0.75}N surface was studied using *in situ* XPS, after each individual “half cycle” of the ALD process. Initially, Al₂O₃, Ga₂O₃ and N-O states were detected on both surfaces at differing concentrations. During the course of the deposition process, the N-O bonds are seen to decrease to within XPS detection limits, as well as a small decrease in the Ga₂O₃ concentration. The Al₂O₃ growth rate initially is seen to be very low, indication of low reactivity between the TMA molecule and the AlGa_{0.25}N surface.

The contents of this chapter are adapted with permission from a paper entitled “*In situ* atomic layer deposition half cycle study of Al₂O₃ growth on AlGa_{0.25}N” [*Applied Physics Letters*, **101**, 211604, (2012)]. Copyright [2012], AIP Publishing LLC.

1.2 Introduction

Due to the large bandgap and relatively high mobility of III-V nitride based materials, they are of significant interest in the fabrication of high electron mobility transistors (HEMTs) and other high power, high frequency and high temperature devices.^{1,2} Incorporating a high-k oxide layer between the semiconductor and the gate metal would have the effect of significantly reducing leakage current.^{3,4} In terms of high-k deposition on these surfaces, ALD provides the most likely candidate for advanced device fabrication, due to the potential for high sample throughput, controlled growth rates and high aspect ratio conformal growth.

A number of studies have looked at the effect of different wet chemical treatments at removing native oxides and surface contamination from III-V nitride surfaces.^{5,6} Hydrofluoric acid (HF) etching of GaN surfaces has previously been shown to produce one of the lowest oxide concentrations when compared to various other wet chemical treatments,⁷ with only HCl seen to produce a marginally more oxide free surface.⁸ Previous studies looking at SiN_x/Al₂O₃/AlGaIn/GaN heterostructures showed low D_{it} levels at the oxide/semiconductor interface,⁹ and using a high-k LaAlO₃/SiO₂ bi-layers also on AlGaIn/GaN structures, high drive currents, low threshold voltages, and high mobility was achieved with a capacitance extracted thickness for the high-k of 3 nm.¹⁰ Hori et al. also report a reduction in interface state density on ALD Al₂O₃/AlGaIn/GaN devices by employing an N₂O radical treatment prior to ALD.¹¹ However, very little is reported about the chemical interactions that take place between deposited high-k materials and III-V nitride surfaces.¹² For this reason, this study looks at the effect of depositing Al₂O₃ by ALD on the native oxide and HF etched Al_{0.25}Ga_{0.75}N surface, with XPS carried out after successive “half cycles” of the ALD process,¹³ to monitor the chemical changes at the semiconductor/high-k interface.

1.3 Experimental

1.3.1 *Ex Situ* Wet Chemical Pretreatments

Undoped Al_{0.25}Ga_{0.75}N (30 nm) samples, grown on a 1.2 μm GaN layer on a Si(111) substrate by metal organic chemical vapor deposition from DOWA Electronics Materials (see Figure 1.1 (b)), were used in this work. Four undoped Al_{0.25}Ga_{0.75}N samples from AlGaIn wafer were first solvent cleaned in acetone, methanol and isopropanol for one minute each. The first sample was used as the control sample. The other three samples were etched by 10% ammonium hydroxide (NH₄OH) for 5 min, 10% ammonium sulfide ((NH₄)₂S) for 10 min and 2% hydrofluoric acid (HF) for 2 min, respectively. Then these four samples mounted to a sample plate were loaded to the ultra-high vacuum (UHV) system. The XPS is performed on them.

1.3.2 *In Situ* ALD Half Cycle Setup

For ALD study, one sample was then etched in a 2% HF solution for 2 minutes, followed by a 2 minute rinse in flowing deionized water and dried with nitrogen¹² The sample was then

immediately mounted to a sample plate along with an un-etched native oxide sample and introduced to the (UHV) system as shown in Figure 1.1 (a). In this study, ALD of Al_2O_3 was carried out on the AlGaIn surfaces in a Picosun ALD reactor, at a substrate temperature of 300 °C. Trimethyl-aluminum (TMA) and H_2O were used as the precursors for ALD, with a precursor pulse and purge time of 0.1 and 4 s respectively. The base pressure of the ALD reactor was ~12 mbar, with ultra-high purity N_2 used as the carrier and purging gas.

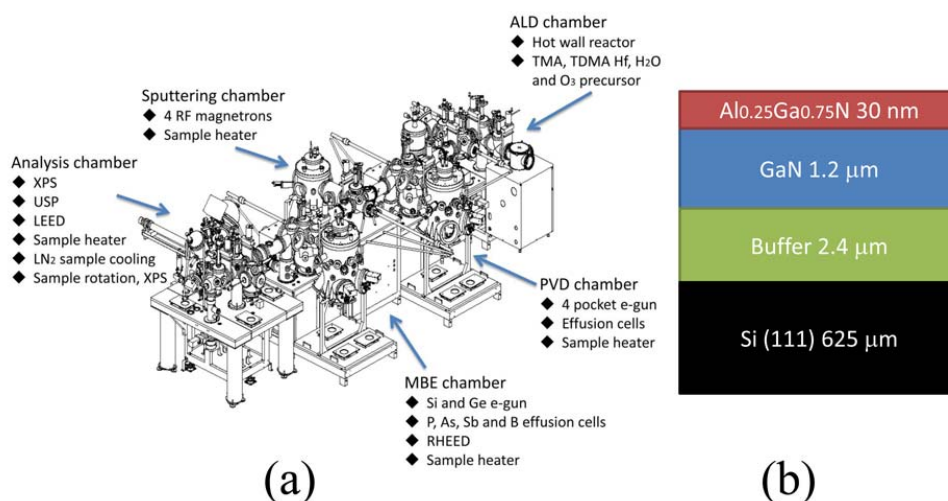


Figure 1.1. (a) UHV cluster system (b) the epilayer structure used in this study.

In order to monitor the Al_2O_3 growth on the AlGaIn surfaces, XPS was carried out after loading the samples to the UHV system, upon exposing the samples to the ALD reactor at 300 °C under typical ALD conditions for 30 mins, and after each individual “half cycle” pulse of the ALD process (such that the samples were first exposed to one pulse of TMA and scanned with XPS and then transferred back to the ALD reactor and exposed to one pulse of H_2O and again scanned with XPS) up to two full cycles, as well as after 5, 10 and 20 full cycles (TMA + H_2O). The XPS was carried out using a monochromated Al $K\alpha$ ($h\nu = 1486.7$) X-ray source, equipped with a 7 channel analyzer, using a pass energy of 15 eV, with all scans taken at 45° with respect to the sample normal. Spectra were taken of the Ga $2p_{3/2}$, Ga $3d$, N $1s$, Al $2p$, O $1s$, C $1s$, F $1s$ core level regions as well as of the valence band edges. XPS peak deconvolution was carried out using AAnalyzer software^{14,15} with a detailed peak fitting procedure described elsewhere. All

peaks were referenced to the N 1s peak at 397.0 eV.

Atomic force microscope (AFM) images were obtained using an *ex situ* Veeco (Bruker) Multimode system in non-contact tapping mode, with root mean square (RMS) roughness measurements calculated using WSxM software,¹⁶ and the final values determined by averaging RMS values taken from a number of regions on the surfaces. Images were taken of the initial surfaces, (native oxide and HF etched) and after 20 cycles of Al₂O₃.

1.4 Results and Discussion

While all treatment show a decrease in the amount of oxygen, particularly in the form of hydroxides (at ~533.5eV), none was able to fully remove the native oxides. The level of gallium oxide states present in Figure 1.2 (c) was also seen to decrease, with HF most effective. However, carbon levels were detected to increase on all samples with wet chemical treatment. Residual F was seen to remain on HF treated surfaces (see Figure 1.7). Etching of the sample in HF reduced the concentration of oxygen by >40% relative to that seen on the native oxide sample as Figure 1.2 shows.

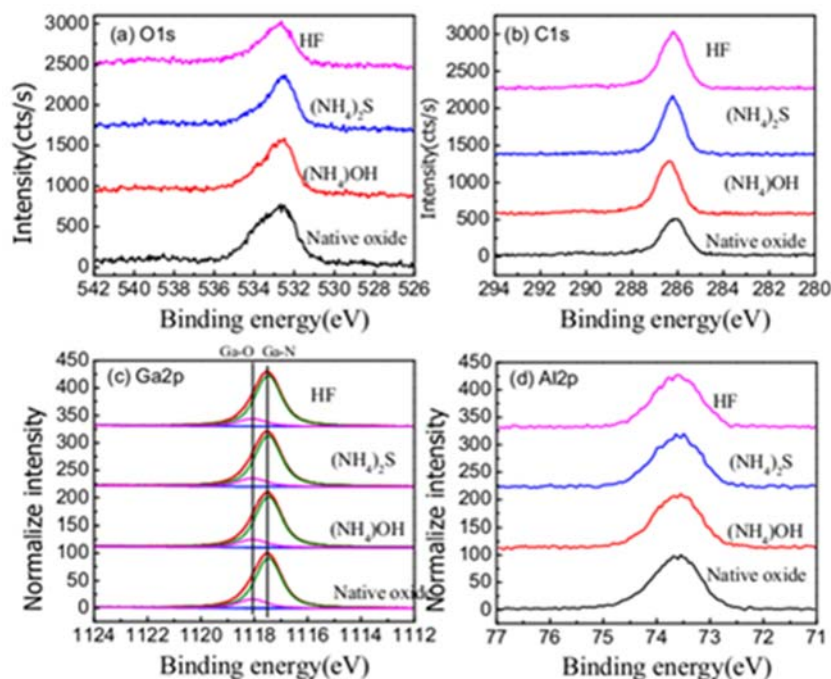


Figure 1.2. (a) O 1s, (b) C 1s, (c) Ga 2p_{3/2} and (d) Al 2p spectra for native oxide, (NH₄)OH etched, (NH₄)₂S etched and HF etched AlGaIn samples.

In order to determine where these changes to the substrate-oxide bonding were taking place, it was necessary to look at Ga, N and Al core level spectra in more detail. The peak fitted Ga $2p_{3/2}$ and N $1s$ spectra after each individual stage in the deposition process are shown in Figure 1.2. The Ga $2p_{3/2}$ spectra in Figure 1.3 (a) and (b) for the native oxide and HF etched samples, respectively, show evidence of two peaks; one at 1117.5 eV assigned to Ga bonded to N, and the other at 1118.2 eV, indicative of a Ga 3+ oxidation state, likely due to Ga_2O_3 , consistent with previous reports.^{17,18} There is no evidence of a Ga 1+ state, however detection of this state is complicated due to the Ga-N peak having a similar binding energy to that of the Ga_2O_3 peak (1117.55 eV), as seen on GaAs and InGaAs samples.¹⁹ Upon heating of the samples to 300 °C in the ALD reactor there is a slight broadening of the Ga-N peak, such that the FWHM increases from 1.03 eV to 1.11 eV, which persists during subsequent ALD cycles. This could be evidence for the formation of a low concentration of lower binding energy oxidation states or general disorder at the AlGaIn surface.

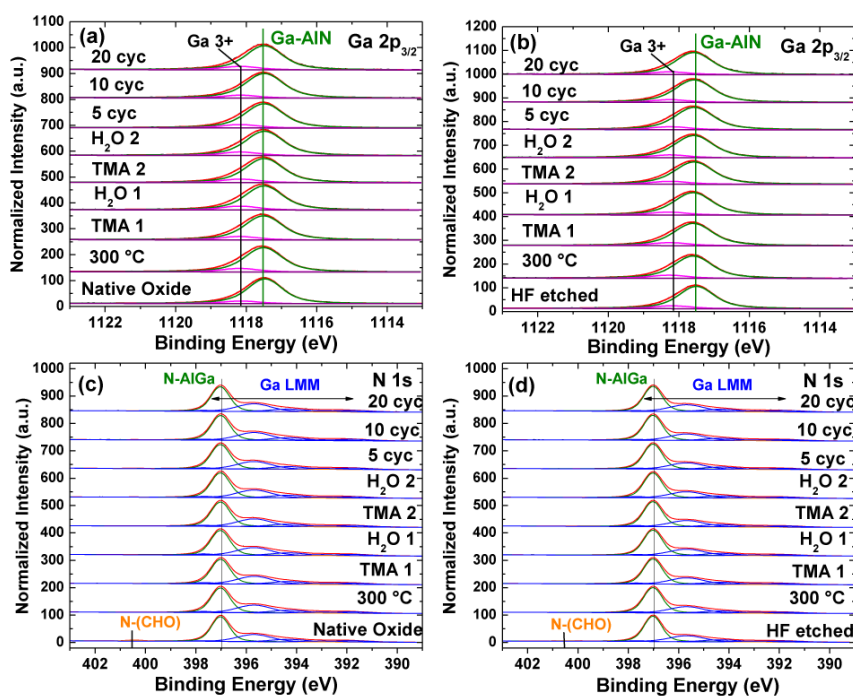


Figure 1.3. XPS spectra of the Ga $2p_{3/2}$ from the native oxide (a) and HF etched (b) surfaces. XPS spectra of N $1s$ from the native oxide (c) and HF etched (d) surfaces.

The corresponding N 1s spectra in Figure 1.3 (c) and (d) show the N-AlGa peak at 397.0 eV,²⁰ a N-O peak (possibly consisting of O, C and H bonds) at ~400.5 eV,²¹ as well as the Ga $L_{2M_{45}M_{45}}$ Auger feature (~392-398 eV). The Auger feature is fitted in such a way that the line-shape remains constant throughout and is consistent with line-shapes from previously reported spectra.²² It should be pointed out that the commonly reported GaN-O bond at ~398 eV is likely to be a component of the Ga LMM Auger line, with an increase in this region usually appearing upon gallium oxidation. In order to show the changes in these spectra more clearly, the Ga $2p_{3/2}$ and N 1s core level spectra from the initial surfaces, after 300 °C anneal and after the first TMA pulse, are shown in Figure 1.4. Upon the first pulse of TMA, it is difficult to detect any obvious change in the Ga $2p_{3/2}$ spectra, however from the ratio of the Ga 3+ peak area to that of the bulk peak, plotted in Figure 1.4 (e), we find that there is a slight decrease in the concentration of Ga-O present on the surface as a result of interaction with TMA molecule. The extent of this interaction is much less on these surfaces, suggesting that there is a stronger bond between the Ga 3+ state and AlGaIn surface than with other materials. This inherent stability is also reflected in the oxide ratios when comparing the native oxide and HF etched surfaces, with the oxide ratio initially seen to be greater on the HF etched surface. This inherent stability is reflected in a previous study by Sivasubramani *et al.* which compared exposure of a GaN substrate to either H₂O or O₃ pulses,¹² and revealed that no oxidation was seen to take place upon exposure of the surface to H₂O. Upon exposure to the more aggressive O₃ oxidation, however, surface oxides were seen to form which helped to promote subsequent Al₂O₃ nucleation. With successive cycles of TMA, we do detect an incremental decrease in the Ga-O:Ga-AlN ratio, which is likely due to the formation of Ga-O-Al which will be further discussed in Chapter 4, however, this trend is close to the associated error in the measurement. After 20 full cycles, the ratio is seen to increase again, with the highest level seen on the native oxide sample. From the N 1s spectra in Figure 1.4 (c) and (d), we find that the N-O signal reduces to within detection limits after introduction to the ALD reactor at 300 °C. This is concurrent with an increase in gallium and aluminum oxide peaks, suggesting oxygen is transferring from the N-O bonding environments to form gallium and aluminum oxide. No further changes are detected in the N 1s spectra throughout the remainder of the deposition process.

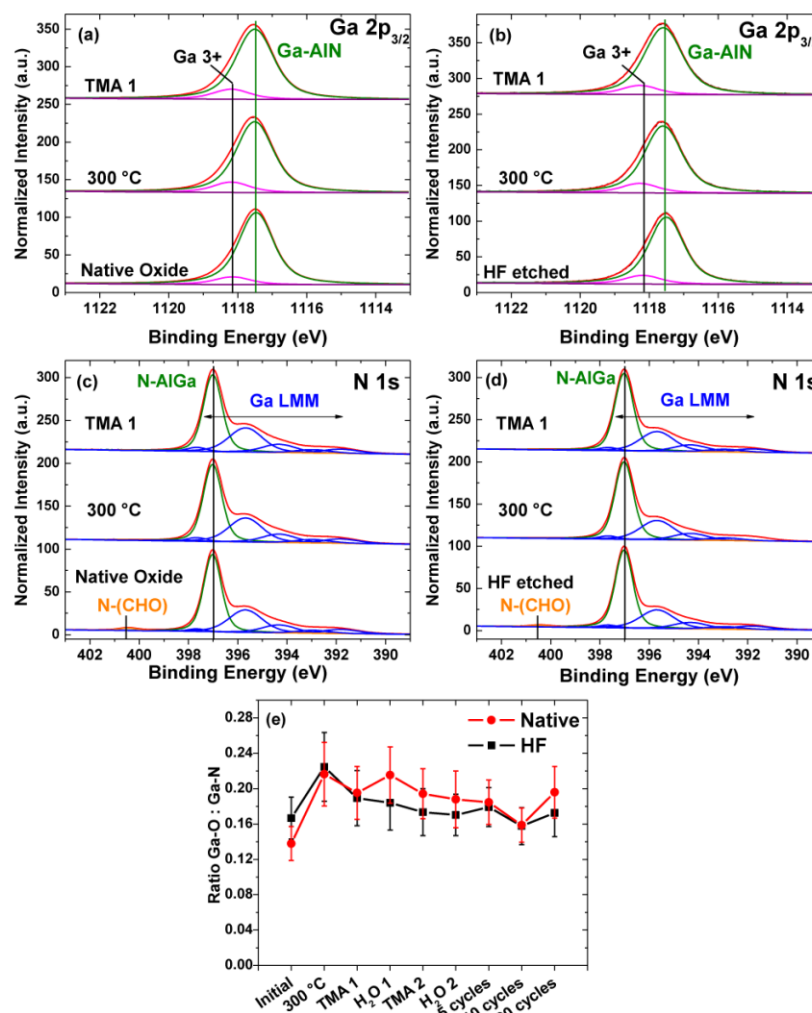


Figure 1.4. XPS spectra of the Ga 2p_{3/2} core levels from the native oxide (a) and HF etched (b) surfaces, from the initial surfaces, after annealing at 300 °C and after one pulse of TMA. XPS spectra of the N 1s core levels from the native oxide (c) and HF etched (d) surfaces, from the initial surfaces, after annealing at 300 °C and after one pulse of TMA. Figure 1.4 (e) shows the ratio of gallium oxide to the bulk Ga-AlN peak from the Ga 2p_{3/2} spectra, indicating the changes in the gallium oxide present on the surface over the course of the deposition. Error bars were estimated to be $\pm 9\%$ based on the peak deconvolution and fitting procedures employed here.

Looking at the Al 2p spectra for the complete deposition process in Figure 1.5 (a) and (b), and for the 300 °C annealed, after first “half cycle” of TMA and after 20 full cycles spectra in (c)

and (d), we detect the Al-GaN bulk peak at 73.5 eV, as well as trace amounts of Al_2O_3 at 74.4 eV. This is present on both the native oxide and HF etched surface initially and is observed to increase upon annealing, shown most clearly in the ratio of oxide to the bulk peaks in Figure 1.5 (e). Subsequently we detect an incremental increase in the Al_2O_3 peak after each successive TMA pulse, as indicated by the plot inset in Figure 1.5 (e) showing the change in the ratio during the initial stages of growth. However, this growth rate is much lower than typically expected.

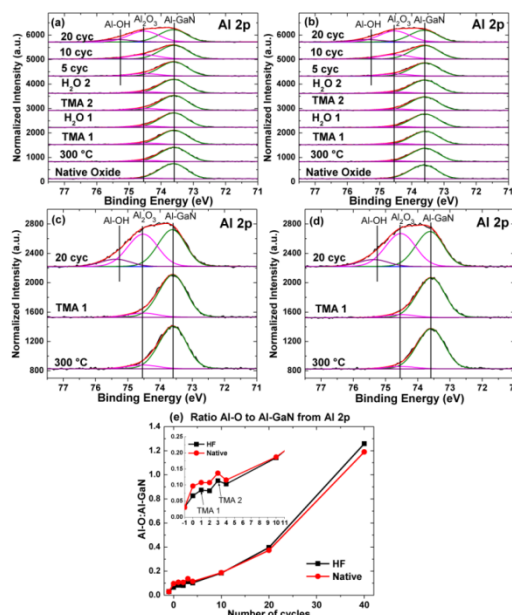


Figure 1.5. Al 2p core level spectra from the native oxide (a) and HF etched (b) samples at various stages in the Al_2O_3 deposition process. Al 2p core level spectra from the native oxide (c) and HF etched (d) samples after 300 °C annealing, first pulse of TMA and 20 cycles of Al_2O_3 . Figure 1.5 (e) shows the ratio of Al-O to Al-GaN from the same spectra indicating the change in Al_2O_3 growth rate with increasing number of ALD cycles. Inset shows the change in the ratio during the initial ALD cycles.

From XPS thickness calculations, based on the attenuation of the Ga $2p_{3/2}$ peak upon Al_2O_3 deposition, after 5 full cycles, we detect < 0.1 nm of Al_2O_3 growth on both surfaces. With a further 5 full cycles, a similar growth rate is seen with ~ 0.2 nm of Al_2O_3 detected. However, after the next 10 cycles the growth rate is observed to increase significantly, such that the final calculated thickness is 0.9 nm on the native oxide sample and 1.0 nm on the HF etched sample.

This suggests that true ALD growth does not occur until a complete monolayer of oxide is formed on the surface and a number of ALD cycles are needed to instigate this growth. This variation in Al_2O_3 thickness on the two samples is further confirmed by the Al-O to Al-GaN ratio in Figure 1.5 (e), with a greater final value observed for the HF etched sample, despite an initially higher ratio seen on the native oxide sample. With increasing Al_2O_3 thickness, the emergence of a higher binding energy peak in the Al $2p$ spectra takes place, which suggests that there is some Al-OH incorporation into the films. A peak at 532.8 eV in the O $1s$ spectra in Figure 1.6 on both samples, also suggests the presence of an -OH related state on both samples. With more cycles of Al_2O_3 , the O $1s$ peak intensity increases indicating the formation of Al_2O_3 .

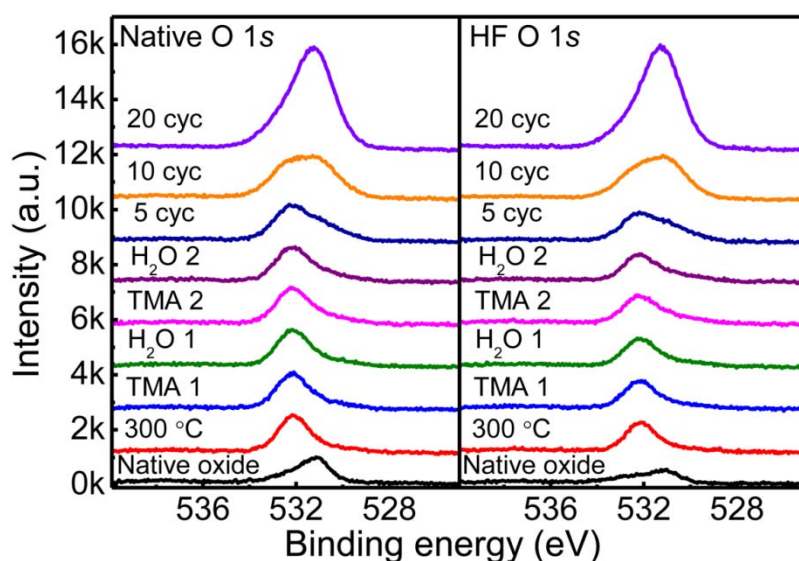


Figure 1.6. O $1s$ core level spectra from the native oxide and HF etched samples at various stages in the Al_2O_3 deposition process.

The F $1s$ spectra and C $1s$ spectra for naïve oxide and HF etched samples are shown in Figure 1.7. A small concentration of fluorine was also detected on the HF etched sample, which was seen to decrease in concentration after annealing at 300 °C. However, upon subsequent ALD no further changes in the level were detected. There was no evidence of any Ga or Al-F bonding in the Ga $2p_{3/2}$ or Al $2p$ spectra, where these bonds would be expected to form at higher binding energies than the oxide states due to the increased electronegativity of F relative to O, suggesting

the F may at least initially be physisorbed to the surface. It is not clear what impact the presence of F at the interface between the AlGaIn and Al₂O₃ layer would have in terms of device performance. Further, there was no evidence of increased carbon concentration levels on the surfaces as a result of ALD, suggesting that there is no decomposition of the TMA molecule, other than that during ALD growth to form Al₂O₃.

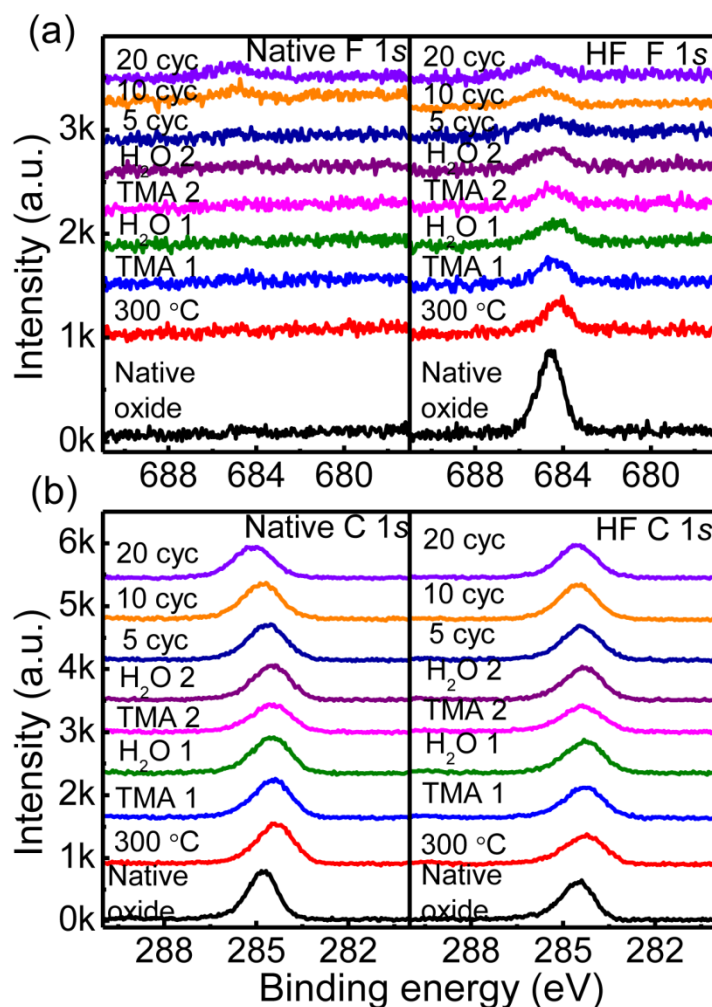


Figure 1.7. (a) F 1s and (b) C 1s core level spectra from the native oxide and HF etched samples at various stages in the Al₂O₃ deposition process.

To comment further on the carbon present (see Figure 1.7(b)) on the surface of the samples, on both samples the level of carbon detected, on the order of a monolayer in concentration, is not

seen to increase over the course of the experiment, suggesting there is no significant incorporation of carbon into the Al_2O_3 film as a result of the ALD process. During the ALD half cycles, there is evidence of C-H (likely AlCH_3) and C-OH bonding detected in the XPS spectra at various stages. Particularly on the HF etched sample, we see an increase in C-H bonding and a decrease in C-OH after TMA pulses, with the process reversed during the H_2O pulses, consistent with a typical ALD process,²⁴ where a CH_4 molecule is removed upon interaction with the oxygen precursor, again, with no change in the total amount of carbon present.

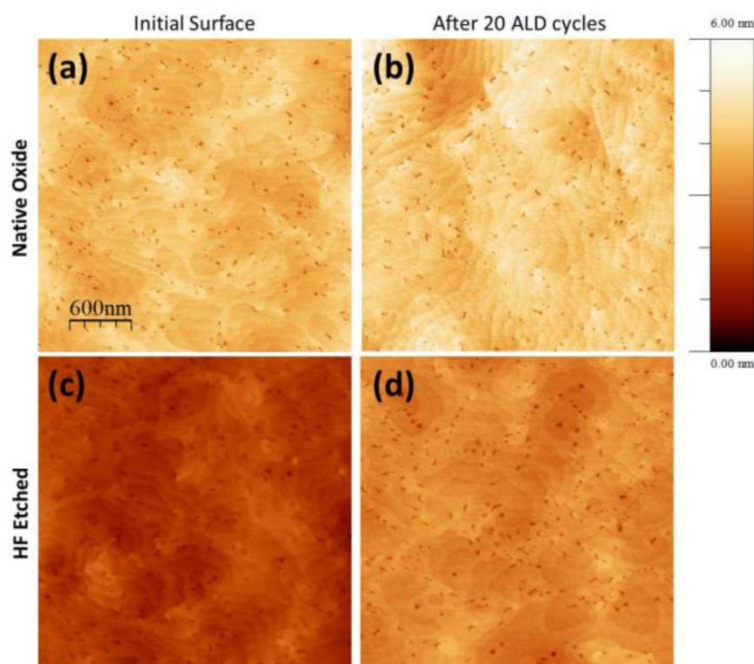


Figure 1.8. AFM images ($3\ \mu\text{m} \times 3\ \mu\text{m}$) of the native oxide (a) and HF etched samples (c) from the initial surfaces. AFM images of the native oxide (b) and HF etched samples (d) after 20 cycles of ALD. The contrasts have been adjusted so that all images have the same height scale.

In order to investigate whether there were any changes in the surface roughness as a result of the HF etch, AFM images were taken from the AlGaIn samples before and after deposition. AFM images ($3\ \mu\text{m} \times 3\ \mu\text{m}$) were taken from at least four different locations on the two samples, before and after 20 cycles of TMA, are shown in Figure 1.8, with clear evidence of the characteristic monolayer steps of the $(\text{Al})\text{GaIn}$ surface seen,²⁵ even after deposition, indicating the conformal growth of the ALD Al_2O_3 despite the initial slow nucleation rate on the surface.

The RMS roughness of the native oxide surface was calculated to be 0.30 ± 0.05 nm, increasing to 0.39 ± 0.05 nm after deposition. With HF etching, the RMS roughness is seen to decrease to 0.29 ± 0.01 nm, with only a slight increase, to 0.32 ± 0.03 nm, after ALD. This suggests that HF etching produces a more uniform surface, which may help to promote Al_2O_3 nucleation as evidenced by the increased final Al_2O_3 thickness on this surface. Reduced surface roughness is also likely to lead to improved carrier mobility by reducing the effect of surface scattering.²⁶ The appearance of dark regions are attributed to pits in the substrate that originate from the epitaxial process, and are widely reported in the literature (e.g. ref. 25).

1.5 Conclusion

In conclusion, the initial stages of Al_2O_3 growth on the native oxide and HF treated AlGaN surface was investigated by XPS. Results suggest that the AlGaN surface is chemically very stable and that a number (>10) of ALD cycles are needed to initially nucleate the surface with Al_2O_3 before ALD growth is seen to take place. The ALD could not remove the native oxides from the $\text{Al}_2\text{O}_3/\text{AlGaN}$ interface. AFM measurements show a reduced surface roughness on the HF etched surface, with conformal ALD growth seen on both surfaces.

1.6 References

- ¹ S.J. Pearton and F. Ren, Adv. Mater. **12**, 1571 (2000).
- ² S. Strite, J. Vac. Sci. Technol. B **10**, 1237 (1992).
- ³ T. Mizutani, Y. Ohno, M. Akita, S. Kishimoto, and K. Maezawa, IEEE Trans. Electron Devices **50**, 2015 (2003).
- ⁴ Y. Ohno, T. Nakao, S. Kishimoto, K. Maezawa, and T. Mizutani, Appl. Phys. Lett. **84**, 2184 (2004).
- ⁵ M. Diale, F.D. Aurret, N.G. van der Berg, R.Q. Odendaal, and W.D. Roos, Appl. Surf. Sci. **246**, 279 (2005).
- ⁶ H. Ishikawa, S. Kobayashi, Y. Koide, S. Yamasaki, S. Nagai, J. Umezaki, M. Koike, and M. Murakami, J. Appl. Phys. **81**, 1315 (1997).
- ⁷ S.W. King, J.P. Barnak, M.D. Bremser, K.M. Tracy, C. Ronning, R.F. Davis, and R.J. Nemanich, J. Appl. Phys. **84**, 5248 (1998).
- ⁸ R. Sohal, P. Dudek, and O. Hilt, Appl. Surf. Sci. **256**, 2210 (2010).

- ⁹ M. Miczek, C. Mizue, T. Hashizume, and B. Adamowicz, J. Appl. Phys. **103**, 104510 (2008).
- ¹⁰ C. Tsai, T. Wu, and A. Chin, IEEE Electron Device Lett. **33**, 2011 (2012).
- ¹¹ Y. Hori, C. Mizue, and T. Hashizume, Phys. Status Solidi **9**, 1356 (2012).
- ¹² P. Sivasubramani, T.J. Park, B.E. Coss, A. Lucero, J. Huang, B. Brennan, Y. Cao, D. Jena, H.G. Xing, R.M. Wallace, and J. Kim, Phys. Status Solidi - Rapid Res. Lett. **6**, 22 (2012).
- ¹³ M. Milojevic, C.L. Hinkle, F.S. Aguirre-Tostado, H.C. Kim, E.M. Vogel, J. Kim, and R.M. Wallace, Appl. Phys. Lett. **93**, 252905 (2008).
- ¹⁴ A. Herrera-Gómez, P. Pianetta, and D. Marshall, Phys. Rev. B **61**, 988 (2000).
- ¹⁵ B. Brennan and G. Hughes, J. Appl. Phys. **108**, 053516 (2010).
- ¹⁶ I. Horcas, R. Fernández, J.M. Gómez-Rodríguez, J. Colchero, J. Gómez-Herrero, and a M. Baro, Rev. Sci. Instrum. **78**, 013705 (2007).
- ¹⁷ C.L. Hinkle, a. M. Sonnet, M. Milojevic, F.S. Aguirre-Tostado, H.C. Kim, J. Kim, R.M. Wallace, and E.M. Vogel, Appl. Phys. Lett. **93**, 113506 (2008).
- ¹⁸ C.L. Hinkle, M. Milojevic, B. Brennan, a. M. Sonnet, F.S. Aguirre-Tostado, G.J. Hughes, E.M. Vogel, and R.M. Wallace, Appl. Phys. Lett. **94**, 162101 (2009).
- ¹⁹ C.L. Hinkle, E.M. Vogel, P.D. Ye, and R.M. Wallace, Curr. Opin. Solid State Mater. Sci. **15**, 188 (2011).
- ²⁰ F. González-Posada, J. a. Bardwell, S. Moisa, S. Haffouz, H. Tang, A.F. Braña, and E. Muñoz, Appl. Surf. Sci. **253**, 6185 (2007).
- ²¹ F. Moulder, J. F. Stickle, W. E. Sobol, P. and D. Bomben, K, *Handbook of X-Ray Photoelectron Spectroscopy* (Perkin-Elmer Corp, Minnesota, 1992).
- ²² E. Antonides, E. Janse, and G. Sawatzky, Phys. Rev. B **15**, (1977).
- ²³ P.D. Ye, G.D. Wilk, B. Yang, J. Kwo, S.N.G. Chu, S. Nakahara, H.-J.L. Gossmann, J.P. Mannaerts, M. Hong, K.K. Ng, and J. Bude, Appl. Phys. Lett. **83**, 180 (2003).
- ²⁴ R.L. Puurunen, J. Appl. Phys. **97**, 121301 (2005).
- ²⁵ T. Hashizume, S. Ootomo, S. Oyama, M. Konishi, and H. Hasegawa, J. Vac. Sci. Technol. B **19**, 1675 (2001).
- ²⁶ B. Liu, Y.W. Lu, G.R. Jin, Y. Zhao, X.L. Wang, Q.S. Zhu, and Z.G. Wang, Appl. Phys. Lett. **97**, 262111 (2010).

CHAPTER 2

In Situ Atomic Layer Deposition Study of HfO₂ Growth on NH₄OH and Atomic Hydrogen Treated AlGaN

2.1 Preface

The previous chapter (Chapter 1) is about the atomic layer deposition (ALD) of Al₂O₃ on AlGaN. HfO₂ is another important high k dielectric which also widely used as oxide layer in metal oxide semiconductor (AlGaN/GaN) high electron mobility transistors, the initial study for ALD of HfO₂ on AlGaN is discussed in this chapter. The *in situ* X-ray photoelectron spectroscopy (XPS) results in Chapter 1 detect a slow initial Al₂O₃ nucleation on native oxide AlGaN and HF etched AlGaN. Either carbon contamination or native oxide is hardly removed by wet chemical pretreatments. In this chapter, the focus is to optimize the nucleation and cleaning of AlGaN surface using an *in situ* atomic hydrogen pretreatment. The ALD of HfO₂ on the native oxide, NH₄OH and atomic hydrogen treated Al_{0.25}Ga_{0.75}N surface was studied using XPS, after each individual “half cycle” of the ALD process. During the deposition process, minimal change in the chemical states of Ga and Al is detected, with no evidence of interfacial oxide generation. The initial HfO₂ growth rate on the native oxide Al_{0.25}Ga_{0.75}N surface is very low, however exposure of the Al_{0.25}Ga_{0.75}N surface to atomic hydrogen decreases the concentration of carbon and oxygen and enhances the HfO₂ growth rate.

The contents of this chapter are adapted with permission from a paper entitled “***In situ* atomic layer deposition half cycle study of HfO₂ growth on NH₄OH and atomic hydrogen treated Al_{0.25}Ga_{0.75}N**” [*Journal of Applied Physics*, **113**, 244102 (2013)]. Copyright [2013], AIP Publishing LLC.

2.2 Introduction

HfO₂ with a high dielectric constant (20~25) and a large band gap (5.6~5.8 eV), has been studied extensively as a gate dielectric for Si and III-V semiconductor devices.^{1,2} J. Shi *et al.* have

previously reported the formation of AlGaIn/GaN MOS-high field effect transistor (HFET) devices incorporating a HfO₂ gate layer deposited by ALD, showing significantly lower leakage current than without the HfO₂ layer in place.³ However, the chemical interactions and growth process taking place during the initial stages of ALD HfO₂ on AlGaIn, which establishes interface state properties, is still not well understood.

Studies concerning the cleaning of AlGaIn and GaN surfaces have investigated many chemical processes, with a good review of these recently presented by R.D. Long et. al.⁴ Although HF and HCl based treatments have been shown to produce the lowest coverage of oxygen on the AlGaIn or GaN surface, residual F and Cl can be left on the surface.^{5,6} The residual F Atomic hydrogen cleaning has been used to clean InAs, InSb, InP, InN, GaAs, InGaAs, and GaSb surfaces,⁷⁻⁹ however there are few investigations which look at atomic hydrogen cleaning of the AlGaIn surface.¹⁰ The effect of *in situ* atomic hydrogen treatments on the growth of high-k dielectrics on the AlGaIn surface has not been reported.

This study looks at the effect of depositing HfO₂ by ALD on the native oxide, NH₄OH etched and atomic hydrogen treated Al_{0.25}Ga_{0.75}N surface, with XPS carried out after a successive “half cycles” of the ALD process, to monitor the chemical changes at the semiconductor/ high-k interface and assess the impact of the surface pre-treatments.

2.3 Experimental

Three undoped Al_{0.25}Ga_{0.75}N samples (30 nm), grown on a 1.2 μm GaN layer on a p-type Si(111) substrate by metal organic chemical vapor deposition, obtained from DOWA Electronics Materials (see Figure 1.1(b)), were first solvent cleaned in acetone, methanol and isopropanol for one minute each. One sample was then etched in 10% NH₄OH for 5 minutes, followed by a 10s rinse in flowing deionized water and dried with nitrogen. This etched sample and a separate companion native oxide sample were then immediately mounted to a sample plate. A second native oxide sample was mounted to another sample plate, and these two plates were introduced into the ultra-high vacuum (UHV) system described in Chapter 1, allowing for *in situ* surface treatments, thin film depositions, and surface characterization without exposure to atmospheric conditions, preventing spurious surface contamination.

XPS was carried out after immediately loading the samples to UHV to determine the initial

starting surfaces. The native oxide and NH_4OH treated samples mounted on the same plate were annealed in UHV (the PVD chamber in Figure 1.1) at $\sim 8 \times 10^{-9}$ mbar at 300 °C for 30 minutes. The other native oxide sample was treated by atomic hydrogen (AH) at 300 °C for 30 minutes in the same UHV chamber. The AH was obtained by using a H_2 thermal cracking source consisting of a fine capillary tube, through which H_2 is flowed, surrounded by a tungsten filament heated to ~ 1400 °C by direct current heating (Dr. Eberl MBE Komponenten) which dissociates the molecular H_2 into atomic hydrogen.^{11,12} The total background pressure of H in the chamber during exposure was 2.5×10^{-6} mbar (which corresponds to ~ 3.4 kL of H exposure). XPS was then carried out after annealing or AH exposure.¹³

A Picosun ALD reactor integrated to the system by a buffer chamber and transfer tube was used for this *in situ* study. Tetrakis(dimethylamino) hafnium (TDMA-Hf) and $\text{DI-H}_2\text{O}$ were used as the precursors for HfO_2 formation. In this study, one full ALD cycle is 0.1s TDMA-Hf/ N_2 + 20s N_2 purge + 0.1s $\text{H}_2\text{O}/\text{N}_2$ + 20s N_2 purge. High purity (99.999%) N_2 is used as the precursor carrier and purging gas. The base pressure of the ALD reactor is ~ 10 mbar and the HfO_2 deposition temperature is 250 °C. In order to monitor the HfO_2 growth on the $\text{Al}_{0.25}\text{Ga}_{0.75}\text{N}$ surfaces, XPS was carried out after each individual “half cycle”¹⁴ pulse of the ALD process up to two full cycles; i.e., the samples were first exposed to one pulse of TDMA-Hf and interrogated with XPS, then transferred back to the ALD reactor and exposed to one pulse of H_2O prior to again being examined with XPS). The samples were also examined with XPS after 5 and 10 full cycles (TDMA-Hf + H_2O). Two further native oxide and AH treated samples were similarly prepared with subsequent ALD of 120 cycles of HfO_2 (for a nominal HfO_2 thickness of 10 nm), with XPS scans taken again of the treated surfaces and after 10 and 120 cycles of ALD to determine if there were any variations in the bulk deposited HfO_2 films due to the surface treatment.

The XPS in this study was carried out using a monochromated Al $K\alpha$ ($h\nu = 1486.7$ eV) X-ray source, equipped with a 7 channel analyzer, using a pass energy of 15 eV, with all scans taken at 45° with respect to the sample normal. Spectra were taken of the Ga $2p_{3/2}$, Ga $3d$, Hf $4f$, Hf $4d$, N $1s$, Al $2p$, O $1s$ and C $1s$ core level regions. XPS peak deconvolution was carried out using AAnalyzer¹⁵ software with a detailed peak fitting procedure described elsewhere.¹⁶ All

peaks were referenced to the N 1s peak at 397.0 eV to compensate for any changes in the peak core level positions due to band bending or surface charging. The variation of the shift among the samples investigated was within 1.5 eV.

2.4 Results and Discussion

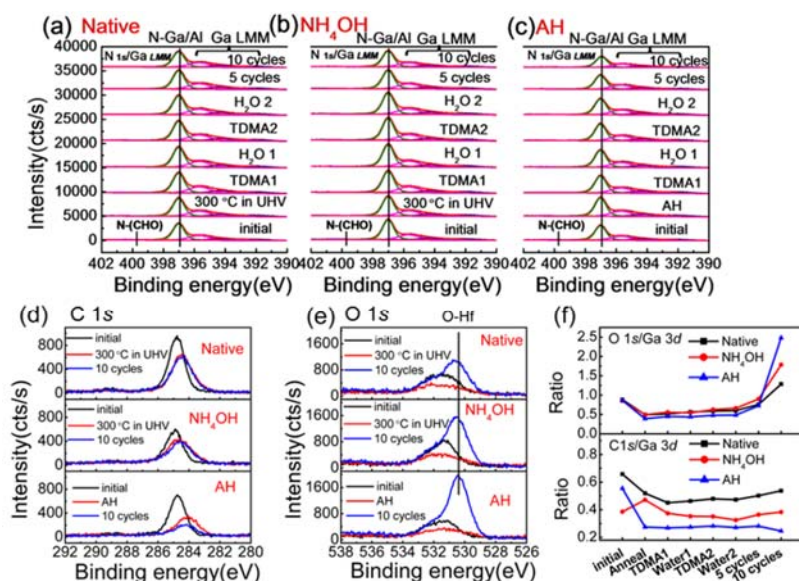


Figure 2.1. XPS spectra of the N 1s (a, b, c) core levels from the native oxide (a), NH₄OH etched (b) and AH treated (c) surface, from the initial surfaces, after annealing at 300 °C in UHV/AH cleaning and each individual ALD half cycle deposition. (d) and (e) show XPS spectra of C 1s and O 1s core levels from the initial surfaces, after annealing at 300 °C in UHV/AH cleaning and 20 full cycles HfO₂ deposition. Figure 2.1(f) shows the ratio of C 1s and O 1s to the Ga 3d.

N 1s and Ga Auger spectra are shown in Figure 2.1 for the (a) native oxide, (b) NH₄OH treated and (c) AH exposed samples. The complicated nature of the Ga *L*₂*M*₄₅*M*₄₅ Auger feature makes accurate deconvolution of the N 1s difficult. The fitting process is consistent with our previous reported work on ALD Al₂O₃ on AlGa_{0.5}N.¹⁷ All initial peaks show the N-Al/Ga peaks (set at 397.0 eV), a N-O peak (possibly consisting of O, C and H bonds) at ~400.5 eV, and the Ga *L*₂*M*₄₅*M*₄₅ Auger feature (spanning ~392-398 eV). After 300 °C anneal or AH treatment, N-O peaks in all samples are below the XPS detection limit, indicating that heating of the substrate alone is

sufficient to decompose any N-O bonding present on the surface. During the subsequent ALD process, no further changes in the N 1s core level spectra are observed. There is no obvious change in the intensity of N 1s peaks until 10 cycles of HfO₂ have been deposited suggesting a slow HfO₂ nucleation rate.

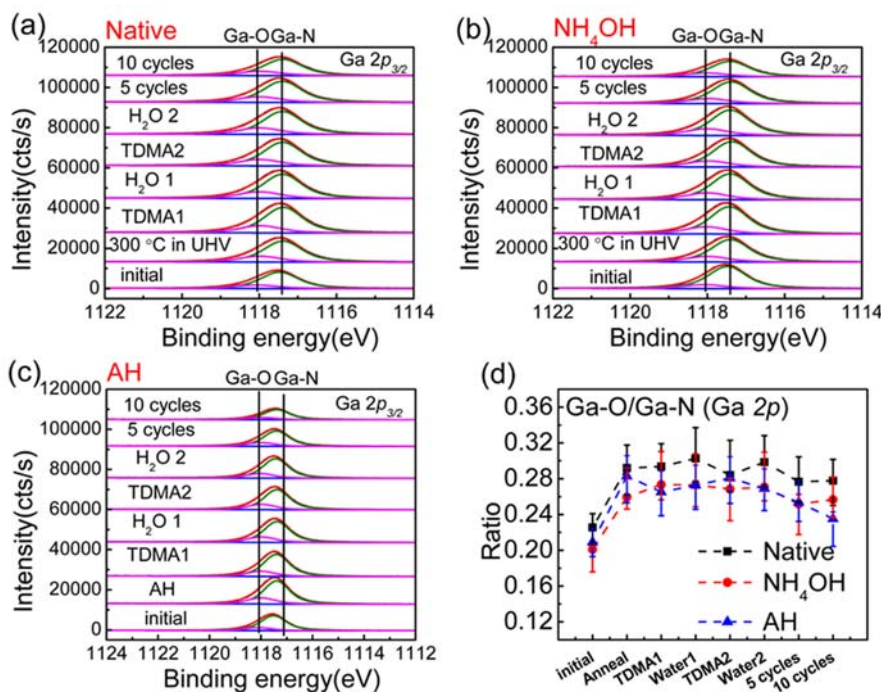


Figure 2.2. XPS spectra of Ga 2p_{3/2} (a, b, c) core levels from the native oxide (a), NH₄OH etched (b) and atomic hydrogen treated (c) surfaces, from the initial surfaces, after annealing at 300 °C in UHV/atomic hydrogen cleaning and each individual ALD half cycle deposition. Figure 2.2 (d) shows the ratio of gallium oxide to the bulk Ga-AlN from the Ga 2p_{3/2} spectra.

Examination of the C 1s spectra in Figure 2.1(d) for the initial surfaces, after 300 °C anneal or AH exposure, and after 10 full of HfO₂ cycles, the NH₄OH etch is shown to decrease the concentration of carbon present relative to the native oxide surface. A 300 °C anneal in UHV condition and AH exposure at 300 °C are both observed to reduce the concentration of carbon contamination on the native oxide surface, with atomic hydrogen being the more effective of the two. After anneal or atomic hydrogen treatment, the C 1s peak is observed to shift to a lower binding energy, likely due to decomposition of C-O(-H) bonds. At the same time, the data also

indicates that there is no increase in the amount of carbon on the surface during ALD, suggesting that the reaction between the TDMA-Hf and H₂O precursors is complete during each cycle.

Figure 2.1(e) shows the O 1s spectra at the same stages during the deposition process for the three samples. The 300 °C anneal in UHV and atomic hydrogen exposure are observed to cause a decrease in the concentration of oxygen present on the surfaces, particularly evident as a reduction in the O 1s peak intensity at ~531 eV, indicative of a decrease in native oxides and C-O bonding. This is also consistent with the trend of C concentration in Figure 2.1(f) which further indicates that the AH surface has the lowest concentration of carbon and oxygen (based on the peak area ratio of carbon and oxygen to gallium from the fitted C 1s, O 1s and Ga 3d core level spectra). After 10 full ALD cycles, the O 1s peak is seen to shift to a lower binding energy of ~530.4 eV, indicative of the formation of Hf-O bonding. The peak at 532 eV, likely due to hydroxide related species, is seen to persist throughout the deposition process, and at an increased level after 10 cycles of HfO₂ relative to the annealed and AH exposed surfaces, suggesting that there may be some –OH bond incorporation into the HfO₂ film.

The peak fitted Ga 2p_{3/2} spectra after each individual stage in the deposition process are shown in Figure 2.2. The spectra from the (a) native oxide, (b) NH₄OH etched and (c) atomic hydrogen treated samples show two peaks, indicative of Ga-N substrate bonding and the presence of Ga₂O₃, separated from the bulk peak by 0.68 eV.²¹ After 300 °C anneal or atomic hydrogen treatment, the ratio of the Ga-O to Ga-N peak areas, plotted in Figure 2.2 (d), shows an obvious increase, likely due to oxygen transferring from N-O and C-O bonding to form Ga-O. The error bars are calculated by varying the energy separation between the Ga-O and Ga-N peaks by ±0.025 eV and recalculating the peak areas, and is related to the energy resolution of the analyzer^{18,19} (the error in the Al 2p peak areas is also addressed in this way). Upon the first pulse of TDMA-Hf, there is no change detected in the Ga 2p_{3/2} spectra within experimental error. During the complete deposition process this ratio is relatively stable, suggesting again that there is a strong bond between the gallium oxide and the Al_{0.25}Ga_{0.75}N surface. However, after 10 full cycles of ALD of HfO₂, the AH treated sample does indicate a slight decrease in Ga-O concentration. This decrease is possibly due to the “clean up” effect that is widely reported on other III-V semiconductors,³ or the formation Hf-O-Ga environment which will be further

discussed in Chapter 4.

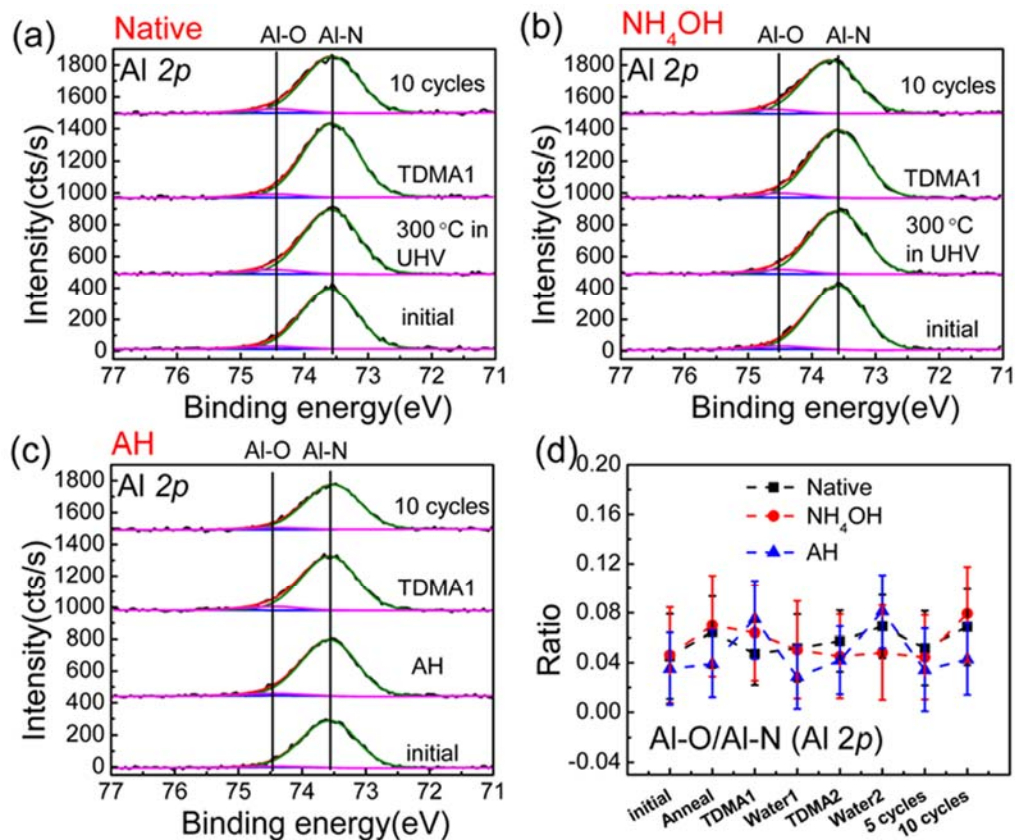


Figure 2.3. XPS spectra of Al 2p (a, b, c) core levels from the native oxide (a), NH₄OH etched (b) and AH (c) surfaces, from the initial surfaces, after annealing at 300 °C in UHV/atomic hydrogen cleaning, after first pulse of TDMA-Hf and after 10 full cycles. Figure 2.3 (d) shows the ratio of Al-O to the bulk Al-GaN from the Al 2p spectra.

Due to the inherent stability of the native oxide on Al_{0.25}Ga_{0.75}N, it is difficult to observe “clean up” effect on native oxide and NH₄OH samples, however, it is possible that the atomic hydrogen treatment produces more Ga-OH bonds on the Al_{0.25}Ga_{0.75}N surface with which the TDMA-Hf can react. The removal of carbon contamination by the *in situ* AH pretreatment is another possible reason. The lack of interfacial gallium oxide growth during ALD is in contrast to the results reported by Y.C. Chang et. al, where the emergence of a significant concentration of gallium oxide was detected by *ex situ* XPS and TEM after HfO₂ ALD on GaN, using TEMAH

and H₂O, at 200 °C.²⁰ We have previously shown that profound differences in the reported interfacial chemistry can occur when comparing *in situ* and *ex situ* XPS analysis,²⁶ however in this case where a relatively thick HfO₂ layer was deposited, it is likely that the oxidation occurs during the deposition process, as is indicated by the authors.

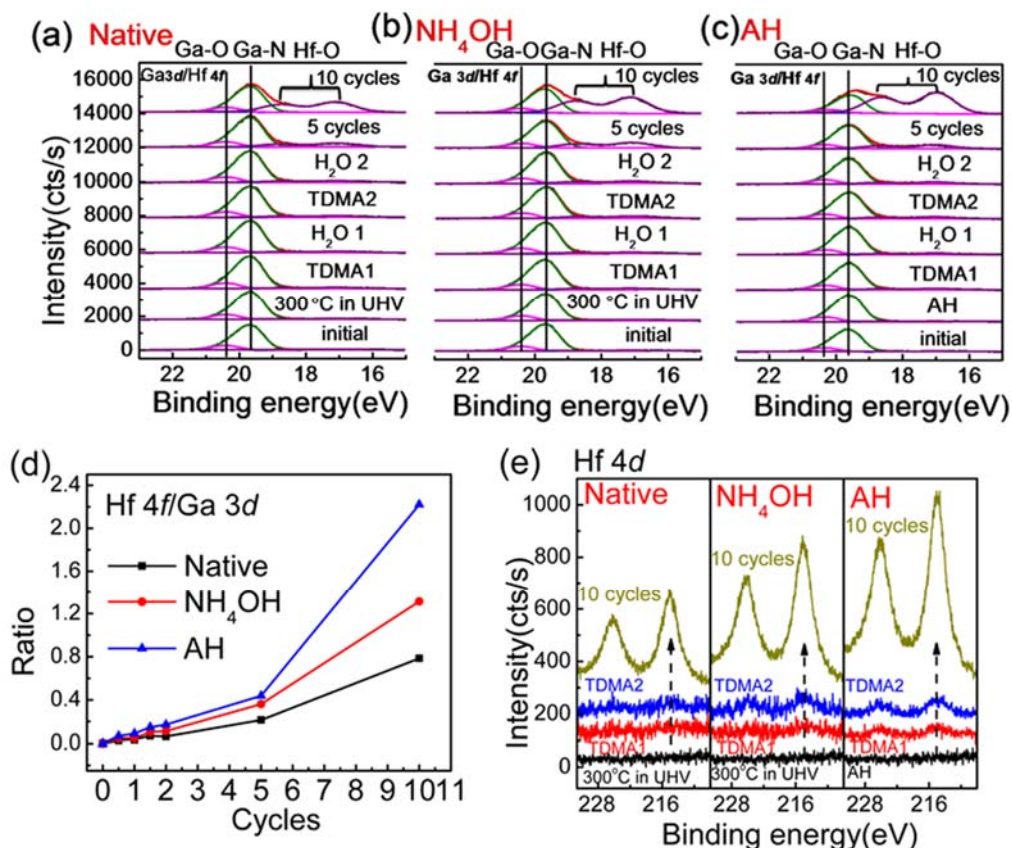


Figure 2.4. XPS spectra of Ga 3d and Hf 4f (a, b, c) core levels from the native oxide (a), NH₄OH etched (b) and AH (c) surfaces from the complete process. Figure 2.4 (d) shows the ratio of Hf 4f to the b Ga 3d. Figure 2.4 (e) shows Hf 4d from native oxide, NH₄OH etched and AH surfaces after annealing at 300 °C in UHV/atomic hydrogen cleaning, after first pulse of TDMA-Hf, after second pulse of TDMA-Hf and after 10 full cycles.

Al 2p spectra for the complete deposition process for the initial, 300 °C anneal/AH, after first “half cycle” of TDMA-Hf and after 20 full cycles spectra are shown in Figure 2.3 (a), (b) and (c) respectively. We are able to detect the Al-GaN bulk peak at 73.5 eV, as well as trace

amount of Al_2O_3 at 74.4 eV on all samples,²¹ however it is worth pointing out that this is close to XPS detection limits, (as indicated by the error bars from the ratio of Al-O:Al-GaN in Figure 2.3 (d)). Because of this low concentration of Al_2O_3 and the error associated with the deconvolution process, it is difficult to make a clear conclusion regarding changes in the concentration of Al_2O_3 present on the different samples. However, the ratio is relatively stable, which is consistent with $\text{Al}_{0.25}\text{Ga}_{0.75}\text{N}$'s inherent stability, and the initial and final area ratios are lowest on the AH treated surface.

Figure 2.4, shows the Ga 3*d* and Hf 4*f* spectra from the (a) native oxide, (b) NH_4OH etched and (c) AH treated $\text{Al}_{0.25}\text{Ga}_{0.75}\text{N}$ samples during the “half cycle” deposition process. The Ga-N bulk peaks were detected at 19.5eV, and Ga-O peaks located at ~20.2eV, consistent with the binding energy separation seen in the Ga 2*p*_{3/2} spectra. Hf 4*f*_{5/2} and Hf 4*f*_{7/2} peaks were detected after the first half cycle of TDMA-Hf for the three samples, however at a very low concentrations ($\ll 0.1$ nm). This initial growth rate is much lower than typical ALD HfO_2 growth on Si.^{21,22} and is also in contrast to previous half cycle studies investigating oxide deposition on other III-V semiconductor materials, where the first cycle of ALD was shown to deposit > 0.1 nm of HfO_2 or Al_2O_3 , under the same ALD conditions, reflecting the inherent stability and low reactivity of the III-N based materials.^{22,23–25} With subsequent cycles, a linear incremental increase was detected in the Hf 4*f* peaks after each TDMA-Hf pulse up to 5 full cycles. Figure 2.4 (d) shows most clearly the growth in HfO_2 by monitoring the change in the peak area ratio between the fitted Hf 4*f* and Ga 3*d* spectra during HfO_2 growth. Similar growth characteristics were also found for ALD Al_2O_3 on HF treated AlGaN and GaN.^{22,26}

From XPS thickness calculations, based on the attenuation of the Ga 2*p*_{3/2} peaks, after 10 full cycles, we detect about 0.2, 0.3 and 0.4 nm of HfO_2 on native oxide, NH_4OH and AH samples, respectively. This low growth rate of HfO_2 indicates that there is an initial nucleation period before the atomic layer deposition will take place, however it is possible that this growth rate may be improved through initial oxidation or functionalization of the surface.²⁹ Since this initial growth rate is faster on the AH treated surface, full nucleation is achieved earlier, and as a result we see a significant difference in the peak area ratios after 10 full cycles, as well as a clear variation in the intensities of the Hf 4*d* peaks from Figure 2.4(e) for the three samples. These Hf

4*d* spectra after 300 °C anneal or AH, after the first and second “half cycle” of TDMA-Hf, as well as after 10 full cycles make it easier to visually observe the growth of the HfO₂ layer compared to the Hf 4*f* peaks, which is significantly dominated in intensity during the early stages of deposition by the presence of the Ga 3*d* peak. Obvious Hf 4*d* peaks could be detected after the first “half cycle” of TDMA-Hf for AH sample whereas the signal was much lower on the other two samples. Again, after 10 cycles of HfO₂ deposition, the Hf concentration is highest for the AH exposed sample, and lowest for the native oxide sample, which is consistent with results from the Hf 4*f* peaks. Methods to further enhance ALD nucleation are currently under investigation, such as UV ozone oxidation,³² H₂O pretreatments,²⁷ and alternative surface pre-treatments.²⁸

In order to further compare the impact of AH treatment on the HfO₂ deposition and growth, a further 110 cycles of HfO₂ were deposited on the native oxide and AH treated surfaces, to give a nominal 10 nm HfO₂ thickness (based on a deposition rate of 0.08 nm/cycle extracted from depositions on a Si spectator sample). After this deposition it was no longer possible to detect any substrate signals in the XPS spectra due to the thickness of the oxide being greater than the sampling depth of the measurement, thus ruling out signal coming from the interface. While the HfO₂ spectra from the Hf 4*f* core levels were identical for both samples, there was a variation in the concentration of carbon detected, as indicated by the C 1*s* spectra in Figure 2.5. While the level of carbon detected from the AH exposed sample is close to XPS detection limits, there is still a clear carbon signal on the native oxide treated surface. This would seem to suggest that there is carbon incorporated into the HfO₂ film during deposition on the native oxide surface, which is not taking place on the AH sample.

We also observe that after the first 10 cycles of HfO₂ on the AH exposed surface there is a decrease in the carbon signal detected. This is possibly due to attenuation of the carbon signal by the thicker HfO₂ overlayer on this sample, or by the AH promoting increased interaction between the residual carbon and the TDMA-Hf precursor. This is not the case on the native oxide sample, where an increase in carbon is detected. This suggests that the AH exposure promotes the deposition of a HfO₂ film with less carbon contamination incorporated. However, it is not possible to comment at this time in relation to the location of this carbon, whether it is distributed

throughout the HfO₂ layer, which would indicate that it is incorporated during deposition, or whether it is located just at the HfO₂ surface, which could indicate carbon migration that originated at the AlGaN surface.

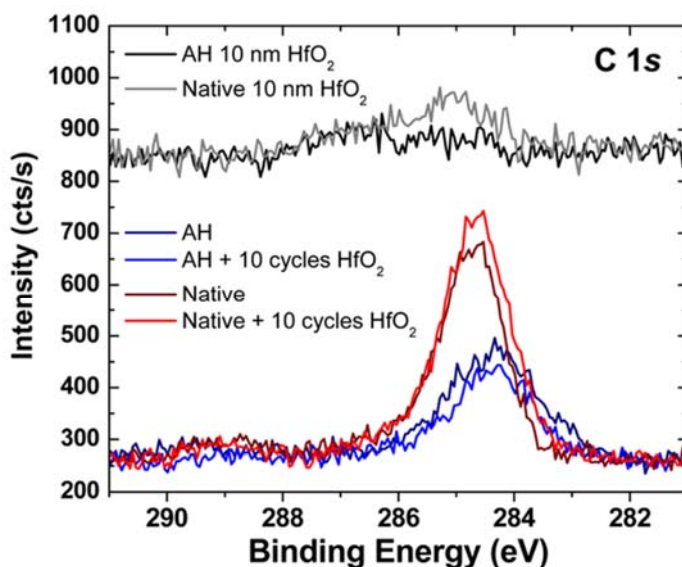


Figure 2.5. XPS spectra of C 1s from the native oxide and AH surfaces from the initial surface, after 10 cycles HfO₂, and after 120 cycles HfO₂ (~10 nm).

2.5 Conclusion

In conclusion, the initial stages of HfO₂ growth on the native oxide, NH₄OH treated, and atomic hydrogen treated Al_{0.25}Ga_{0.75}N surface was investigated by XPS by interrupting the deposition process after each individual ALD “half cycle”. Results suggests that while the Al_{0.25}Ga_{0.75}N surface is inherently chemically very stable in comparison to other III-V materials, annealing in UHV and atomic hydrogen both facilitate removal of carbon from the surface, with atomic hydrogen more effective. While no interfacial oxide growth was detected on any of the samples, the HfO₂ growth rates on the three surfaces was seen to vary, with atomic hydrogen treatment enhancing the nucleation rate of ALD HfO₂.

2.6 References

¹ S.M. George, Chem. Rev. **110**, 111 (2010).

- ² C. Hinkle, M. Milojevic, A. Sonnet, H. Kim, J. Kim, E.M. Vogel, and R.M. Wallace, ECS Trans. **19**, 387 (2009).
- ³ J. Shi, L.F. Eastman, X. Xin, and M. Pophristic, Appl. Phys. Lett. **95**, 042103 (2009).
- ⁴ R.D. Long and P.C. McIntyre, Materials (Basel). **5**, 1297 (2012).
- ⁵ S.W. King, J.P. Barnak, M.D. Bremser, K.M. Tracy, C. Ronning, R.F. Davis, and R.J. Nemanich, J. Appl. Phys. **84**, 5248 (1998).
- ⁶ R. Sohal, P. Dudek, and O. Hilt, Appl. Surf. Sci. **256**, 2210 (2010).
- ⁷ L.F.J. Piper, T.D. Veal, M. Walker, I. Mahboob, C.F. McConville, H. Lu, and W.J. Schaff, J. Vac. Sci. Technol. A Vacuum, Surfaces, Film. **23**, 617 (2005).
- ⁸ K. a. Elamrawi, M. a. Hafez, and H.E. Elsayed-Ali, J. Appl. Phys. **84**, 4568 (1998).
- ⁹ G. Bell, N. Kaijaks, R. Dixon, and C. McConville, Surf. Sci. **401**, 125 (1998).
- ¹⁰ M. Losurdo, J. Appl. Phys. **95**, 8408 (2004).
- ¹¹ H. Shimomura, Y. Okada, and M. Kawabe, Jap. J. Appl. Phys. **31**, L628 (1992).
- ¹² T. Sugaya and M. Kawabe, Jpn. J. Appl. Phys (1991).
- ¹³ F.S. Aguirre-Tostado, M. Milojevic, K.J. Choi, H.C. Kim, C.L. Hinkle, E.M. Vogel, J. Kim, T. Yang, Y. Xuan, P.D. Ye, and R.M. Wallace, Appl. Phys. Lett. **93**, 061907 (2008).
- ¹⁴ M. Milojevic, F.S. Aguirre-Tostado, C.L. Hinkle, H.C. Kim, E.M. Vogel, J. Kim, and R.M. Wallace, Appl. Phys. Lett. **93**, 202902 (2008).
- ¹⁵ A. Herrera-Gómez, P. Pianetta, and D. Marshall, Phys. Rev. B **61**, 988 (2000).
- ¹⁶ B. Brennan and G. Hughes, J. Appl. Phys. **108**, 053516 (2010).
- ¹⁷ B. Brennan, X. Qin, H. Dong, J. Kim, and R.M. Wallace, Appl. Phys. Lett. **101**, 211604 (2012).
- ¹⁸ P. Streubel, R. Szargan, R. Hesse, and T. Chass'e, Surf. Interface Anal. **36**, 1373 (2004).
- ¹⁹ P. Cumpson and M. Seah, Surf. Interface Anal. (1992).
- ²⁰ Y.C. Chang, M.L. Huang, Y.H. Chang, Y.J. Lee, H.C. Chiu, J. Kwo, and M. Hong, Microelectron. Eng. **88**, 1207 (2011).
- ²¹ D. Triyoso, R. Liu, D. Roan, M. Ramon, N. V. Edwards, R. Gregory, D. Werho, J. Kulik, G. Tam, E. Irwin, X.-D. Wang, L.B. La, C. Hobbs, R. Garcia, J. Baker, B.E. White, and P. Tobin, J. Electrochem. Soc. **151**, F220 (2004).

- ²² M.L. Green, M.-Y. Ho, B. Busch, G.D. Wilk, T. Sorsch, T. Conard, B. Brijs, W. Vandervorst, P.I. Raˆˆisaˆˆnen, D. Muller, M. Bude, and J. Grazul, J. Appl. Phys. **92**, 7168 (2002).
- ²³ M. Milojevic, C.L. Hinkle, F.S. Aguirre-Tostado, H.C. Kim, E.M. Vogel, J. Kim, and R.M. Wallace, Appl. Phys. Lett. **93**, 252905 (2008).
- ²⁴ B. Brennan, M. Milojevic, H.C. Kim, P.K. Hurley, J. Kim, G. Hughes, and R.M. Wallace, Electrochem. Solid-State Lett. **12**, H205 (2009).
- ²⁵ B. Brennan, H. Dong, D. Zhernokletov, J. Kim, and R.M. Wallace, Appl. Phys. Express **4**, 125701 (2011).
- ²⁶ P. Sivasubramani, T.J. Park, B.E. Coss, A. Lucero, J. Huang, B. Brennan, Y. Cao, D. Jena, H.G. Xing, R.M. Wallace, and J. Kim, Phys. Status Solidi - Rapid Res. Lett. **6**, 22 (2012).
- ²⁷ X. Liu, R. Yeluri, J. Lu, and U.K. Mishra, J. Electron. Mater. **42**, 33 (2012).
- ²⁸ N. Nepal, N.Y. Garces, D.J. Meyer, J.K. Hite, M. A. Mastro, and C.R. Eddy, Appl. Phys. Express **4**, 055802 (2011).

CHAPTER 3

A Comparative Study of Atomic Layer Deposition of Al₂O₃ and HfO₂ on AlGa_N/Ga_N

3.1 Preface

Chapters 1 and 2 have investigated the atomic layer deposition (ALD) of Al₂O₃ and HfO₂ on AlGa_N using *in situ* X-ray photoelectron spectroscopy (XPS), respectively. Obviously, an initial nucleation around 10 cycles of ALD is needed. There is no obvious detectable chemical change on AlGa_N after ALD of Al₂O₃ or HfO₂. In this chapter, the device performances and surface state types are investigated by capacitance voltage (C-V) and gate leakage measurements. The ALD of Al₂O₃ and HfO₂ on AlGa_N/Ga_N were systematically studied. The band alignments of Al₂O₃/AlGa_N and HfO₂/AlGa_N were investigated using the *in situ* XPS. Band offsets of 1.8 and 1.1 eV were observed for Al₂O₃/AlGa_N and HfO₂/AlGa_N, respectively. The Al₂O₃ and HfO₂ dielectric layers were found to reduce the leakage current as expected, but neither of them changes the density of surface states. The positive ionized surface donor states density and average interface state density (D_{it}) below the conduction band edge ($0.34 < E_C - E_T < 0.50$ eV), is crudely extracted from C-V characterization, and were $\sim 1.7 \times 10^{13} \text{cm}^{-3}$ and $1.1 \times 10^{14} \text{cm}^{-2} \text{eV}^{-1}$, respectively.

The contents of this chapter are adapted from a manuscript entitled “**A comparative study of atomic layer deposition of Al₂O₃ and HfO₂ on AlGa_N/Ga_N**” which will be submitted soon.

3.2 Introduction

Although, the high k oxide is able to reduce the high leakage current, there are still some challenges for AlGa_N/Ga_N due to its unique properties. For example, the insertion of an insulator layer would shift the threshold voltage to negative values, which is not desirable for enhancement mode AlGa_N/Ga_N HEMT.¹ Similar phenomenon have also been reported by Al₂O₃/Ga_N devices.^{2,3} The negative shift for oxide/AlGa_N is induced by the positive charges at the AlGa_N surface which is considered as the origin of free electron for two dimension electron

gas.⁴ Thus, the evaluation and modulation of the positive AlGaIn surface state is important for AlGaIn/GaN device designs. The D_{it} occupying levels below the conduction band edge at the oxide/AlGaIn interface, which degrades the device stability, is another concern.^{5,6} Whether ALD of Al₂O₃ or HfO₂ could passivate such states and reduce the D_{it} is still not clear. In this work, the Al₂O₃/AlGaIn and HfO₂/AlGaIn interface was systematically investigated using *in situ* XPS, and *ex situ* C-V as well as gate leakage current measurements. Band alignments are proposed from high resolution XPS measurements, and the interface charge density and D_{it} are extracted by the C-V curves from various thicknesses of oxide/AlGaIn/GaN metal-oxide-semiconductor (MOS) diodes.

3.3 Experimental

Metal organic chemical vapor deposited Al_{0.25}Ga_{0.75}N (30 nm)/ GaN (1.2 μ m) layer on a p-type Si(111) substrate HEMTs wafers obtained from DOWA Electronics Materials (Tokyo, Japan) were used in this study. Two samples ($\sim 1 \times 1$ cm²) cut from the same wafer were first solvent cleaned in acetone, methanol and isopropanol for one minute each to reduce the surface organic contamination, and then were introduced to an ultra-high vacuum (UHV) cluster system described in Chapter 1 and in detail elsewhere.⁷ After initial XPS analysis, samples were transferred to a Picosun ALD reactor through a transfer tube (operation pressure: 1×10^{-10} mbar) to avoid spurious atmospheric contamination. After 20 cycles of Al₂O₃ or HfO₂ ALD, *in situ* XPS was performed again on each sample after transferring them back to the analysis chamber. Each sample was also examined by XPS after another 80 cycles of Al₂O₃ or HfO₂ (totally 100 cycles). One ALD cycle for Al₂O₃ was 0.1 s Trimethyl-aluminum (TMA) + 4 s purge + 0.1 s H₂O + 4 s purge, while that for HfO₂ was 0.1 s Tetrakis (dimethylamino) hafnium (TDMA-Hf) + 20 s purge + 0.1 s H₂O + 20 s purge. The TMA and H₂O precursors were kept at room temperature and the TDMA-Hf was heated at 75 °C. High purity (99.999%) N₂ (200 sccm) was used as the precursor carrier and purge gas. The working pressure of the ALD reactor was ~ 10 mbar and the Al₂O₃ and HfO₂ deposition temperature were 300 °C and 250 °C, respectively. XPS was carried out using a monochromatic Al K α_1 ($h\nu = 1486.7$ eV) X-ray source, equipped with a 7 channel analyzer, using a pass energy of 15 eV, with all scans taken at 45° with respect to the sample normal.

For MOS diode fabrication, 50, 100 and 150 cycles of Al₂O₃ and HfO₂ (nominal 5 nm, 10

nm and 15 nm) were deposited on AlGaIn/GaN/Si samples, respectively using the same ALD deposition conditions described above. Ohmic contact regions were firstly defined using a standard photolithography followed by BCl₃ (15 sccm)/Ar (5 sccm) reactive ion etching (RIE) to open up the contact regions. The ohmic contacts (resistivity $\rho \sim 1 \times 10^{-6} \Omega \cdot \text{cm}^2$)⁸ were formed by e-beam evaporation deposition (base pressure $\sim 1 \times 10^{-6}$ mbar) of Ti/Al/Ni/Au (20 nm / 100 nm / 50 nm / 50nm) followed by a rapid thermal annealing at 850 °C in N₂ atmosphere at a flow rate of 2000 sccm for 30s after patterning by lift off.⁹ Circular gate electrodes were then defined, followed by e-beam deposition of Ni/Au (50 nm / 100 nm) and lift off. The leakage current measurements were carried out using a Keithley 4200. C-V measurements were performed using an Agilent 4284 LCR meter at a step of 0.02 V and AC modulation voltage of 50 mV with sweep frequencies varying from 1 to 400 kHz.

3.4 Results and Discussion

Figure 3.1 shows the Ga 2p_{3/2} spectra before and after 20 cycles of Al₂O₃ or HfO₂ deposition, along with the N 1s and Ga LMM regions. For comparison of chemical shifts, the spectra intensity is normalized to the initial peak intensity. Both the Ga 2p_{3/2} and the N 1s and Ga LMM spectra overlap well with each other before and after Al₂O₃ or HfO₂ deposition, and is an indication that no change in the interfacial chemistry is detected for the AlGaIn surface after the ALD. The detailed *in situ* XPS studies on the Al₂O₃/AlGaIn and HfO₂/AlGaIn interfaces have been reported previously,^{8,10–12} in which good stability AlGaIn interface toward ALD have been demonstrated.

The band offsets at the Al₂O₃/AlGaIn and HfO₂/AlGaIn interface are determined by XPS.¹³ Figure 3.2 (a) and (d) show the O 1s core level spectra along with the onset of the O loss features upon 100 cycles of Al₂O₃ and HfO₂ on AlGaIn. The band gap of the Al₂O₃ and HfO₂ films can be extracted from the separation between the O 1s core level feature and the onset of its loss feature originated from the excitation of electrons from the valence band to the conduction band.¹⁴ The extracted ALD Al₂O₃ band gap is 6.9±0.1 eV, which is consist with the work of Hashizume *et al.*¹⁵ The extraction of HfO₂ band gap (Figure 3.2(d)) is more complex than that for Al₂O₃ because of the overlap of the Hf 4s feature. Recently Ohta *et al.*¹⁶ reported that a subtraction of the Hf 4s spectra in the O 1s loss feature is important to decide the accurate band gap of HfO₂.

As shown in Figure 3.2 (d), the reduced O 1s spectra is achieved by subtracting the Hf 4s spectra that is fitted from a pure Hf metal reference sample (also grown by RF sputtering in an interconnected chamber).⁷ With the Hf 4s feature subtraction, a 5.9 ± 0.3 eV of band gap is obtained in this work, consistent with the recently reported band gap of HfO₂ (5.99 ± 0.33 eV).¹⁷

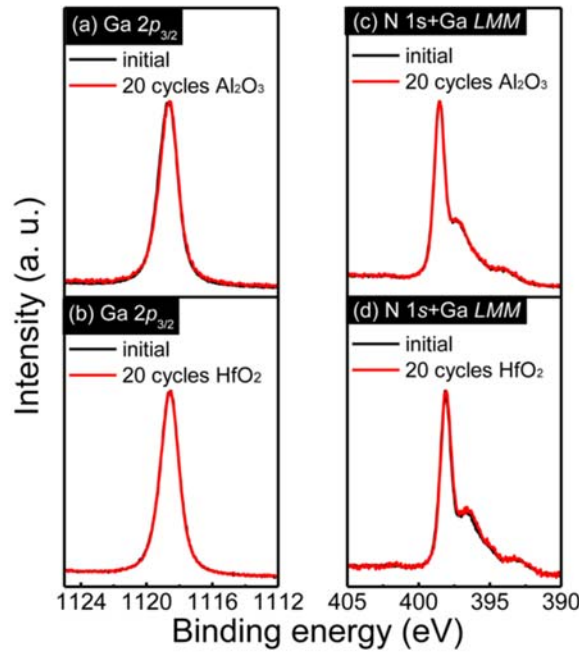


Figure 0.1. *In situ* normalized XPS spectra of the Ga 2p_{3/2} and N 1s/Ga LMM for AlGaN before and after 20 cycles of Al₂O₃ and HfO₂.

The valance band offset (VBO) can be obtained by:¹⁸

$$\Delta E_V = (E_{CL,Ga\ 3d}^{AlGaN} - E_{Valence}^{AlGaN}) - (E_{CL,Al\ 2p\ or\ Hf\ 4f}^{oxide} - E_{Valence}^{oxide}) - \Delta E_{CL} \quad (3.1)$$

where $E_{CL,Ga\ 3d}^{AlGaN}$ and $E_{Valence}^{AlGaN}$ are the Ga 3d core level and the valence band maximum (VBM) extracted from initial AlGaN, while $E_{CL,Al\ 2p\ or\ Hf\ 4f}^{oxide}$ and $E_{Valence}^{oxide}$ are the Al 2p/Hf 4f core level and VBM upon 100 cycles Al₂O₃ or HfO₂ deposited on AlGaN. The thickness assures that the photoelectron information depth is confined to the oxide. In contrast, the core level shift (ΔE_{CL}) is determined by:¹⁸

$$\Delta E_{CL} \equiv E_{CL,Ga\ 3d}^{AlGaN}(Interface) - E_{CL,Al\ 2p\ or\ Hf\ 4f}^{oxide}(Interface) \quad (3.2)$$

where $E_{CL,Ga\ 3d}^{AlGaN}(Interface)$ and $E_{CL,Al\ 2p\ or\ Hf\ 4f}^{oxide}(Interface)$ are the binding energy of

Ga 3d and Al 2p/Hf 4f core levels measured upon 20 cycles of Al₂O₃ or HfO₂ on AlGa_{0.75}N, where the oxide thickness renders photoelectron transparency to the interface. Experimentally, there is no core level binding energy shift detected at the interface after the Al₂O₃ or HfO₂ deposition. Thus equation (3.1) is simplified to equation (3.3):

$$\Delta E_V = E_{Valence}^{oxide} - E_{Valence}^{AlGaN} \quad (3.3)$$

The valance band spectra of the initial AlGa_{0.75}N surface and after 100 cycles of Al₂O₃ and HfO₂ are shown in Figure 3.2 (b) and (e). It is worth noting that the valence band maximum of initial AlGa_{0.75}N surface is $\sim 3.2 \pm 0.1$ eV. If we assume the band gap value of the AlGa_{0.75}N is 3.9 eV,¹⁹ then the Fermi level of Al_{0.25}Ga_{0.75}N is ~ 0.7 eV below the conduction band edge for the unintentional doping AlGa_{0.75}N. The corresponding band diagrams for Al₂O₃/AlGa_{0.75}N and HfO₂ is shown in Figure 3.2(c) and (f), where the deduced conduction band offset (CBO) values for Al₂O₃/AlGa_{0.75}N and HfO₂/AlGa_{0.75}N are 1.8 and 1.1 eV, respectively.

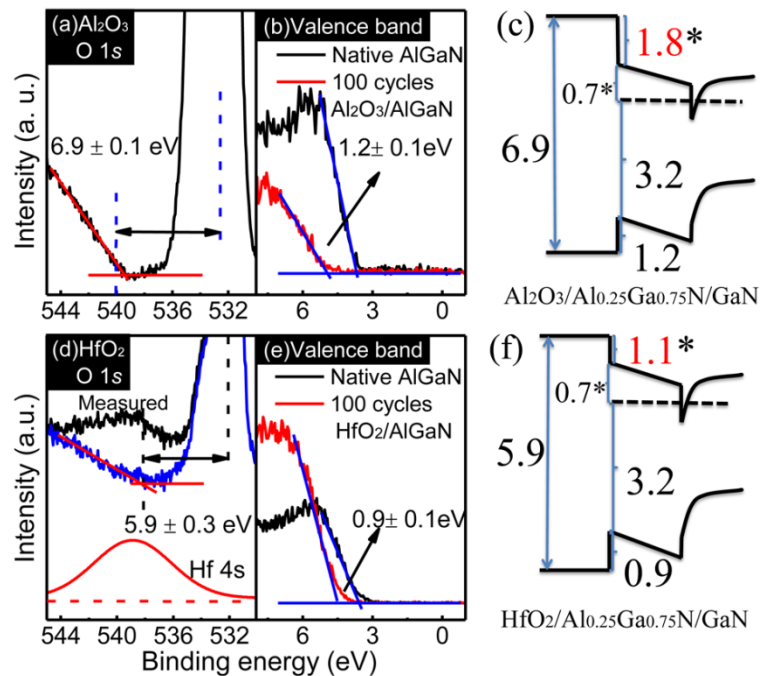


Figure 0.2. XPS of O 1s core level spectra showing the onset of O loss features for 100 cycles of (a) Al₂O₃/AlGa_{0.75}N and (d) HfO₂/AlGa_{0.75}N, XPS valence band spectra for AlGa_{0.75}N and 100 cycles of (b) Al₂O₃/AlGa_{0.75}N and (e) HfO₂/AlGa_{0.75}N, and energy band diagram for (c) Al₂O₃/AlGa_{0.75}N/GaN and (f) HfO₂/AlGa_{0.75}N/GaN interfaces. Subtraction of the Hf 4s peak is applied in (d), see text.

Figure 3.3 (a) and (b) show the gate leakage current density vs applied gate voltage (J-V) plots for the $\text{Al}_2\text{O}_3/\text{AlGaIn}/\text{GaIn}$ and $\text{HfO}_2/\text{AlGaIn}/\text{GaIn}$ MOS diodes with different oxide thicknesses. The corresponding gate leakage current density for a metal (Au/Ni)/AlGaIn/GaN Schottky diode is also included as a reference. From -20 to -4 V (reverse bias, “off” state) for the metal /AlGaIn/GaN Schottky diode, the leakage current density plateaus at $\sim 10^{-2}$ A/cm². From -4 to 0 V, the leakage current density obviously decreases. The leakage current mechanism for the reverse bias condition is complex and related with defect states, polarization and the electric field profile.²⁰ In forward bias (0 to 4 V), the gate leakage current density increases exponentially and is attributed to thermionic (Schottky) emission and thermionic field emission as well as some trap-induced mechanisms.^{20–22} As expected, both the Al_2O_3 and HfO_2 films reduce the leakage current over the whole applied voltage range (from -20 V to 4 V), with the Al_2O_3 more effective. For example, the leakage current densities measured for ~ 10 nm Al_2O_3 and HfO_2 are $\sim 10^{-6}$ and $\sim 10^{-3}$ A/cm², respectively at an applied voltage of 4 V. These results are consistent with the fact that the CBO for $\text{Al}_2\text{O}_3/\text{AlGaIn}$ is larger than that of $\text{HfO}_2/\text{AlGaIn}$ as mentioned earlier (Figure 3.2). In addition, it is noted that for MOS diodes with the Al_2O_3 insulator, the minimum leakage current is found near the threshold voltages (Table 3.1) while such phenomenon is not found for HfO_2 -MOS diodes. The mechanism is still under study.

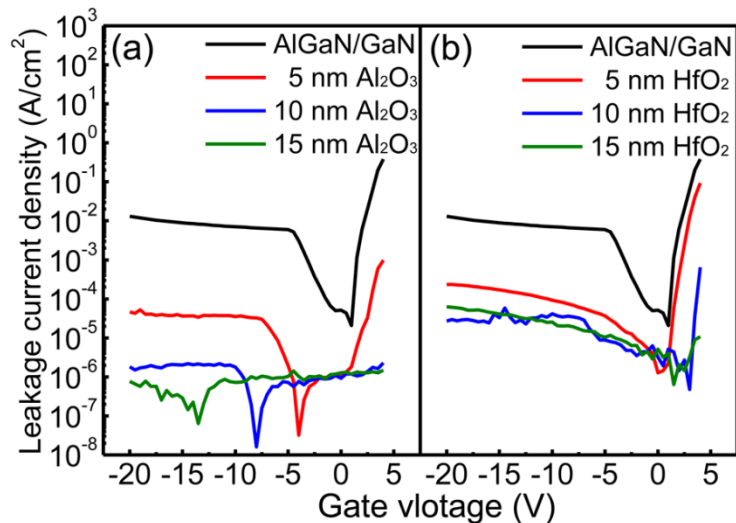


Figure 0.3. Leakage current density-voltage plots for (a) $\text{Al}_2\text{O}_3/\text{AlGaIn}/\text{GaIn}$ and (b) $\text{HfO}_2/\text{AlGaIn}/\text{GaIn}$ MOS diodes.

Figure 3.4 (a) and (b) shows the C-V curves for the MOS diodes fabricated using different thicknesses of Al₂O₃ or HfO₂ measured at 100 kHz at room temperature. The capacitance of the 2D electron gas (2DEG) modulation region decreases with the increasing of Al₂O₃ and HfO₂ thickness.^{8,23,24} The oxide capacitance is extracted by using the capacitance value of oxide/AlGaIn stacks and the AlGaIn capacitance (262 nF/cm² measured from the reference metal(Au/Ni)/AlGaIn/GaN Schottky diode) as shown in Table 5.1. The calculated dielectric constants for Al₂O₃ and HfO₂ is ~9.5 and ~20, which are consistent with the typical values for ALD Al₂O₃ and HfO₂ films.²⁵ A negative threshold voltage shift (see Figure 3.4) is detected in both the Al₂O₃/AlGaIn/GaN and HfO₂/AlGaIn/GaN MOS diodes as a result of the interface charge discussed further below.

Table 0.1. Summary of observed threshold voltages, capacitances at 2DEG plateau and calculated oxide capacitance.

Samples	V _{TH} (V)	Capacitance (oxide/AlGaIn) (nF/cm ²)	Capacitance (oxide) (nF/cm ²)
50 cycles Al ₂ O ₃	-7.1±0.1	225	1593.2
100 cycles Al ₂ O ₃	-9.4±0.1	191	718.6
150 cycles Al ₂ O ₃	-13.1±0.1	178	546.6
50 cycles HfO ₂	-4.94±0.1	242	3170.2
100 cycles HfO ₂	-6.16±0.1	228	1759.0
150 cycles HfO ₂	-7.94±0.1	211	1084.0

The threshold voltage (V_{th}) can be described as equation (3.4):^{26,27}

$$V_{th} = \frac{\Phi_B}{q} - \frac{\Delta E_C^{oxide/AlGaIn} + \Delta E_C^{AlGaIn/GaN}}{q} - \frac{\Phi_f}{q} - \frac{q d_{ox}}{2 C_{ox}} n_{ox} - \frac{q}{C_{ox}} Q_{oxide/AlGaIn} - q \left(\frac{1}{C_{ox}} + \frac{1}{C_{AlGaIn}} \right) Q_{AlGaIn/GaN} , \quad (3.4)$$

where Φ_B is metal barrier height for Ni on oxide (i.e., 3.5 and 3.25 eV for the Ni/Al₂O₃ and Ni/HfO₂ interface, respectively²⁸), q is the elementary charge (1.6×10^{-19} C), $\Delta E_C^{oxide/AlGaIn}$

and $\Delta E_C^{AlGaN/GaN}$ are the CBO of the oxide/AlGaN (1.8 eV and 1.1 eV, see Figure 3.2) and AlGaN/GaN (~ 0.3 eV),²⁹ respectively, Φ_f is described as the energy difference $E_{c,GaN} - E_f$ (E_f is the Fermi energy) in the GaN bulk (~ 0.3 eV),²⁶ d_{ox} is the thickness of oxide, C_{ox} and C_{AlGaN} are the capacitance of the oxide and AlGaN, respectively, n_{ox} is the average oxide bulk charge density (per unit volume, in units of cm^{-3}), $Q_{oxide/AlGaN}$ and $Q_{AlGaN/GaN}$ are corresponding interface charge densities (in units of cm^{-2}) at the oxide/AlGaN and AlGaN/GaN interfaces. $Q_{AlGaN/GaN}$ is the total polarization sheet charge density (given by the sum of spontaneous and piezoelectric polarization) at the AlGaN/GaN interface ($1.4 \times 10^{13} \text{ cm}^{-2}$)²⁹.

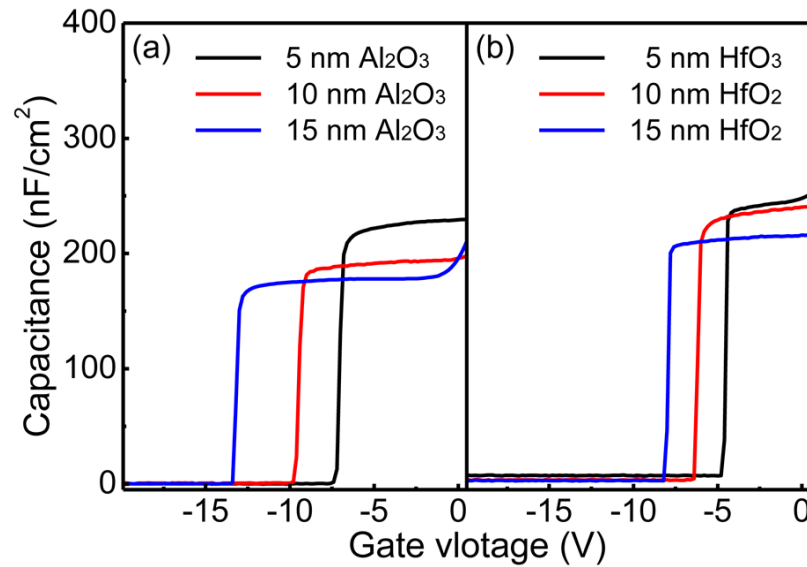


Figure 0.4. C-V curves measured at 100 kHz for (a) Al₂O₃/ AlGaN/ GaN and (b) HfO₂/ AlGaN/ GaN MOS diodes.

The origin of $Q_{oxide/AlGaN}$ is more complex and consists of different components: the sum of spontaneous and piezoelectric polarization induced charge density, the positive charge density of the ionized surface donors (Q_d), of which the origin is still under debate,²⁰ and the negatively charged oxide/AlGaN interface traps (Q_{it}). Among these sources, Q_{it} is usually one order of magnitude smaller than that of the total $Q_{oxide/AlGaN}$,²⁷ which often contributes to a hysteresis in C-V curves. Our previous work has also demonstrated that the small hysteresis results from a low Q_{it} at/near the Al₂O₃/AlGaN interface.⁸ The impact of the oxide fixed charge density n_{ox}

on the threshold voltage shift is much smaller (one order of magnitude smaller) than that from $Q_{oxide/AlGaN}$ and $Q_{AlGaN/GaN}$.^{26,27} Therefore, a linear fitting is performed to solve for the $Q_{oxide/AlGaN}$ by ignoring the n_{ox} term as Figure 3.5 shows.²³ The equation (3.4) could be converted to equation (3.5)

$$\frac{dV_{th}}{d\epsilon_{ox}} = -\frac{q}{\epsilon_0\epsilon_{ox}}(Q_{oxide/AlGaN} + Q_{AlGaN/GaN}) \quad (3.5)$$

ϵ_0 and ϵ_{ox} is the vacuum permittivity and oxide dielectric constant, respectively. The $Q_{oxide/AlGaN}$ values extracted from the fitting for $Al_2O_3/AlGaN$ and $HfO_2/AlGaN$ interface are $1.7\pm0.4\times10^{13}$ and $1.9\pm0.4\times10^{13}$ cm^{-2} , respectively, which indicate an existence of similar levels of positive charge density of the ionized surface donors. According to previous *in situ* XPS results^{8,10-12} as well as Figure 3.1, there is no detectable chemical state variations, suggesting that the ALD Al_2O_3 and HfO_2 insulators do not change or passivate the ionized surface state. In summary, the positive charges at the oxide/ $AlGaN$ interface originating from the surface donor states are considered as the main source for the undesirable negative voltage shift, and this charge is not influenced by the ALD process.

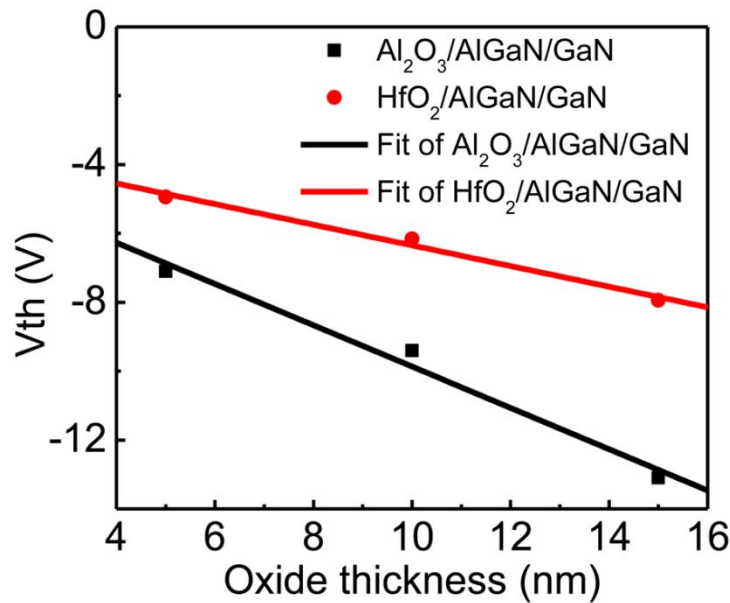


Figure 0.5. Linear fit to V_{th} dependence on the oxide thickness.

Figure 3.6 shows the C-V curves measured at various modulation frequencies from 1 kHz to

400 kHz for ~ 15 nm $\text{Al}_2\text{O}_3/\text{AlGaIn}/\text{GaIn}$ and ~ 15 nm $\text{HfO}_2/\text{AlGaIn}/\text{GaIn}$ MOS diodes. A typical two-step response in the C-V curves is observed.²⁴ Substantial frequency dispersion in the positively applied gate voltage region is detected for both samples as a result of a high D_{it} (“fast” states, i.e., short time constant response) below the conduction band edge that likely originates primarily from the oxide/AlGaIn interface. It should be noted the fast D_{it} does not impact the threshold voltage shift as demonstrated previously.⁸ The extraction of the average D_{it} is presented in our previous work.⁸ The corresponding values of average D_{it} are $1.1 \pm 0.2 \times 10^{14}$ and $1.2 \pm 0.2 \times 10^{14} \text{ cm}^{-2} \text{ eV}^{-1}$ for Al_2O_3 and HfO_2 (see Table 3.2), indicate that neither Al_2O_3 nor HfO_2 can passivate the surface due to the chemical stability of AlGaIn surface during the ALD process.

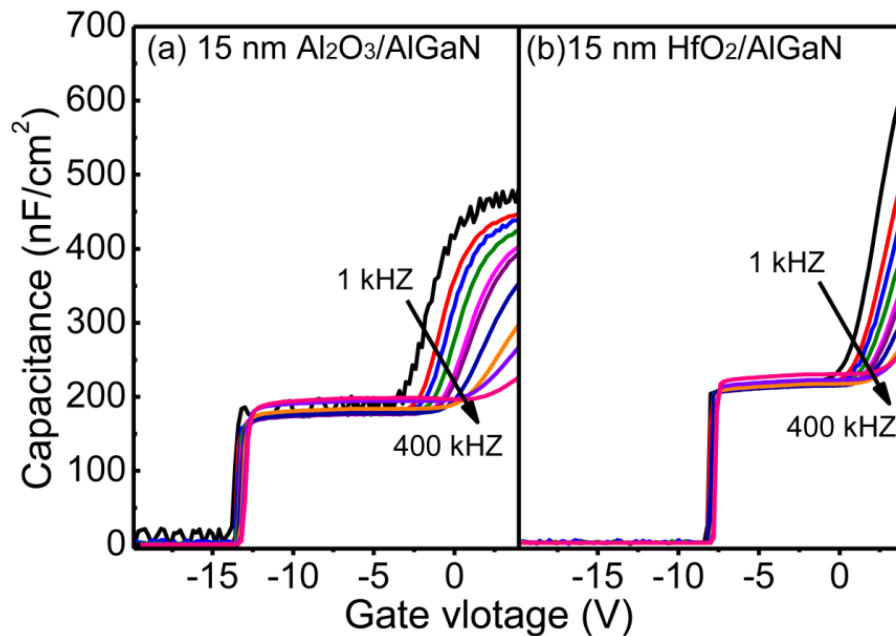


Figure 0.6. Frequency-dependent C-V curves for (a) ~ 15 nm $\text{Al}_2\text{O}_3/\text{AlGaIn}/\text{GaIn}$ and ~ 15 nm $\text{HfO}_2/\text{AlGaIn}/\text{GaIn}$ diodes.

Tapajna *et al.*²³ reported a high D_{it} close to the conduction band edge ($>10^{13} \text{ eV}^{-1} \text{ cm}^{-2}$) and a high positive oxide/AlGaIn(GaIn) donor states change density ($>10^{13} \text{ cm}^{-2}$) for MOSHEMT structures with Al_2O_3 grown by metal organic chemical vapor deposition (MOCVD) at 600°C on GaIn(cap layer, $\sim 3 \text{ nm}$)/ $\text{Al}_{0.24}\text{Ga}_{0.76}\text{N}/\text{GaIn}/\text{sapphire}$ and $\text{Al}_{0.24}\text{Ga}_{0.76}\text{N}/\text{GaIn}/\text{sapphire}$, indicating that the Al_2O_3 grown by MOCVD was also not effective for the passivation of the AlGaIn or GaIn cap. Recently, a monolayer crystalline oxide passivation method has been

reported which is capable of reducing the positive charge density of the ionized surface donors, as well as the D_{it} below the conduction band edge effectively.³¹

Table 0.2. Summary of, surface charge density at oxide/AlGaIn interface ($Q_{oxide/AlGaIn}$), oxide fixed charge (n_{ox}) and fast D_{it} ($0.34 < E_C - E_T < 0.5$ eV).

Structure	$Q_{oxide/AlGaIn}$ (cm^{-2})	D_{it} ($\text{cm}^{-2}\text{eV}^{-1}$)
Al ₂ O ₃ /AlGaIn/GaN	$1.7 \pm 0.4 \times 10^{13}$	$1.1 \pm 0.2 \times 10^{14}$
HfO ₂ /AlGaIn/GaN	$1.9 \pm 0.4 \times 10^{13}$	$1.2 \pm 0.2 \times 10^{14}$

3.5 Conclusion

The ALD Al₂O₃/AlGaIn and HfO₂/AlGaIn interfaces are investigated using *in situ* XPS and *ex situ* electric characterization. It has been demonstrated that both oxide insulating layers reduce the gate leakage current, with a more effective reduction observed for the Al₂O₃ layers due to a higher CBO. The positive charges at the oxide/AlGaIn ($\sim 1.7 \times 10^{13} \text{ cm}^{-2}$) result in a negative threshold voltage as well as a negative shift in the threshold voltage while the oxide capacitance decreases. Neither ALD Al₂O₃ nor HfO₂ changes or passivates the surface charge. A high average fast D_{it} ($1.2 \pm 0.2 \times 10^{14} \text{ cm}^{-2}\text{eV}^{-1}$) is found at AlGaIn surface independent of the oxides employed.

3.6 References

- ¹ C. Mizue, Y. Hori, M. Miczek, and T. Hashizume, Jpn. J. Appl. Phys. **50**, 021001 (2011).
- ² T.H. Hung, S. Krishnamoorthy, M. Esposto, D. Neelim Nath, P. Sung Park, and S. Rajan, Appl. Phys. Lett. **102**, 072105 (2013).
- ³ J. Son, V. Chobpattana, B.M. McSkimming, and S. Stemmer, Appl. Phys. Lett. **101**, 102905 (2012).
- ⁴ J.P. Ibbetson, P.T. Fini, K.D. Ness, S.P. DenBaars, J.S. Speck, and U.K. Mishra, Appl. Phys. Lett. **77**, 250 (2000).
- ⁵ S. Yang, Z. Tang, K. Wong, Y. Lin, C. Liu, Y. Lu, S. Huang, and K.J. Chen, IEEE Electron Device Lett. **34**, 1497 (2013).

- ⁶ H.A. Shih, M. Kudo, and T. Suzuki, Appl. Phys. Lett. **101**, 043501 (2012).
- ⁷ R.M. Wallace, ECS Trans. **16**, 255 (2008).
- ⁸ X. Qin, A. Lucero, A. Azcatl, J. Kim, and R.M. Wallace, Appl. Phys. Lett. **105**, 011602 (2014).
- ⁹ S. Ruvimov, Z. Liliental-Weber, J. Washburn, K.J. Duxstad, E.E. Haller, Z.-F. Fan, S.N. Mohammad, W. Kim, A.E. Botchkarev, and H. Morkoç, Appl. Phys. Lett. **69**, 1556 (1996).
- ¹⁰ X. Qin, H. Dong, B. Brennan, A. Azcatl, J. Kim, and R.M. Wallace, Appl. Phys. Lett. **103**, 221604 (2013).
- ¹¹ X. Qin, B. Brennan, H. Dong, J. Kim, C.L. Hinkle, and R.M. Wallace, J. Appl. Phys. **113**, 244102 (2013).
- ¹² B. Brennan, X. Qin, H. Dong, J. Kim, and R.M. Wallace, Appl. Phys. Lett. **101**, 211604 (2012).
- ¹³ S. Miyazaki, J. Vac. Sci. Technol. B Microelectron. Nanom. Struct. **19**, 2212 (2001).
- ¹⁴ F. Bell and L. Ley, Phys. Rev. B **37**, (1988).
- ¹⁵ T. Hashizume, S. Ootomo, T. Inagaki, and H. Hasegawa, J. Vac. Sci. Technol. B **21**, 1828 (2003).
- ¹⁶ A. Ohta, H. Murakami, S. Higashi, and S. Miyazaki, J. Phys. Conf. Ser. **417**, 012012 (2013).
- ¹⁷ S. McDonnell, B. Brennan, A. Azcatl, N. Lu, H. Dong, C. Buie, J. Kim, C.L. Hinkle, M.J. Kim, and R.M. Wallace, ACS Nano **7**, 10354 (2013).
- ¹⁸ E.A. Kraut, R.W. Grant, J.R. Waldrop, and S.P. Kowalczyk, Phys. Rev. Lett. **44**, 1620 (1980).
- ¹⁹ D. Brunner, H. Angerer, E. Bustarret, F. Freudenberg, R. Höpler, R. Dimitrov, O. Ambacher, and M. Stutzmann, J. Appl. Phys. **82**, 5090 (1997).
- ²⁰ B.S. Eller, J. Yang, and R.J. Nemanich, J. Vac. Sci. Technol. A **31**, 050807 (2013).
- ²¹ J.C. Carrano, T. Li, P. a. Grudowski, C.J. Eiting, R.D. Dupuis, and J.C. Campbell, Appl. Phys. Lett. **72**, 542 (1998).
- ²² E.J. Miller, X.Z. Dang, and E.T. Yu, J. Appl. Phys. **88**, 5951 (2000).
- ²³ M. Ľapajna, M. Jurkovič, L. Válik, Š. Haščík, D. Gregušová, F. Brunner, E.-M. Cho, T. Hashizume, and J. Kuzmík, J. Appl. Phys. **116**, 104501 (2014).
- ²⁴ Z. Yatabe, Y. Hori, W. Ma, J.T. Asubar, M. Akazawa, T. Sato, and T. Hashizume, Jpn. J. Appl. Phys. **53**, 100213 (2014).

- ²⁵ G.D. Wilk, R.M. Wallace, and J.M. Anthony, J. Appl. Phys. **89**, 5243 (2001).
- ²⁶ M. Ľapajna and J. Kuzmík, Appl. Phys. Lett. **100**, 113509 (2012).
- ²⁷ Y. Zhang, M. Sun, S.J. Joglekar, T. Fujishima, and T. Palacios, Appl. Phys. Lett. **103**, 033524 (2013).
- ²⁸ J. Robertson and B. Falabretti, J. Appl. Phys. **100**, 014111 (2006).
- ²⁹ O. Ambacher, J. Smart, J.R. Shealy, N.G. Weimann, K. Chu, and M. Murphy, J. Appl. Phys. **85**, 3222 (1999).
- ³⁰ G. Dingemans, N.M. Terlinden, M.A. Verheijen, M.C.M. van de Sanden, and W.M.M. Kessels, J. Appl. Phys. **110**, 093715 (2011).
- ³¹ X. Qin, H. Dong, J. Kim, and R.M. Wallace, Appl. Phys. Lett. In press (2014).

CHAPTER 4

Impact of N₂ and Forming Gas Plasma Exposure on the Growth and Interfacial Characteristics of Al₂O₃ on AlGaN

4.1 Preface

In Chapters 1 and 2, a slow initial nucleation process is demonstrated using *in situ* x-ray photoelectron spectroscopy (XPS) characterization for atomic layer deposition (ALD) of Al₂O₃ or HfO₂. The device results in Chapter 3 demonstrate a high density of positive fixed charges and a high density of D_{it} below the conduction band edge. In this chapter, the *in situ* N₂ plasma and forming gas plasma pretreatments are used to clean the surface and improve the nucleation. The interface and ALD of Al₂O₃ on the annealed, N₂ plasma and forming gas (N₂:H₂) exposed Al_{0.25}Ga_{0.75}N surface was studied using *in situ* XPS and low energy ion scattering spectroscopy (LEIS). Exposure of the Al_{0.25}Ga_{0.75}N surface to the plasma treatments is able to remove spurious carbon, and readily facilitate uniform ALD Al₂O₃ nucleation.

The contents of this chapter are adapted with permission from a paper entitled “**Impact of N₂ and forming gas plasma exposure on the growth and interfacial characteristics of Al₂O₃ on AlGaN**” [*Applied Physics Letters*, **103**, 2441604 (2013)]. Copyright [2013], AIP Publishing LLC.

4.2 Introduction

Cleaning of the AlGaN surface prior to dielectric layer deposition is a critical step in device fabrication. In previous studies, it has been shown that ALD Al₂O₃/HfO₂ growth is closely related to the quality of the AlGaN interface.^{1,2} To accomplish this cleaning process, a number of studies have investigated *ex-situ* and *in-situ* methods.^{3, 4} In these methods, annealing in plasma, particularly H₂ and N₂ plasma, has been shown to be more effective at removing surface contamination than traditional wet chemical treatment. Hashizume *et al.* reported that H₂ and N₂ plasma at 280 °C is effective at removing oxygen and carbon from the AlGaN surface.⁵ Recently,

Meunier *et al.* also reported the cleaning effect of N₂ and forming gas (FG) plasma.⁶ Similar studies on AlGa_{0.25}N and GaN devices by Romero *et al.* demonstrated that *in situ* N₂ plasma pretreatment reduces current-collapse and gate-lag effects.^{7,8} However, the chemical interactions that take place between AlGa_{0.25}N treated by *in situ* N₂ or FG plasma and a gate oxide layer are still not clear.

This study examines the effect of plasma surface treatments prior to deposition of Al₂O₃ by ALD on ultra-high vacuum (UHV)-annealed, N₂ plasma-exposed and FG plasma-exposed Al_{0.25}Ga_{0.75}N surfaces with *in situ* monochromatic XPS and LEIS to monitor the AlGa_{0.25}N/Al₂O₃ interface and Al₂O₃ growth.

4.3 Experimental

Six undoped Al_{0.25}Ga_{0.75}N samples (30 nm), grown on a 1.2 μm GaN layer on a p-type Si(111) substrate by metal organic chemical vapor deposition, obtained from DOWA Electronics Materials (see Figure 1.1 (b)), were first solvent cleaned in acetone, methanol and isopropanol for one minute each. Then three sample plates, each with two samples mounted, were introduced to the UHV cluster system described in Chapter 1. The apparatus enables the study of *in situ* surface treatments, thin film depositions, and surface characterization without spurious surface contamination.

The first group of samples was annealed in a UHV chamber at 300 °C for 30 minutes. The second group of samples was treated by a N₂ plasma at 300 °C for 30 minutes in the same UHV chamber. The third group of samples was exposed to a FG (N₂(90%):H₂(10%)) plasma at 300 °C for 30 minutes also in the same UHV chamber. The N₂ and FG plasmas were excited by 13.56 MHz rf-excitation with the samples were immersed in the plasma during the process. The pressure in the chamber during exposure was 5×10^{-3} mbar (which corresponds to 45 sccm N₂ or 50 sccm FG flow) and the rf- power was maintained at 100 W. XPS was then carried out after UHV-annealing, N₂ plasma exposure or FG plasma exposure on one of two samples on each sample plate. LEIS analysis was carried out on the companion sample, due to the potential surface damage from the 1 keV He⁺ ion bombardment during the LEIS measurement.

The Picosun ALD reactor integrated to the system by a buffer chamber and transfer tube was used for this *in situ* study. Tri-methyl aluminum (TMA) and H₂O were used as the precursors

for Al₂O₃ formation. In this study, one full ALD cycle was 0.1s TMA/N₂ + 4s N₂ purge + 0.1s H₂O/N₂ + 4s N₂ purge. High purity (99.999%) N₂ was used as the precursor carrier and purging gas. The base pressure of the ALD reactor was ~10 mbar and the Al₂O₃ deposition temperature was 300 °C. XPS was carried out on the samples not analyzed by LEIS after 20 full cycles (TMA + H₂O). LEIS was then carried out on the same samples. One further native oxide sample annealed in UHV was similarly prepared with subsequent 25 cycles of ALD Al₂O₃ to compare the coverage of ALD Al₂O₃ of the similar thickness on different treated Al_{0.25}Ga_{0.75}N surfaces.

XPS was carried out using a monochromatic Al K α (h ν = 1486.7 eV) X-ray source, equipped with a 7 channel analyzer, using a pass energy of 15 eV, with all scans taken at 45° with respect to the sample normal. XPS peak deconvolution was carried out using AAnalyzer software with a detailed peak fitting procedure described elsewhere.⁹ All peaks were referenced to the N 1s peak at 397.0 eV to compensate for any variation in the peak core level positions due to band bending or surface charging. The LEIS was carried out using the same 7 channel analyzer as used for the XPS measurements with biasing conditions suitable for ion detection, and He⁺ ions excited by an ISE 100 fine focus ion gun using 1 kV bias and 10 mA emission current.

4.4 Results and Discussion

The N 1s and Ga Auger spectra normalized to the Ga *LMM* feature are shown in Figure 4.1 (a) for UHV-annealed, N₂-plasma and FG plasma-exposed samples. All initial spectra show the N-Ga/Al peaks (set at 397.0 eV)¹⁰, and the Ga *L₂M₄₅M₄₅* Auger feature (spanning ~392-398 eV).¹¹ A small feature at 398.5 eV¹² attributed to CN_x formation is detected after the N₂ plasma-exposure. Similar peaks at 398.5 eV from FG plasma-exposed sample may also be attributed to N-(CH) bond formation.¹² Apart from the feature attributed to CN_x bonding, the N 1s and Ga *LMM* Auger spectra from the N₂ plasma-exposed samples overlap with the normalized spectra from the UHV-annealed sample. Hashizume *et al.* has demonstrated that the H₂ plasma reacts with the surface to result in a decrease of the N 1s peak intensity indicating the formation of a N-vacancy.^{5,13,14} However, no such decrease is detected after FG plasma treatment, suggesting FG plasma treatment suppresses formation of N-vacancies due to the presence of the N₂ plasma. In contrast, a more intense N 1s peak from the FG plasma-exposed sample is detected

likely due to Ga/Al(surface)-NH_x bonding,^{15,16} where the NH_x is formed by the FG plasma itself. After 20 cycles of ALD Al₂O₃, CN_x and C-(NH) bonding is still detected in N₂ plasma-exposed and FG plasma-exposed samples, respectively. The increased Ga/Al-NH_x concentration from the FG plasma-exposed sample disappears after 20 cycles of ALD Al₂O₃ likely due to the reaction with ALD precursors.

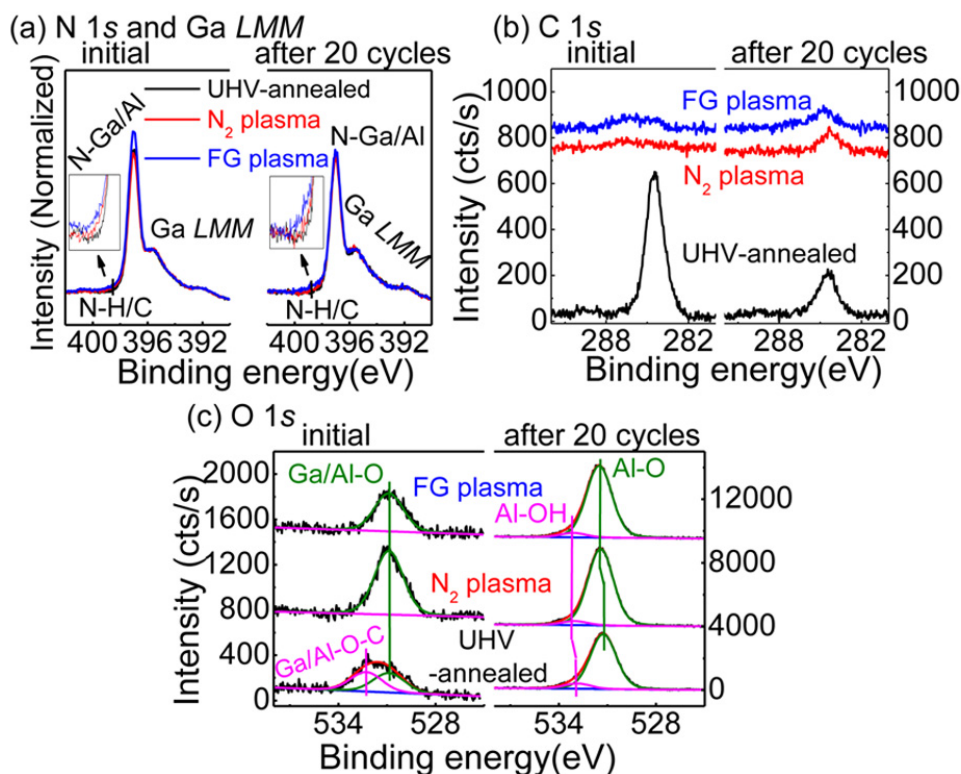


Figure 0.1. (a) N 1s and Ga *LMM* spectra normalized by Ga *LMM* peaks (b) C 1s spectra and (c) O 1s spectra from the UHV-annealed, N₂ plasma-exposed and FG plasma-exposed surface from initial surface and after 20 cycles ALD Al₂O₃.

The C 1s spectra from UHV-annealed, N₂ plasma-exposed and FG plasma-exposed samples are shown in Figure 4.1 (b). Low intensity C1s peaks at 286 eV corresponding to C-(NH)/CN_x,¹⁷ near XPS detection limits, is detected after the plasma treatments. The high efficiency of the N₂ plasma for breaking organic bonds has been widely reported.^{5,18,19} After N₂ or FG plasma treatment, the absolute intensities of N 1s, Ga 2p_{3/2} and Al 2p all increase, suggesting the original carbon is at the top surface of the Al_{0.25}Ga_{0.75}N layer. An obvious C 1s signal is detected from the

UHV-annealed sample. No evidence of carbide formation (e.g. Al/Ga-C (~282eV) or Al/Ga-CH₃ (~283eV)) is observed.^{20,21} In addition, the high bond dissociation energy of Al-O (542 kJ/mol)²² and Ga-O (349±42 kJ/mol)²² also suggests that Al-O and Ga-O bonds are energetically preferable at the Al_{0.25}Ga_{0.75}N surface. The carbon coverage Θ_C can be calculated from the XPS peak intensity as equation (4.1) shows.²³ (The oxygen coverage Θ_O is also calculated by this method)

$$\Theta_C = \left(\frac{I_C}{S_C} \right) / \left\{ \frac{I_{Ga}}{S_{Ga} \times \sum_{n=0}^{\infty} \exp\left[\frac{-nd_{AlGa}N}{\lambda_{Ga} \cos(\theta)}\right]} + \frac{I_{Al}}{S_{Al} \times \sum_{n=0}^{\infty} \exp\left[\frac{-nd_{AlGa}N}{\lambda_{Al} \cos(\theta)}\right]} \right\} \quad (4.1)$$

where Θ_C is the coverage of the number of carbon atoms divided by the number of Ga and Al atoms. I_C , I_{Ga} , and I_{Al} are the peak fitted areas from the C 1s, Ga 3d and Al 2p spectra, and S_C , S_{Ga} , S_{Al} are the atomic sensitivity factors for C 1s, Ga 3d and Al 2p.²⁴ The inelastic mean free path of Ga 3d and Al 2p in Al_{0.25}Ga_{0.75}N are noted as λ_{Ga} and λ_{Al} .²⁵ θ (the angle between the normal direction and the detector) is 45° in this study, and $d_{AlGa}N$ (the distance between two Ga/Al planes) is 0.26 nm. Because the exponential function decreases quickly, the infinite limit is replaced by 40 layers in this study, as greater than 99.9% of Al 2p and Ga 3d XPS signal comes from the first 40 layers. The coverage of oxygen (Θ_O) is calculated by the revised equation (4.1) where $\frac{I_C}{S_C}$ is replaced by $\frac{I_O}{S_O}$.

Θ_C values for the UHV-annealed, N₂ plasma-exposed and FG plasma-exposed samples are ~1.2±0.2 ML, ~0.1 ML and ~0.1 ML respectively. 1 ML is ~5.75×10¹⁴ atoms/cm² for Al_{0.25}Ga_{0.75}N (0001) structure. Figure 4.1 (b) also shows C 1s spectra after 20 cycles of ALD Al₂O₃. An additional carbon concentration (< 0.2 ML) is detected after 20 cycles Al₂O₃ from N₂ plasma-exposed and FG plasma-exposed samples, suggesting that the reaction between TMA and H₂O precursor is almost complete. It also found that the C 1s peak from the UHV-annealed sample after the same ALD process originates almost entirely from the Al_{0.25}Ga_{0.75}N surface. Therefore the pretreatment is highly important to determine the final concentration of carbon contamination at the AlGaN/Al₂O₃ interface. Since carbon contamination at the surface of the AlGaN, in particular organic species, is a significant factor in the magnitude of the current collapse,²⁶ the removal of such carbon by plasma treatments has potential to improve device performance.

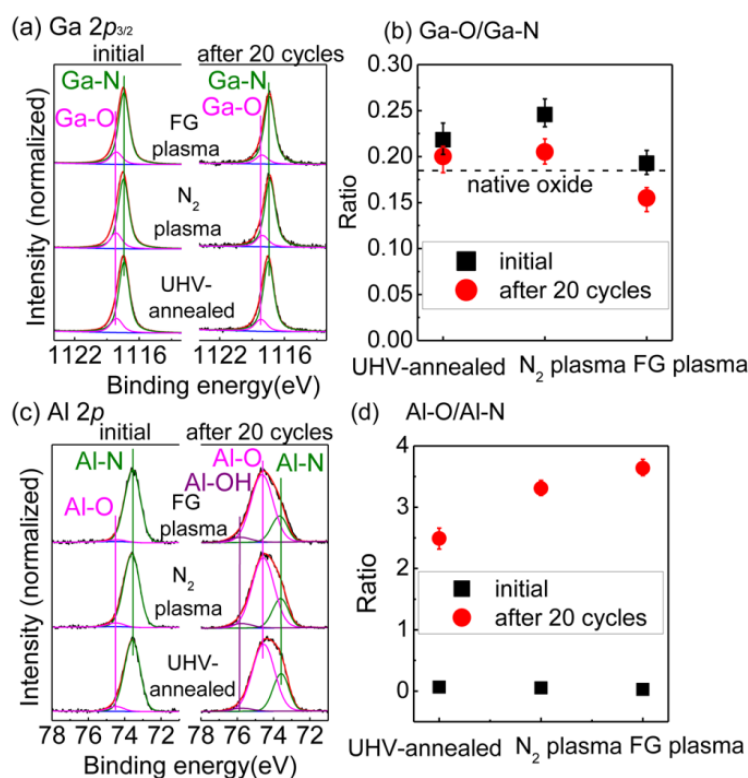


Figure 0.2. Fitting XPS spectra of the normalized (a) Ga $2p_{3/2}$ and (c) Al $2p$ from the UHV-annealed, N₂ plasma-exposed and FG plasma-exposed surface, from the initial surface and after 20 ALD cycles Al₂O₃. Figure 4.2 (b) and (d) show the ratio Ga-O/Ga-N and Al-O/Al-N respectively.

As shown in Figure 4.1 (c), only a single O1s peak (FWHM = 1.8 eV) could be detected from the N₂ plasma-exposed and FG plasma-exposed samples corresponding to Ga/Al-O formation.²⁷ However, except for Ga/Al-O bonding detected at 531 eV, the O 1s peak from UHV-annealed sample shows another chemical state at 532.2 eV, which is attributed to C-O and/or Ga/Al-O-C bonding.²⁸ This is also consistent with the C 1s spectra in Figure 4.1 (b). Although the absolute area of the O 1s peak from the N₂ plasma-exposed sample is somewhat greater than from the UHV-annealed sample, this does not necessarily indicate that a higher concentration of oxygen is detected, as the removal of ~ 1 ML carbon will result in an increase of the O 1s signal. This also supports the hypothesis that carbon is on the surface of the Al_{0.25}Ga_{0.75}N after annealing. Θ_o values for the UHV-annealed, N₂ plasma-exposed and FG

plasma-exposed samples are ~ 0.45 ML, ~ 0.45 ML and ~ 0.35 ML respectively, indicating that the presence of H_2 in the FG plasma results in the lowest concentration of oxygen on the surface. After 20 cycles of ALD Al_2O_3 , Al-O (~ 531.4 eV) and Al-OH bonds (~ 532.8 eV) are detected from all samples, which are also observed in a previous “half cycle” study.¹ The small variation (0.25 eV) between UHV-annealed sample and plasma treated samples is likely due to surface change or band bending after 20 cycles of ALD Al_2O_3 .

The normalized peak-fitted Ga $2p_{3/2}$ spectra are shown in Figure 4.2 (a). All Ga $2p_{3/2}$ spectra show two peaks, indicative of Ga-N substrate bonding and the presence of Ga_2O_3 , separated from the bulk peak by 0.68 eV (fixed in the fitting process).⁹ Based on our prior work carefully assigning chemical states,^{29–31} there the Ga^{1+} state appears to be below the level of detection. No evidence of metal bond formation is detected from the FG plasma-exposed sample, which would be expected with N-vacancy formation resulting from H_2 plasma exposure.¹⁴ The ratio of Ga-O/Ga-N is plotted in Figure 4.2(b). The calculation of error bars is based on fitting procedure and consistent with our previous reports.^{2,32} (The error in the Al $2p$ peak areas is also addressed in this way.) A larger Ga-O concentration is detected from the UHV-annealed and N_2 plasma-exposed samples compared to a native oxide sample without any pretreatment in Figure 4.2 (b), due to the transfer of oxygen from C-O and N-O to Ga-O during the annealing process.^{1,2} However, the Ga-O/Ga-N ratio from the FG plasma-exposed sample is equal to the ratio from native oxide sample. This indicates that FG plasma suppresses the formation of Ga-O during annealing, but does not decrease the ratio or break the strong Ga-O bond at this temperature. This result is also consistent with the Θ_O values. After 20 cycles of ALD Al_2O_3 , a slight decrease in Ga-O concentration is detected suggesting a “clean up” effect^{31,33} most likely due to the formation of a Ga-O-Al environment after ALD Al_2O_3 . After considering the stability of Ga_2O_3 on $Al_{0.25}Ga_{0.75}N$, we can assume that the removal of native oxide by the ALD precursors known as “clean up” effect^{31,33} is difficult on the $Al_{0.25}Ga_{0.75}N$ surface. In all Ga $2p_{3/2}$ spectra fitting, in order to maintain consistency the Gaussian width, Lorentz width and separation value of binding energy between Ga-N and oxide chemical state are fixed. All of these parameters are based on the initial surfaces in Chapters 1 and 2. However, the real separation value after 20 cycles of ALD Al_2O_3 may be smaller than at the initial surfaces due to the formation of Ga-O-Al bonds

with the lower binding energy than Ga_2O_3 at the initial surfaces.^{34,35} While the fitting of Ga $2p_{3/2}$ after 20 cycles of ALD Al_2O_3 are still based on the separation value from initial surface, it will result in a spurious intensity decrease of oxide peaks if Ga-O-Al is formatted as expected. Therefore, the “decrease” reflects the formation of Ga-O-Al. And the smaller “decrease” after 20 cycles of ALD Al_2O_3 from the UHV-annealed sample indicates the diminished formation of Ga-O-Al bonds than for the N_2 plasma-exposed and FG plasma-exposed sample.

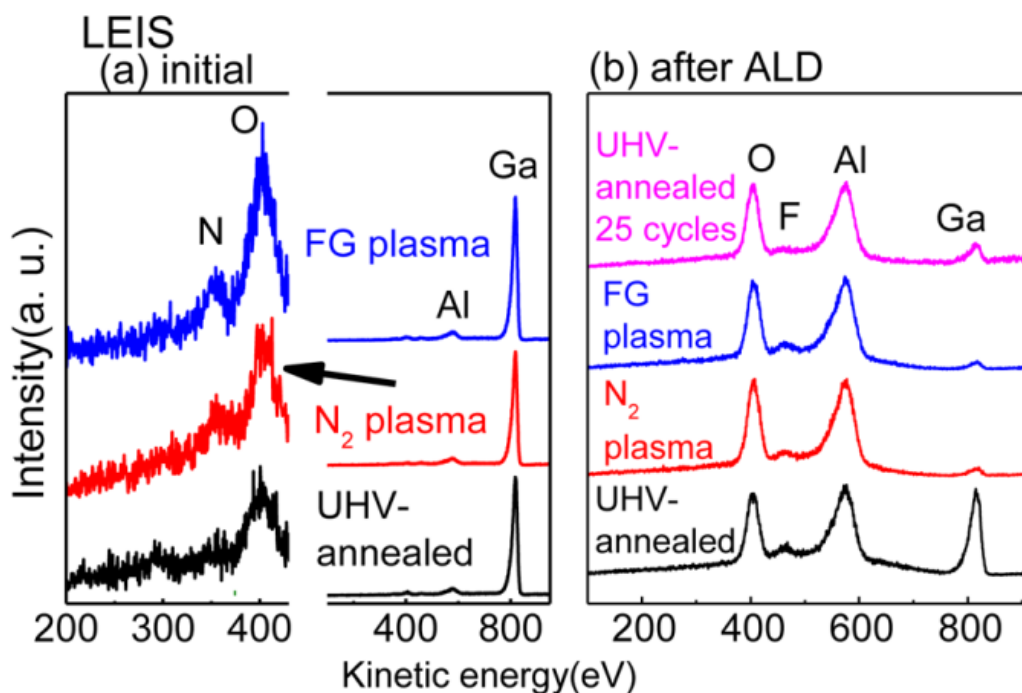


Figure 0.3. LEIS spectra from the UHV-annealed, N_2 plasma-exposed and FG plasma-exposed surface from (a) initial surface and (b) after 20 or 25 cycles ALD Al_2O_3 .

The normalized peak fitted Al $2p$ spectra are shown in Figure 4.2 (c). A small feature attributed to Al_2O_3 formation at 74.4 eV is close to XPS detection limits. An intense Al-N bulk peak at 73.5 eV is detected from all samples,^{1,2} and the ratio of Al-O/Al-N in Figure 4.2 (d) is $\sim 5\%$ from all initial samples. Due to a high bond dissociation energy anticipated for Al-O (542 kJ/mol),²² no change is detected after N_2 plasma or FG plasma treatments. After 20 cycles of ALD Al_2O_3 , intense Al-O peaks at 74.4 eV and Al-OH peaks at 75.3 eV are detected. The intensity ratio of Al-O (Al_2O_3) / Al-N ($\text{Al}_{0.25}\text{Ga}_{0.75}\text{N}$) is plotted in Figure 4.2 (d). It is noted that

the ratio from the UHV-annealed sample is significantly lower than that from the N₂ plasma-exposed and FG plasma-exposed samples, indicating that N₂ plasma or FG plasma treatments accelerate nucleation of ALD Al₂O₃ on Al_{0.25}Ga_{0.75}N.

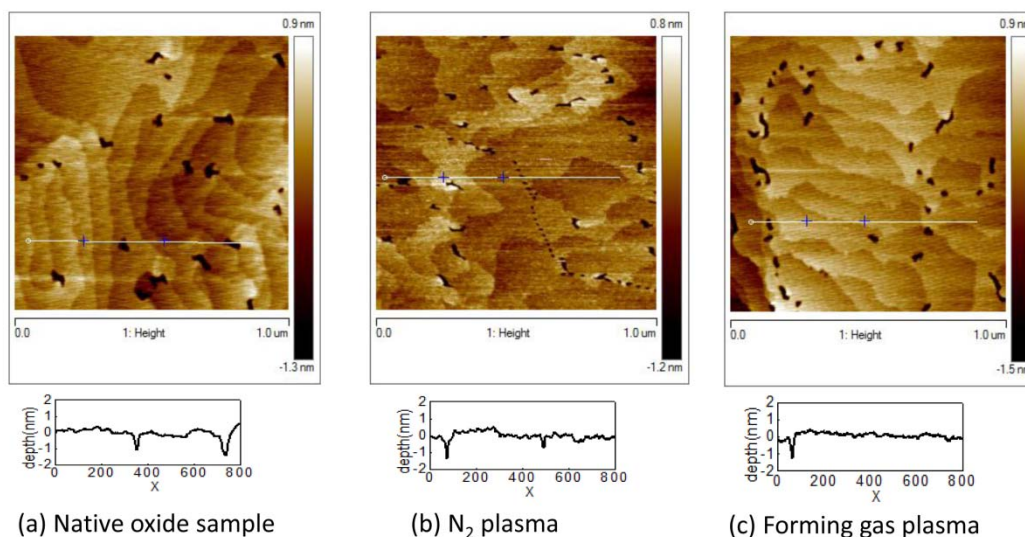


Figure 0.4. AFM picture from (a) native oxide, (b) N₂ plasma-exposed and (c) FG plasma-exposed AlGaIn surface.

In order to further study the nucleation process, LEIS is carried out, which is sensitive to only the first atomic layer of the surface.³⁶ The LEIS spectra are shown in Figure 4.3 (a) for UHV-annealed, N₂ plasma-exposed, and FG plasma-exposed samples. The elemental composition is determined by elastic collision principles.³⁷ The first layer is occupied mainly by Ga (818 eV) and Al (578 eV) atoms for the three surfaces, agreeing with the metal face of Al_{0.25}Ga_{0.75}N. In addition, small O peaks (403 eV) are observed, however it is difficult to detect C due to its low scattering cross section (carbon sensitivity = 1/3 × oxygen sensitivity).³⁸ After the FG plasma treatment, an obvious N peak at 355 eV could be detected, which is much lower on the other samples, and is consistent with the elevated N 1s peak intensity for the same sample in Figure 4.1 (a).

LEIS after 20 of ALD cycles of Al₂O₃ and 25 of cycles of Al₂O₃ on another UHV-annealed sample are shown in Figure 4.3 (b), with Al and O peaks from the Al₂O₃ film clearly detected. A small F peak from originating from the ALD process is detected in the LEIS and attributed to a

decomposition of the reactor elastomer seals. The concentration of F is below XPS detection limits and does not affect the discussion here. After 20 cycles of ALD Al_2O_3 , an intense Ga peak is detected on the UHV-annealed sample, while the signal was much lower on the other two samples. This indicates that the coverage of Al_2O_3 on the N_2 plasma and FG plasma-treated sample is greater than on UHV-annealed sample. Assuming an Al_2O_3 density of 3.5 g/cm^3 ,³⁹ the thickness of the Al_2O_3 thin film based on Ga $2p_{3/2}$ peaks ratios¹ can be estimated. After 20 cycles of Al_2O_3 , a thickness of 1.10 nm, 1.46 nm and 1.50 nm of Al_2O_3 is deposited on UHV-annealed, N_2 plasma-exposed and FG plasma-exposed samples, respectively.

The thicker Al_2O_3 layer on N_2 -exposed and FG plasma-exposed samples is strong evidence that the N_2 plasma and FG plasma treatments both enhance the nucleation of Al_2O_3 . The thickness of 25 cycles of ALD Al_2O_3 on another UHV-annealed sample is about 1.54 nm, which is thicker than 20 cycles of Al_2O_3 ALD on N_2 plasma-exposed and FG plasma-exposed samples. However the Ga peak from LEIS in Figure 4.3 (b) is still ~ 3 times greater than from the plasma treated samples, indicating that the ALD Al_2O_3 film on the UHV-annealed sample is not as uniform as on the N_2 plasma-exposed/FG plasma-exposed samples. We note that *ex situ* AFM measurements as Figure 4.4 shows could not detect the change in the ALD Al_2O_3 coverage due to extensive steps at the $\text{Al}_{0.25}\text{Ga}_{0.75}\text{N}$ surface.¹ The marked difference between the UHV-annealed sample and the N_2 plasma-exposed and FG plasma-exposed samples is the removal of carbon. Carbon is likely to saturate oxygen dangling bonds, the nucleation center,³¹ at the surface of UHV-annealed samples by generating Ga/Al-O-C and C-C bonds, which do not allow for reaction of either TMA or H_2O .⁴⁰ In contrast the removal of the carbon passivation layer by N_2 and FG plasma treatments results in the faster nucleation, which is expected to improve the quality of the ALD Al_2O_3 film.⁴¹ The trend of the “decrease” of Ga-O after ALD Al_2O_3 also shows the removal of carbon provides more nucleation sites for formation of Ga-O-Al bond.

4.5 Conclusion

In conclusion, the initial interface and Al_2O_3 growth on UHV-annealed, N_2 plasma treated and FG plasma treated $\text{Al}_{0.25}\text{Ga}_{0.75}\text{N}$ surfaces were investigated by *in situ* XPS and LEIS. Results suggest that the N_2 plasma and forming gas plasma both facilitate removal of carbon contamination, while FG plasma suppresses formation of oxide in the annealing process. The

removal of the carbon passivation layer by N₂ and FG plasma pretreatment enhances nucleation of ALD Al₂O₃.

4.6 References

- ¹ B. Brennan, X. Qin, H. Dong, J. Kim, and R.M. Wallace, *Appl. Phys. Lett.* **101**, 211604 (2012).
- ² X. Qin, B. Brennan, H. Dong, J. Kim, C.L. Hinkle, and R.M. Wallace, *J. Appl. Phys.* **113**, 244102 (2013).
- ³ R.D. Long and P.C. McIntyre, *Materials (Basel)*. **5**, 1297 (2012).
- ⁴ B.S. Eller, J. Yang, and R.J. Nemanich, *J. Vac. Sci. Technol. A* **31**, 050807 (2013).
- ⁵ T. Hashizume, S. Ootomo, T. Inagaki, and H. Hasegawa, *J. Vac. Sci. Technol. B* **21**, 1828 (2003).
- ⁶ R. Meunier, A. Torres, and M. Charles, *ECS Trans.* **50**, 451 (2013).
- ⁷ F. Romero, M. A. Jiménez, A.F. Braña, F. González-Posada, R. Cuervo, F. Calle, and E. Muñoz, *IEEE Electron Device Lett.* **29**, 209 (2008).
- ⁸ M. Romero, A. Jiménez, F. González-Posada, S. Martín-Horcajo, F. Calle, and E. Muñoz, *IEEE Trans. Electron Devices* **59**, 374 (2012).
- ⁹ B. Brennan and G. Hughes, *J. Appl. Phys.* **108**, 053516 (2010).
- ¹⁰ F. González-Posada, J. a. Bardwell, S. Moisa, S. Haffouz, H. Tang, A.F. Braña, and E. Muñoz, *Appl. Surf. Sci.* **253**, 6185 (2007).
- ¹¹ E. Antonides, E. Janse, and G. Sawatzky, *Phys. Rev. B* **15**, (1977).
- ¹² M. Tabbal, P. Mérel, S. Moisa, M. Chaker, E. Gat, a. Ricard, M. Moisan, and S. Gujrathi, *Surf. Coatings Technol.* **98**, 1092 (1998).
- ¹³ T. Hashizume and H. Hasegawa, *Appl. Surf. Sci.* **234**, 387 (2004).
- ¹⁴ T. Hashizume and R. Nakasaki, *Appl. Phys. Lett.* **80**, 4564 (2002).
- ¹⁵ M.A. Centeno, S. Delsarte, and P. Grange, *J. Phys. Chem. B* **103**, 7214 (1999).
- ¹⁶ D. Paget, V.L. Berkovits, V.P. Ulin, F. Ozanam, P. Dumas, S. Kubsy, K. Lahlil, L. Bideux, and G. Monier, *J. Electrochem. Soc.* **160**, H229 (2013).
- ¹⁷ E. Ech-chamikh, a. Essafti, Y. Ijdiyaou, and M. Azizan, *Sol. Energy Mater. Sol. Cells* **90**, 1420 (2006).
- ¹⁸ A. Callegari, P.D. Hoh, D. a. Buchanan, and D. Lacey, *Appl. Phys. Lett.* **54**, 332 (1989).

- ¹⁹ C. Schulz, S. Kuhr, H. Geffers, T. Schmidt, J.I. Flege, T. Aschenbrenner, D. Hommel, and J. Falta, *J. Vac. Sci. Technol. A* **29**, 011013 (2011).
- ²⁰ S.L. Peczonczyk, J. Mukherjee, A.I. Carim, and S. Maldonado, *Langmuir* **28**, 4672 (2012).
- ²¹ J. Mukherjee, S. Peczonczyk, and S. Maldonado, *Langmuir* **26**, 10890 (2010).
- ²² Y. Luo, *Comprehensive Handbook of Chemical Bond Energies* (CRC Press, Boca Raton, FL, 2010).
- ²³ V.M. Bermudez, *J. Appl. Phys.* **80**, 1190 (1996).
- ²⁴ F. Moulder, J. F. Stickle, W. E. Sobol, P. and D. Bomben, K, *Handbook of X-Ray Photoelectron Spectroscopy* (Perkin-Elmer Corp, Minnesota, 1992).
- ²⁵ C. Powell and M. Seah, *J. Vac. Sci. Technol. A* **8**, 735 (1990).
- ²⁶ J.A. Bardwell, S. Haffouz, W.R. McKinnon, C. Storey, H. Tang, G.I. Sproule, D. Roth, and R. Wang, *Electrochem. Solid-State Lett.* **10**, H46 (2007).
- ²⁷ H.W. Jang, J.M. Baik, M.-K. Lee, H.-J. Shin, and J.-L. Lee, *J. Electrochem. Soc.* **151**, G536 (2004).
- ²⁸ M.S. Lim, K. Feng, X. Chen, N. Wu, A. Raman, J. Nightingale, E.S. Gawalt, D. Korakakis, L. a Hornak, and A.T. Timperman, *Langmuir* **23**, 2444 (2007).
- ²⁹ C.L. Hinkle, E.M. Vogel, P.D. Ye, and R.M. Wallace, *Curr. Opin. Solid State Mater. Sci.* **15**, 188 (2011).
- ³⁰ B. Brennan, M. Milojevic, H.C. Kim, P.K. Hurley, J. Kim, G. Hughes, and R.M. Wallace, *Electrochem. Solid-State Lett.* **12**, H205 (2009).
- ³¹ M. Milojevic, F.S. Aguirre-Tostado, C.L. Hinkle, H.C. Kim, E.M. Vogel, J. Kim, and R.M. Wallace, *Appl. Phys. Lett.* **93**, 202902 (2008).
- ³² H. Dong, B. Brennan, D. Zhernokletov, J. Kim, C.L. Hinkle, and R.M. Wallace, *Appl. Phys. Lett.* **102**, 171602 (2013).
- ³³ R.M. Wallace, *ECS Trans.* **16**, 255 (2008).
- ³⁴ S. Ingrey, *J. Vac. Sci. Technol. A Vacuum, Surfaces, Film.* **4**, 984 (1986).
- ³⁵ F.S. Aguirre-Tostado, M. Milojevic, B. Lee, J. Kim, and R.M. Wallace, *Appl. Phys. Lett.* **93**, 172907 (2008).
- ³⁶ F. Zhang, B. King, and D. O'connor, *Phys. Rev. Lett.* **75**, 4646 (1995).

- ³⁷ D.P. Smith, J. Appl. Phys. **38**, 340 (1967).
- ³⁸ H. Niehus and R. Spitzl, Surf. Interface Anal. **17**, 287 (1991).
- ³⁹ A.W. Ott, J.W. Klaus, J.M. Johnson, and S.M. George, Thin Solid Films **292**, 135 (1997).
- ⁴⁰ P. Sivasubramani, T.J. Park, B.E. Coss, A. Lucero, J. Huang, B. Brennan, Y. Cao, D. Jena, H.G. Xing, R.M. Wallace, and J. Kim, Phys. Status Solidi - Rapid Res. Lett. **6**, 22 (2012).
- ⁴¹ S.M. George, Chem. Rev. **110**, 111 (2010).

CHAPTER 5

In Situ X-Ray Photoelectron Spectroscopy and Capacitance Voltage Characterization of Plasma Treatments for Al₂O₃/ AlGaN/ GaN

5.1 Preface

In the previous chapters, we focus on the impact of N₂ and forming gas plasma pretreatments on device performances. As Chapter 4 shows, the *in situ* N₂ and forming plasma is effective for the removal of carbon contamination and improvement of initial nucleation. We investigate the Al₂O₃/AlGaN/GaN metal-oxide-semiconductor structure pretreated by O₂ anneals, N₂ remote plasma and forming gas remote plasma prior to atomic layer deposition of Al₂O₃ using *in situ* X-ray photoelectron spectroscopy (XPS), low energy electron diffraction (LEED) and capacitance- voltage (C-V) measurements. Plasma pretreatments reduce the Ga-oxide/oxy-nitride formation and the interface state density, while inducing a threshold voltage instability.

The contents of this chapter are adapted with permission from a paper entitled “**In situ x-ray photoelectron spectroscopy and capacitance voltage characterization of plasma treatments for Al₂O₃/ AlGaN/ GaN stacks**” [*Applied Physics Letters*, **105**, 011602 (2014)]. Copyright [2014], AIP Publishing LLC.

5.2 Introduction

In metal oxide semiconductor AlGaN/GaN high electron mobility transistors (MOSHEMTs), the interface between the high k oxide dielectric layer and AlGaN is related to device performance, such as threshold voltage¹ and radio frequency performance.² Some papers have reported that the formation of Ga-oxide/oxy-nitride at the GaN-*capped* Al₂O₃/GaN/AlGaN/GaN interface contributes a high density of interface trap states (D_{it}) and a significant voltage shift for MOSHEMTs.^{3,4} However systematic work to clarify the impact of Ga-oxide/oxy-nitride on *uncapped* Al₂O₃/AlGaN/GaN MOSHEMTs is needed. In particular, the reactivity of GaN *capped* surface and exposed AlGaN is very different (e.g. a higher oxide or oxy-nitride concentration on the thin GaN capped surface is observed⁵). Plasma pretreatments, especially plasma nitridation,

has been an important method to improve the interface quality prior to the gate dielectric deposition by removing surface contamination and reducing the native oxide in the AlGaIn/GaN MOSHEMTs.^{3,6} We have recently reported the impact of N₂ plasma and forming gas (FG) plasma on the resultant interfacial chemistry for atomic layer deposition (ALD) Al₂O₃ growth on *uncapped* AlGaIn/GaN (Chapter 4).⁷ However, whether the plasma treatments result in device degradation is still unclear. In this study, we use C-V measurements and *in situ* XPS to reveal the impact of oxide, N₂ and FG plasma pretreatments on the ALD- Al₂O₃/AlGaIn interface.

5.3 Experimental

Metal organic chemical vapor deposited Al_{0.25}Ga_{0.75}N (30 nm)/ GaN (1.2 μm) layer on a p-type Si(111) substrate HEMTs wafers obtained from DOWA Electronics Materials (Tokyo, Japan) were used in this study (see Figure 1.1 (b)). Four samples (~ 1 × 1 cm²) from the same wafer were first solvent cleaned in acetone, methanol and isopropanol for one minute each to remove organic contamination. In order to avoid both the contamination from the photolithography process and a possible increase of oxide originating from the ohmic contact annealing step, a dielectric “first” process was used. Sample “A” consisted of a native oxide AlGaIn/GaN/Si control sample and sample “B” was *ex situ* annealed at 500 °C with 2000 standard cm³/min (sccm) O₂ gas flow for 5min. Subsequently, 100 cycles of ALD Al₂O₃ (~10 nm) was deposited in a Picosun ALD reactor integrated to an *in situ* ultra- high vacuum (UHV) tool described in Chapter 1 and elsewhere.⁸ In contrast, sample “C” was treated with an *in situ* remote N₂ plasma at 300 °C for 30 minutes in a connected chamber in the UHV tool, while sample “D” was similarly exposed to a forming gas (FG: (N₂(90%):H₂(10%)) remote plasma at 300 °C for 30 minutes, also in the same chamber. The plasma processes’ parameters and details have been described in our previous report (Ref. ⁷). Samples C and D were then transferred to the Picosun ALD chamber through a transfer tube (1×10⁻¹¹ mbar) followed again by a 100 cycles (~10nm) of Al₂O₃. All ALD was performed in the attached Picosun ALD reactor used the same parameters as described in the reference ⁷.

The ohmic contact regions were defined by a standard photolithography and contact windows were opened by 20s BCl₃ (15 sccm)/Ar (5 sccm) reactive ion etching (RIE). Then

ohmic contacts (resistivity $\sim 1 \times 10^{-6} \Omega \cdot \text{cm}^2$) were formed by e-beam evaporation deposition (base pressure $\sim 1 \times 10^{-6}$ mbar) of Ti/Al/Ni/Au followed by rapid thermal annealing at 850 °C for 30 s with 2000 SCCM N₂ after patterning by lift off. Circular gate electrodes were defined by standard photolithography, followed by the e-beam deposition of Ni/Au and lift off. C-V measurements were performed by an Agilent 4284A LCR meter with a step size of 0.02 V and an AC magnitude of 50 mV.

In situ XPS and LEED were also performed on all samples. The XPS uses a monochromatic Al K α ($h\nu = 1486.7$ eV) X-ray source, equipped with a 7 channel analyzer, using a pass energy of 15 eV, with all scans taken at 45° with respect to the sample normal. In addition, XPS was performed on a native AlGa_N sample and a native AlGa_N sample with 20 cycles of ALD Al₂O₃ before and after the 850°C ohmic annealing to observe the impact of the rapid thermal annealing process.

5.4 Results and Discussion

Figure 5.1(a) shows that the *in situ* Ga 2p_{3/2} spectra after 20 cycles of Al₂O₃. The impact of N₂ and FG plasma pretreatments has been described in our previous paper.⁷ The N₂ and FG plasma pretreatments are effective in removing the most carbon contamination, while the FG plasma avoids increasing the surface oxide concentration,⁷ as the Ga-O/Ga-N area ratio values in Table 7.1 indicates. The 500 °C O₂ annealing generated more Ga-O bonding as expected. Since the Ga-N bonding in AlGa_N has a similar binding energy to that of the Ga₂O bonding (1117.55 eV), as seen on GaAs and InGaAs samples,⁹ the unique assignment of the Ga¹⁺ chemical state is complicated. In contrast, the increase of Ga³⁺ at 1118.2 eV from sample B is obvious. Similarly, it is also complicated to deconvolve Ga-ON bonding from Ga 2p_{3/2} peak, however evidence for Ga-ON bonding can be extracted from the N 1s spectra, where the binding energy is ~ 1 eV higher than Ga-N.¹⁰ In order to avoid the possible error from small Ga LMM peak at 398 eV¹¹ overlapping with Ga-ON, the normalized spectra to the Ga LMM feature are used. A small feature at ~ 398 eV in Figure 5.1 (b) attributed to Ga-ON formation is detected from sample B. The N 1s and Ga LMM spectra from samples C and D have been discussed in reference ⁷. The oxide/oxynitride thickness from sample B is ~ 0.2 nm calculated by the N 1s ratio¹¹ before and after the O₂ annealing. The Ga 2p_{3/2} spectra before and after the 850°C N₂ annealing are shown

in Figure 5.1 (c) to evaluate the impact of the rapid annealing for ohmic contacts. For the native AlGa_N sample, the rapid annealing process results in more Ga-oxide formation, even with the 2000 sccm N₂ flow. The top ALD Al₂O₃ (~ 2nm) layer inhibits the oxidation of AlGa_N as the Ga-O/GaN intensity ratio (“R”) shown in Figure 5.1 (c). This is one of reasons a dielectric gate first fabrication process is employed here.

Table 0.1. Summary of sample pretreatments, observed threshold voltage, voltage shifts and Ga-O(N) relative concentration.

Samples	Pretreatments	V _{TH} (V)	ΔV ₁ (V)	ΔV ₂ (V)	Ga-O(N)/Ga-N
A	Native oxide	-10.5	0	0.13	8.7%
B	O ₂ annealed	-7.2	0.08	0.67	48.7%
C	N ₂ plasma	-8.7	0.7	0.20	8.7%
D	FG plasma	-8.1	0.5	0.18	5.3%

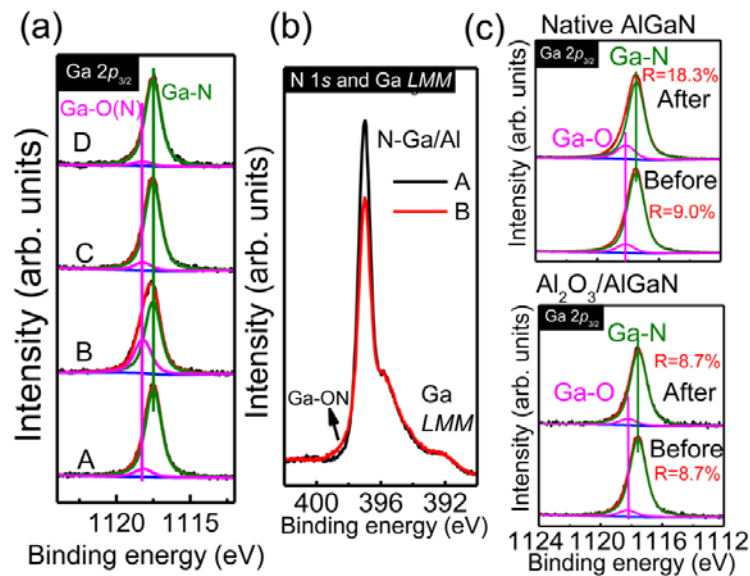


Figure 0.1. XPS spectra of (a) the normalized Ga 2p_{3/2} from samples A, B, C and D after 20 cycles of ALD Al₂O₃ and (b) normalized N 1s by Ga LMM from samples A and B after 20 cycles of ALD Al₂O₃. (c) Ga 2p_{3/2} from the native AlGa_N and Al₂O₃ (2nm)/AlGa_N before and after the 850 °C N₂ rapid thermal annealing.

The forward and backward C-V curves, measured at room temperature at 400 kHz from all samples are shown in Figure 5.2. The observed threshold (V_{TH}) voltage from the forward C-V curves in Figure 5.2 in Table 5.1 shows that O_2 annealing, N_2 and FG plasma pretreatments all increase V_{TH} , indicating that these pretreatments likely reduce the high fixed positive charge density at the $Al_2O_3/AlGaN$ interface.^{12,13} Two abrupt slopes are observed in all C-V curves. The presence of the hysteresis ΔV_1 and ΔV_2 is caused by the slow acceptor traps in the measured trap energy levels with a response time that is comparable to the sweep time of the applied gate voltage. Since the applied negative voltage at first slope is larger, the ΔV_1 represents deeper traps than the ΔV_2 .^{4,14,15} In the first slope to the 2DEG capacitance plateau, no hysteresis loop or threshold voltage shift (ΔV_1) is detected (see also Table 5.1). The ΔV_1 from sample B is ~ 0.08 V, indicating that the interface oxide/oxy-nitride contributes to the threshold voltage shift. The ΔV_1 values of C and D samples are ~ 0.7 and ~ 0.5 V, respectively, and lead to the conclusion that plasma pretreatments result in a higher deep level trap state density.

The plasma pretreatments apparently induce deep acceptors charge traps at the surface, and the CN_x species formed by the plasma pretreatments at the surface of samples C and D, (see ref. 7), is likely responsible for these traps. No obvious physical damage was detected after the remote plasma treatments by *ex situ* atomic force microscopy (Figure 5.4) and the *in situ* LEED patterns (Figure 5.3), which is sensitive to the surface structure, where sharp hexagonal patterns indicative of long range order are observed from samples C and D. No ordered crystal structure is observed from the surface exposed to thermal oxidation (Sample B), as expected. A similar threshold voltage shift/hysteresis loop phenomenon has been reported in some plasma-enhanced chemistry vapor deposited (PECVD) SiN_x passivated $AlGaN/GaN$ devices.^{16,17,18} Thus, the plasma appears to be likely responsible for the voltage instability for $Al_2O_3/AlGaN/GaN$ MOSHEMTs in these studies. The threshold voltage (V_{TH}) instability that has also been reported widely in *capped* $Al_2O_3(HfO_2)GaN/AlGaN/GaN$ MOSHEMTs where the main contributing factor is the Ga-oxide/oxy-nitride.³⁻⁵ It is also noted that the Ga-oxide/oxy-nitride concentration for the GaN cap is much higher than that for the $AlGaN$ surface.⁵ The thick Ga-oxide (>1 nm) for the $Al_2O_3(HfO_2)/GaN$ interface likely contributes to a high V_{TH} shift (>1 V) as a result of deep level trap states.^{3,5} However, for the native $AlGaN$ surface, the thickness of Ga/Al-oxide is less

than one monolayer according to *in situ* XPS.^{7,11,19} Moreover, as Figure 5.2 shows, no V_{TH} shift and a small ΔV_1 is detected from native oxide sample A or from the thermal oxide treatment of sample B. Therefore, it is necessary to consider the differences in the associated interfacial chemistry in the evaluation of the *capped* an *uncapped* AlGaN/GaN device.

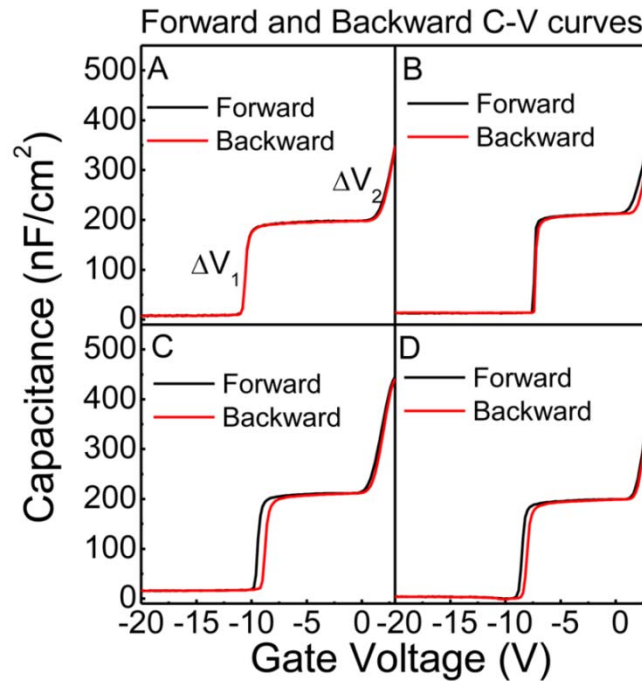


Figure 0.2. Forward and backward C- V curves of capacitors for samples A, B, C and D.

The voltage shift phenomenon from the second abrupt slope in Figure 5.2 is also observed in all samples, and is associated with the high-k/AlGaN interface.¹⁴ The maximum shift values (ΔV_2) measured at $V_G > 0$ for samples A, B, C and D are also shown in Table 5.1, indicating that the oxide/oxynitride interface induces an increase of ΔV_2 , which originates from a shift in capacitance due to charge trapping, and is correlated with D_{it} near the AlGaN conduction band. Measurement of the frequency-dependent C-V curves can enable the extraction of the relatively fast trap D_{it} of the high-k/AlGaN(GaN) interface in MOSHEMTs.^{3,20} The forward C-V curves with the measurement frequency varied from 50 kHz to 400 kHz at room temperature are shown in Figure 5.4 (a). The frequency dispersion due to the Al_2O_3 /AlGaN interface trap response is visible in the second slope region for all samples. The largest (smallest) amount of frequency

dispersion is detected from sample B (D), respectively, indicating that interfacial oxide/oxy-nitride, which is clearly detected in Ga $2p_{3/2}$ and N $1s$ spectra, contribute to the frequency dispersion in the second slope bias region.

Equation (5.1) provides a simple quantitative method to evaluate average D_{it} between two trapping states by assuming that the higher measurement frequency f detects shallower interface states which time constant (τ_e) is shorter than the inverse of the measurement frequency ($1/f$).¹⁴

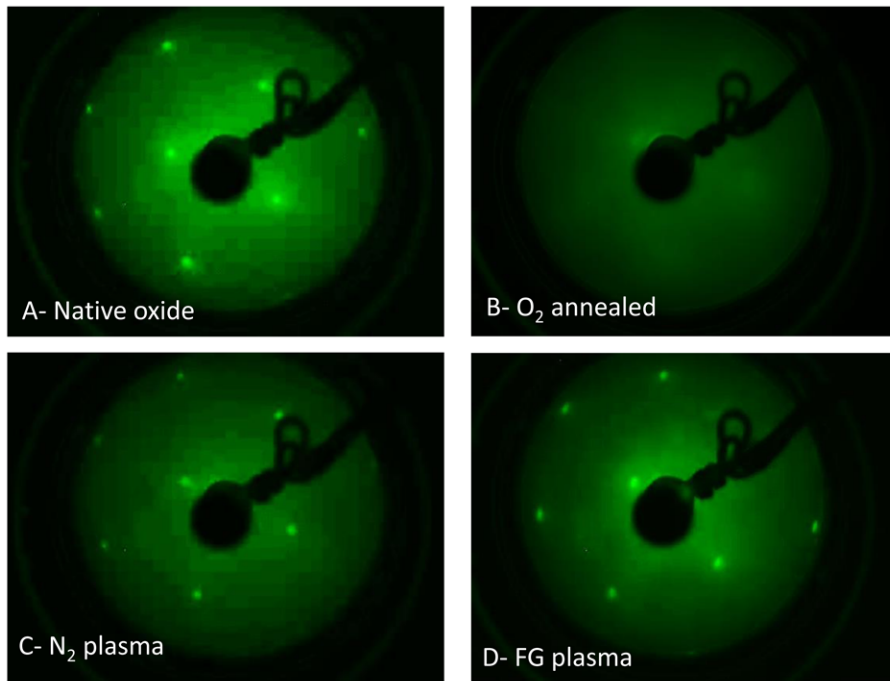


Figure 0.3. LEED patterns from samples A, B, C and D.

$$D_{it} = \frac{\Delta V \cdot C_{Al_2O_3 \text{ insulator}}}{q \Delta E}, \quad \Delta E = (E_C - E_{T1}) - (E_C - E_{T2}) \quad (5.1)$$

$$\tau_e = \frac{1}{v_{th} \cdot \sigma_n \cdot N_c} \exp\left(\frac{E_C - E_T}{kT}\right), \quad \tau_e = \frac{1}{f} \quad (5.2)$$

where ΔE is effective trapping energy difference between high and low measurement frequencies. The trapping energy $E_C - E_T$ at different frequencies could be deduced by Shockley-Read-Hall statistics (equation (5.2)), where $N_c = 2.2 \times 10^{18} \text{ cm}^{-3}$ is the effective density of states in the conduction band in $Al_{0.25}Ga_{0.75}N$, $v_{th} = 2 \times 10^7 \text{ cm/s}$ is the thermal velocity of

electron, and $\sigma_n = 3.4 \times 10^{-15} \text{ cm}^2$ is the electron capture cross section.²¹ $C_{\text{Al}_2\text{O}_3}$ is the capacitance of Al_2O_3 insulator layer, which may be extracted by the capacitances of $\text{Al}_2\text{O}_3/\text{AlGaIn}$ stack and AlGaIn , which are measured directly by C-V curves from the $\text{Al}_2\text{O}_3/\text{AlGaIn}/\text{GaIn}$ MOS capacitances (see Figure 5.4) and $\text{AlGaIn}/\text{GaIn}$ capacitance, respectively. The capacitance of Al_2O_3 is calculated to be $C_{\text{Al}_2\text{O}_3} \sim 841 \text{ nF/cm}^2$, suggesting that the dielectric constant of the $\sim 10 \text{ nm}$ Al_2O_3 is 9.5, consistent with the reported values.^{22,23}

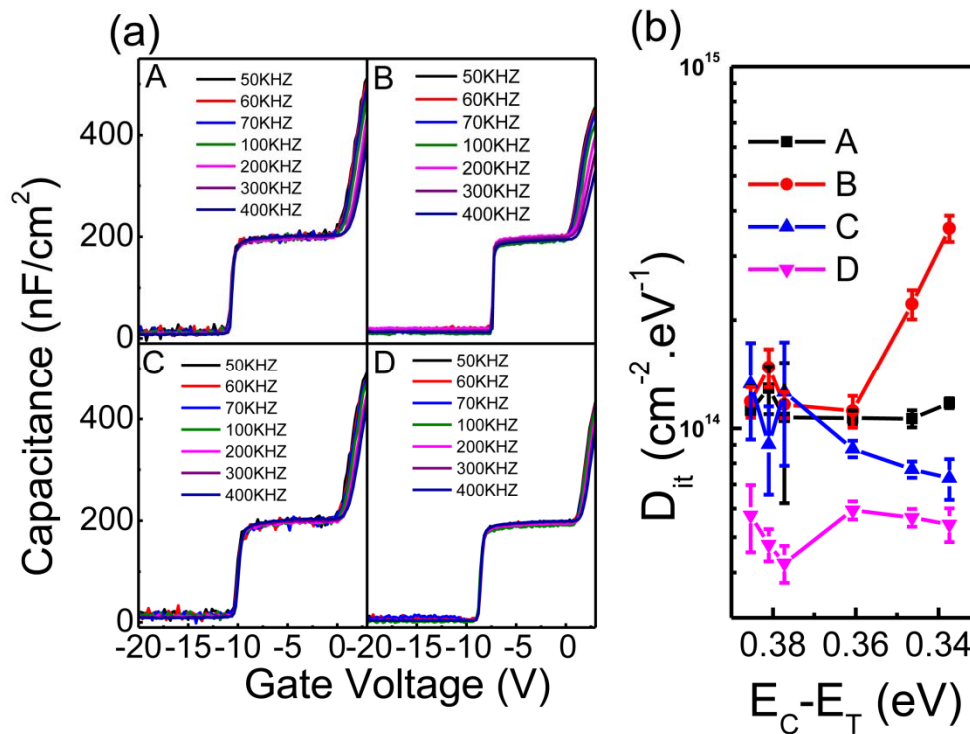


Figure 0.4. (a) Frequency-dependent C-V curves from capacitors for samples A, B, C, and D. (b) associated D_{it} - ($E_C - E_T$) plots.

The D_{it} is plotted in the Figure 5.4 (b). An obvious D_{it} increase ($0.36 > E_C - E_T > 0.33 \text{ eV}$) is detected from the O_2 annealed sample consistent with ΔV_2 results in Table 7.1 indicating that the oxide/oxy-nitride related defects result in an increase of D_{it} in the upper range of the band gap ($E_C - E_T < 0.36 \text{ eV}$). The plasma pretreatments do not contribute to such shallow energy level defects. The deconvolution of Ga-O(N) bonding concentration is difficult, and so it is unclear

whether Ga-O vs. Ga-ON bonding is responsible for the D_{it} response observed. The N₂ plasma and FG plasma pretreatments both decrease the amount of D_{it} , with FG more effective. This behavior is consistent with our previous interface chemistry study.⁷ The N₂ plasma and FG plasma pretreatments are both associated with a higher quality Al₂O₃/AlGa_{0.75}N interface, where the removal of a spurious carbon “passivation” layer provides more nucleation sites for formation of stable Ga-O-Al bonds. The carbon likely originates from the atmospheric exposure prior to the ALD Al₂O₃ growth. The FG plasma pretreatment could not only improve the ALD nucleation, but also is able to avoid the increase of Ga-oxide formation (see Table 5.1). Therefore the lowest D_{it} near the conduction band is obtained from the FG remote plasma treated sample. It is noted that no frequency dispersion could be detected at the first slope because long time constant for electrons.^{14,20} For example, the time constant τ_e for near midgap states (i.e., $E_C - E_T = 2$ eV) is 10^{22} s at room temperature according to equation (5.2). Therefore, the charge of such deep states does not respond to a standard multi-frequency C-V measurement.¹⁴ However, we also should point out the current modulation only considers all D_{it} is at the interface which is likely not the actual. A more accurate quantitative is required.

5.5 Conclusion

In conclusion, the relationship between the interface chemistry and electrical behavior of the Al₂O₃/Al_{0.25}Ga_{0.75}N interface treated by O₂ annealing, N₂ plasma and FG plasma pretreatments was investigated by *in situ* XPS, LEED and C-V measurement. The oxide/oxy-nitride bonding contributes to the D_{it} near the conduction band edge at the Al₂O₃/AlGa_{0.75}N interface, and pretreatments with a N₂ and FG plasma reduces the D_{it} . This response is attributed to the passivation of oxide/oxy-nitride-related defects, with the FG plasma more effective because of inhibiting the increase of oxide formation. Further development of the remote plasma pretreatment to avoid the observed threshold voltage shift as a result of deep traps is underway.

5.6 References

- ¹ P. Lager, C. Ostermaier, G. Pobegen, and D. Pogany, Electron Device Meet. 2012. IEDM 299 (2012).
- ² B.M. Green, K.K. Chu, E.M. Chumbes, J.A. Smart, J.R. Shealy, and L.F. Eastman, IEEE Electron Device Lett. Lett. IEEE **21**, 268 (2000).

- ³ S. Yang, Z. Tang, K. Wong, Y. Lin, C. Liu, Y. Lu, S. Huang, and K.J. Chen, *IEEE Electron Device Lett.* **34**, 1497 (2013).
- ⁴ S. Ozaki, T. Ohki, M. Kanamura, T. Imada, N. Nakamura, N. Okamoto, T. Miyajima, and T. Kikkawa, *CS MANTECH Conf.* 1 (2012).
- ⁵ D.W. Johnson, R.T.P. Lee, R.J.W. Hill, M.H. Wong, G. Bersuker, E.L. Piner, P.D. Kirsch, and H.R. Harris, *IEEE Trans. Electron Devices* **60**, 3197 (2013).
- ⁶ T. Hashizume, S. Ootomo, T. Inagaki, and H. Hasegawa, *J. Vac. Sci. Technol. B* **21**, 1828 (2003).
- ⁷ X. Qin, H. Dong, B. Brennan, A. Azacatl, J. Kim, and R.M. Wallace, *Appl. Phys. Lett.* **103**, 221604 (2013).
- ⁸ R.M. Wallace, *ECS Trans.* **16**, 255 (2008).
- ⁹ C.L. Hinkle, E.M. Vogel, P.D. Ye, and R.M. Wallace, *Curr. Opin. Solid State Mater. Sci.* **15**, 188 (2011).
- ¹⁰ Z.L. Fang, J.Y. Kang, and W.Z. Shen, *Nanotechnology* **20**, 045401 (2009).
- ¹¹ B. Brennan, X. Qin, H. Dong, J. Kim, and R.M. Wallace, *Appl. Phys. Lett.* **101**, 211604 (2012).
- ¹² J. Son, V. Chobpattana, B.M. McSkimming, and S. Stemmer, *Appl. Phys. Lett.* **101**, 102905 (2012).
- ¹³ T.H. Hung, S. Krishnamoorthy, M. Esposto, D.N. Nath, P.S. Park, and S. Rajan, *Appl. Phys. Lett.* **102**, 072105 (2013).
- ¹⁴ C. Mizue, Y. Hori, M. Miczek, and T. Hashizume, *Jpn. J. Appl. Phys.* **50**, 021001 (2011).
- ¹⁵ T. Sato, J. Okayasu, M. Takikawa, and T. Suzuki, *IEEE Electron Device Lett.* **34**, 2012 (2013).
- ¹⁶ M. Fagerlind, F. Allerstam, E.Ö. Sveinbjörnsson, N. Rorsman, A. Kakanakova-Georgieva, A. Lundskog, U. Forsberg, and E. Janzén, *J. Appl. Phys.* **108**, 014508 (2010).
- ¹⁷ Y. Cai, Y. Zhou, K.M. Lau, and K.J. Chen, *IEEE Trans. Electron Devices* **53**, 2207 (2006).
- ¹⁸ Y. Lu, S. Yang, Q. Jiang, Z. Tang, B. Li, and K.J. Chen, *Phys. Status Solidi C* **10**, 1397 (2013).
- ¹⁹ X. Qin, B. Brennan, H. Dong, J. Kim, C.L. Hinkle, and R.M. Wallace, *J. Appl. Phys.* **113**, 244102 (2013).

- ²⁰ H.A. Shih, M. Kudo, and T. Suzuki, Appl. Phys. Lett. **101**, 043501 (2012).
- ²¹ P. Kordoš, R. Stoklas, D. Gregušová, and J. Novák, Appl. Phys. Lett. **94**, 223512 (2009).
- ²² G.D. Wilk, R.M. Wallace, and J.M. Anthony, J. Appl. Phys. **89**, 5243 (2001).
- ²³ D.A. Buchanan, E.P. Gusev, E. Cartier, H. Okorn-Schmidt, K. Rim, M.A. Gribelyuk, A. Mocuta, A. Ajmera, M. Copel, S. Guha, N. Bojarczuk, A. Callegari, C.D. Eme, P. Kozlowski, K. Chan, R.J. Fleming, P.C. Jamison, J. Brown, and R. Arndt, Electron Device Meet. 2000. IEDM 223 (2000).

CHAPTER 6

A Crystalline Oxide Passivation for Al₂O₃/ AlGa_N/ Ga_N

6.1 Preface

According to previous studies, neither the atomic layer deposition (ALD) of Al₂O₃ nor HfO₂ could passivate the interface due to the AlGa_N surface is stable. The high density of positive charges results in a large negative threshold voltage shift. In addition, the high interface state density (D_{it}) could not be passivated by the ALD. Although N₂ and forming gas plasma pretreatments are helpful for the removal of carbon contamination and initial nucleation of ALD, it is not effective for the decreasing of the interface state density. In this chapter, it is demonstrated that a crystalline oxide structure enable to passivate the surface. *In situ* X-ray photoelectron spectroscopy (XPS) and low energy electron diffraction (LEED) are performed to study the formation of a crystalline oxide on the AlGa_N surface. The oxidation of the AlGa_N surface is prepared by annealing and remote N₂+O₂ plasma pretreatments resulting in a stable crystalline oxide. The impact of the oxide on the interface state density is studied by capacitance voltage measurements. It is found that a remote plasma exposure at 550 °C shows the smallest frequency dispersion. Crystalline oxide formation may provide a novel passivation method for high quality AlGa_N/Ga_N devices.

The contents of this chapter are adapted from a paper entitled “**A crystalline oxide passivation for Al₂O₃/AlGa_N/Ga_N**” [*Applied Physics Letters*, **105**, 141604 (2014)]. Copyright [2014], AIP Publishing LLC.

6.2 Introduction

As mentioned in previous chapters which demonstrated a high interface state density, the quality of the Al₂O₃(HfO₂)/AlGa_N interface remains a challenge.¹⁻³ In contrast, Miao *et al.*⁴ proposed the possibility of an energetically favorable 2 monolayer (ML) crystalline oxide structure obeying the electron counting rule (“2 ML EC”)⁵ on Ga_N and Al_N using first-principles

simulations. In that work, it was noted that the “2 ML EC” structure was likely to form under realistic oxidation conditions and had a relatively low density of surface states within the band gap. Moreover, partially ordered oxide structures have been reported to form on GaN upon O₂ exposure at 550°C.⁶ However, the impact of oxidation of AlGa_{0.25}N on device performance is still under much debate with apparently contrasting experimental outcomes.^{7,8} Additionally, the prospect of a high quality interfacial passivation layer, stable to high-k ALD processes, may enable improve MOSHEMT performance.

To examine this possibility, we employ *in situ* monochromatic XPS and LEED characterization to study the interfacial chemistry and structure of the oxidation of AlGa_{0.25}N by annealing and remote N₂+O₂ plasma pretreatments. A stable crystalline oxide layer, ~2 ML thick, is detected on the AlGa_{0.25}N surface pretreated by the remote plasma at 550 °C. Unlike the case for III-arsenides,⁹ the ordered oxide appears to persist upon subsequent exposure to aggressive ALD precursors at 300°C. Frequency dependent capacitance-voltage (C-V) measurements confirm that the crystalline oxide layer reduces the positive fixed charge and interface state density for ALD-Al₂O₃ on AlGa_{0.25}N significantly.

6.3 Experimental

Metal organic chemical vapor deposited Al_{0.25}Ga_{0.75}N (30 nm)/ GaN (1.2 μm) layer on a p-type Si(111) substrate HEMTs wafers obtained from DOWA Electronics Materials (Tokyo, Japan) were used in this study (see Figure 1.1 (b)). The AlGa_{0.25}N orientation was (0001). Four samples (~1 × 1 cm²) from the same wafer were first solvent cleaned in acetone, methanol and isopropanol for one minute each to reduce surface organic contamination and then introduced to an ultra-high vacuum (UHV) cluster system described in Chapter 1 and detail elsewhere⁹. Sample “A” consisted of a native oxide AlGa_{0.25}N/GaN/Si control sample. Sample “B” was exposed to a N₂:O₂ anneal (45 sccm N₂ + 0.5 sccm O₂) at 550 °C for 10 minutes in a connected UHV preparation chamber. Samples “C” and “D” were exposed to a N₂:O₂ remote plasma (45 sccm N₂ + 0.5 sccm O₂) at 300 °C and 550 °C for 10 min, respectively, in the same preparation chamber. After these pretreatments, *in situ* XPS and LEED were performed on all samples. Then the samples were transferred to a Picosun ALD reactor through a transfer tube (operating pressure: 1×10⁻¹⁰ mbar) to avoid spurious atmospheric contamination followed by exposure to one pulse of Tri-methyl

Aluminum (TMA). Then *in situ* XPS and LEED were again performed for on all samples after they were similarly transferred to the analysis chamber. After subsequent exposure to 20 and 80 full ALD cycles (total 100 cycles) of Al_2O_3 , XPS was performed again to monitor the chemical changes at interfaces. All ALD was performed using TMA and H_2O as precursors. One full ALD cycle was 0.1 s TMA + 4 s purge + 0.1 s H_2O + 4 s purge. High purity (99.999%) N_2 (200 sccm) was used as the precursor carrier and purging gas. The working pressure of the ALD reactor was ~ 10 mbar and the Al_2O_3 deposition temperature was 300 °C.

After the total of 100 cycles (~ 10 nm) of ALD Al_2O_3 , the samples were taken out of the deposition and analysis system for capacitor fabrication. Ohmic contact regions were defined firstly by standard photolithography and contact regions to the AlGaIn layer were opened by BCl_3 (15 sccm)/Ar (5 sccm) reactive ion etching (RIE). The ohmic contacts (resistivity $\rho \sim 1 \times 10^{-6} \Omega \cdot \text{cm}^2$) were formed by e-beam evaporation deposition (base pressure $\sim 1 \times 10^{-6}$ mbar) of Ti/Al/Ni/Au followed by rapid thermal annealing at 850 °C for 30 s with 2000 sccm N_2 after patterning by lift off.¹⁰ Circular gate electrodes were then defined, followed by e-beam deposition of Ni/Au and lift off. C-V measurements were performed by an Agilent 4284 LCR meter with step of 0.02 V and AC modulation voltage of 50 mV with sweep frequencies varying from 5 to 400 kHz.

XPS was carried out using a monochromated Al $K\alpha_1$ ($h\nu = 1486.7$ eV) X-ray source, equipped with a 7 channel analyzer, using a pass energy of 15 eV, with all scans taken at 45° with respect to the sample normal. XPS peak deconvolution was accomplished using AAnalyzer software.¹¹ All peaks were referenced to the N 1s peak at 397.0 eV to compensate for any changes in the peak core level positions due to band bending.

6.4 Results and Discussion

Figure 6.1 shows *in situ* N 1s and Ga *LMM* Auger spectra for samples A, B, C and D. The spectra for sample A are shown for reference with the N-Ga/Al N1s peaks (set at 397.0 eV), and the Ga $L_{2M_{45}M_{45}}$ Auger feature (spanning ~ 392 -398 eV)¹². As shown in Figure 6.1 (a), the N 1s and Ga *LMM* spectra for the samples A and B overlap fully, clearly showing that the 550 °C annealing pretreatment in the 45 sccm N_2 + 0.5 sccm O_2 flow does not change the chemical state of nitrogen or the Ga/N ratio (Ga *LMM* area/N 1s area). However an obvious peak at 402 eV,

corresponding to N-O bonding for sample B,¹³ is detected (Figure 6.1 (b)). The detection of N-O bonding indicates that the oxidation layer generated by the 300 °C plasma does not conform to the proposed “2 ML EC” structure that does not formally contain N-O bonds,⁴ as seen in Figure 6.1 (e).

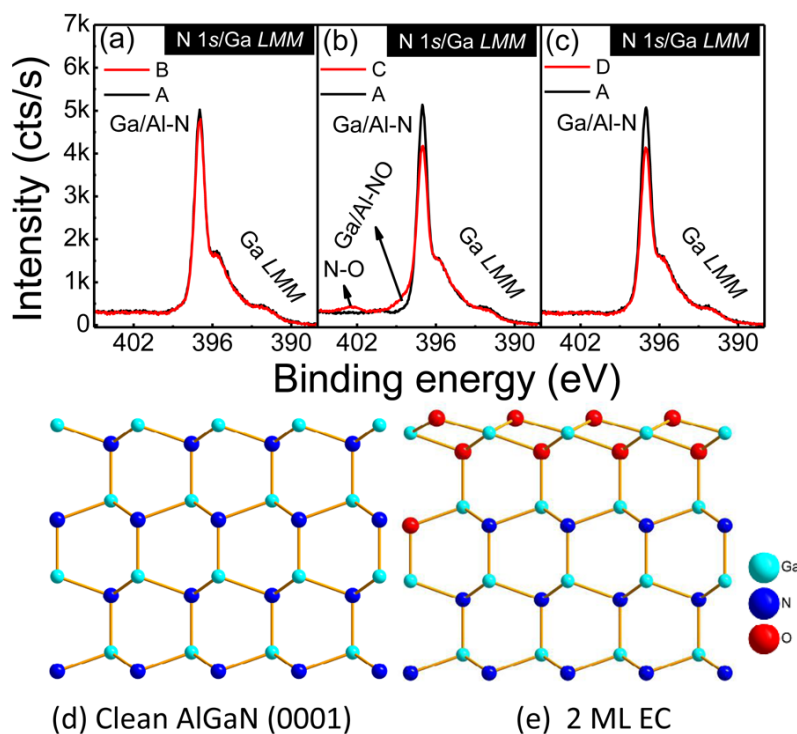


Figure 0.1. *In situ* XPS spectra of the N 1s and Ga LMM for samples A, B, C and D. Schematic of the side view of (d) clean and (e) 2 ML EC AlGaN (0001) structures.

Apart from the N-O bonding, a feature at 398 eV is also detected, which likely originates from Ga/Al-ON¹⁴ and N-C(H)¹⁵. However, since the C 1s intensity for sample C is near the XPS detection limits (see Figure 6.3) and the intensity of N-C(H) is very low according to our previous study for *in situ* N₂ and forming gas plasma pretreatments on AlGaN.¹⁵ This observation leads to the conclusion that the feature mainly originates from Ga/Al-ON bonding. In contrast, there is no evidence of N-O or Ga/Al-O-N feature detected for sample D (Figure 6.1 (c)), which is in agreement with the proposed “2 ML EC” model.⁴ These results indicate that the 550 °C is likely able to oxidize the AlGaN surface to saturation, similar to that reported previously for GaN.⁶ It is noted that the Ga/Al-N peak intensity for samples C and D (Figure 6.1 (b) and (c)) is

lower than that for sample A, but the Ga *LMM* Auger feature intensity remains constant for all samples, indicating that the N intensity is attenuated by the oxide/oxynitride present on the surface of samples C and D, which will be discussed further below.

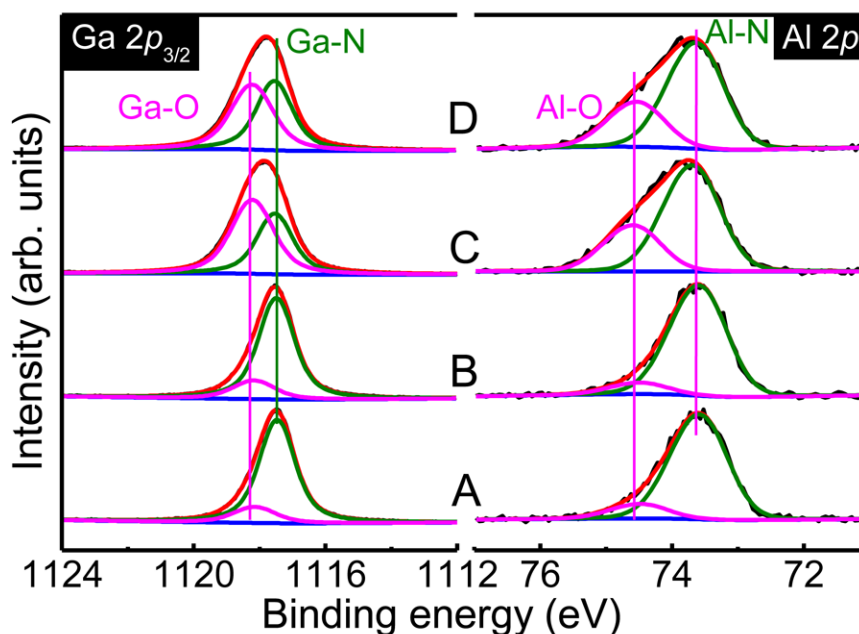


Figure 0.2. *In situ* XPS spectra of the normalized Ga $2p_{3/2}$ and Al $2p$ for samples A, B, C and D.

Figure 6.2 shows that the *in situ* normalized Ga $2p_{3/2}$ and Al $2p$ spectra for samples A, B, C and D. Consistent with our prior work,^{15–17} the Ga $2p_{3/2}$ spectra from sample A shows two peaks, indicative of Ga-N (at 1117.8 eV) from the AlGa₃N substrate and the presence of a Ga³⁺ oxidation state (1118.5 eV) from the surface. Additionally, the Al $2p$ spectra for sample A also shows two peaks consistent with Al-N bonding (at 73.5 eV) and Al-O bonding (at 74.4 eV). It is noted that the “2 ML EC” model of the oxidation layer of GaN/AlN consists of Ga-O/Al-O, while Ga-Ga/Al-Al or Ga/Al-ON bonds should not be detected in the structure.⁴ The same spectral fitting parameters are used as in previous work^{15–17} and the ratios of Ga-O(N)/Ga-N and Al-O(N)/Al-N are shown in Table 6.1. The estimated error of ratio is based on the fitting procedure.^{15,16} The 550 °C annealing pretreatment results in a slight increase of the Ga-O and Al-O concentrations (see Table 6.1). Larger Ga-O and Al-O concentrations are detected from samples C and D compared to B due to the remote plasma exposure, while the 550 °C plasma

pretreatment does not contribute to additional oxide formation than the 300 °C remote plasma pretreatment.

Table 0.1. Summary of sample pretreatments, ratios of Ga-O(N)/Ga-N and Al-O(N)/ Al-N, observed threshold voltage.

Samples	Pretreatments	Ga-O(N) /Ga-N	Al-O(N) /Al-N	V_{TH} (V)	D_{it} (cm ⁻² eV ⁻¹) (0.34 < $E_C - E_T$ < 0.45 eV)
A	Native	0.17±0.01	0.10±0.006	-9.4	2.00×10 ¹⁴
B	550 °C N ₂ +O ₂ anneal	0.19±0.01	0.11±0.006	-11	2.79×10 ¹⁴
C	300 °C N ₂ +O ₂ plasma	0.99±0.09	0.44±0.01	-8.6	3.27×10 ¹⁴
D	550 °C N ₂ +O ₂ plasma	0.84±0.08	0.42±0.01	-5.6	3.81×10 ¹³

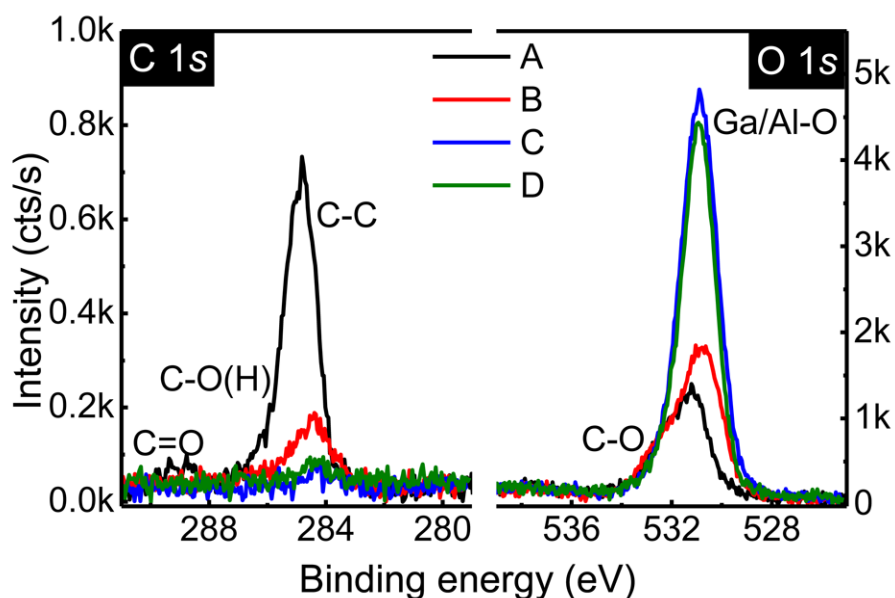


Figure 0.3. *In situ* XPS spectra of the C 1s and O 1s for samples A, B, C and D.

Although the Ga/Al-ON state is clearly detected from the N 1s spectra for sample C, it is complicated to deconvolve the Ga/Al-ON from Ga 2p_{3/2}/Al 2p due to ambiguous Ga-ON peak parameters (such as the associated binding energy¹⁸). Therefore, the fitting for sample C is still

based on the two peaks for a consistent fit in this work. The concentration of Ga-ON could be evaluated simply by the intensity of Ga-ON in N 1s in Figure 6.1 (b). Assuming that Ga-ON contributes entirely to the peak at 398 eV (see Figure 6.1 (b)), the concentration of Ga-ON is ~17% of the oxide/oxy-nitride on sample C. From XPS thickness calculations, based on the attenuation of N 1s spectra in Figure 6.1 (b) and (c), a ~0.3 nm oxide layer for samples C and D is detected, indicating that almost 1 ML of nitrogen on samples C and D is replaced by oxygen from the remote plasma process and 2 ML of oxide is formed which is consistent with the “2 ML EC” structure,⁴ as seen in Figure 6.1 (d) and (e).

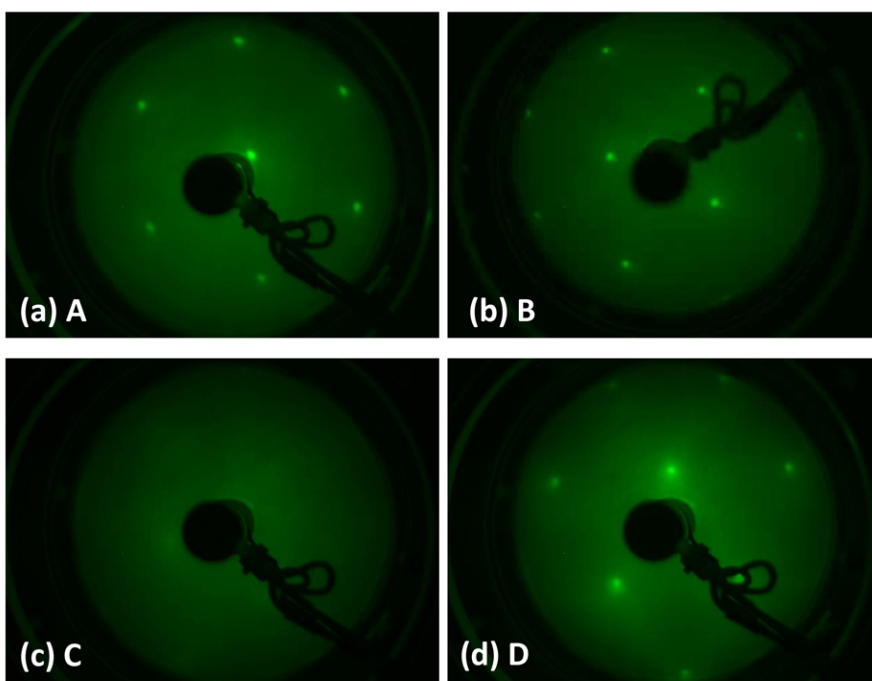


Figure 0.4. LEED patterns for samples A, B, C and D taken with an electron beam energy of 113 eV.

The *in situ* C 1s and O 1s spectra for samples A, B, C and D from the initial surface are shown in Figure 6.3. Carbon contamination is a significant factor in the magnitude of the current collapse observed in devices¹⁹ as well as in the nucleation rates in ALD dielectric growth.¹⁵ The C 1s peak for the sample A shows the following bond formation: C=O at 289 eV, C-O(H) at 285.4 and C-C at 284.5 eV.²⁰ The annealing pretreatment reduces the carbon contamination on

the AlGaN surface by $\sim 75\%$ as a result of decomposition and volatile product formation. In contrast, either the 300 °C or the 500 °C remote plasma pretreatment is more effective for the removal of the carbon contamination than the annealing pretreatment, which is mainly effective for the removal of C=O and C-O(H). The low C 1s intensity for samples C and D are near the XPS detection limits as a result of N₂ based plasma pretreatments, which is highly effective for the removal of carbon.¹⁵

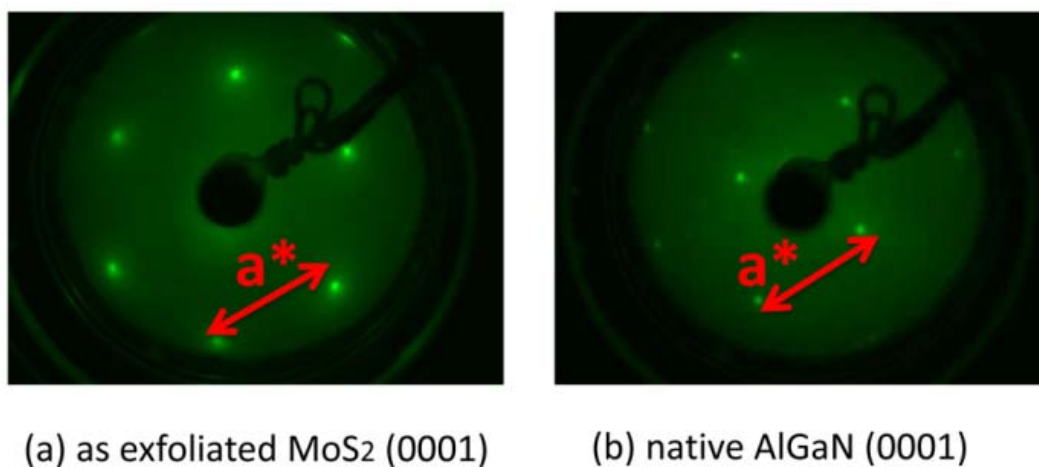


Figure 0.5. LEED pattern for (a) as exfoliated MoS₂ (0001) and (b) native AlGaN (0001) taken at a beam energy of 113 eV.

The LEED characterization, which is sensitive to the surface atom order, is performed to evaluate the surface structure for samples A, B, C and D. Figure 6.4 (a) shows the LEED pattern for the sample A as reference, which shows a sharp (1×1) hexagonal pattern indicative of the AlGaN surface, albeit with a 0.8 ± 0.2 ML nonuniform physisorbed carbon contamination layer. The (1×1) pattern is consistent with LEED patterns from as exfoliated MoS₂²¹ as a reference sample. Figure 6.5 shows the in LEED patterns from as-exfoliated MoS₂ (0001) surface²¹ and native AlGaN taken at a beam energy of 113 eV. Clear hexagonal patterns are obtained from both surfaces. The reciprocal 2D lattice vectors of surface structure are obtained by measuring the distance between the spots (see “a*” Figure 6.5). The relationship of lattice parameters in the real space is expressed in equation (6.1). The calculated lattice constant of AlGaN $a = 3.19$ Å ($a_{\text{MoS}_2} = 3.16$ Å,²² $a^*_{\text{MoS}_2}/a^*_{\text{AlGaN}} = 1.01$), which indicates that the AlGaN surface is an

unreconstructed (1×1) structure.

$$\frac{a^*_{\text{MoS}_2}}{a^*_{\text{AlGaN}}} = \frac{a_{\text{AlGaN}}}{a_{\text{MoS}_2}} \quad (6.1)$$

The carbon coverage is calculated from XPS intensity.¹⁵ Figure 6.4 (b) also shows the same hexagonal pattern as the sample A, indicating that the annealing pretreatment does not change the surface structure. It should be noted that samples A and B do not correspond to the clean surface shown in Figure 6.1(d). However, the oxygen on the surfaces of samples A or B, which is less than 1 ML,¹⁶ does not change the (1×1) surface structure. This is also observed by Bermudez by comparison of clean and O₂ exposed surfaces.²³ The possible adsorption site for oxygen on the surface is at the “on top” or fcc position.²⁴ However, a LEED pattern in Figure 6.4 (c) for sample C does not show any ordered structure, suggesting that the 300 °C plasma pretreatment produces an amorphous oxide/oxynitride layer. Considering the presence of the Ga-ON and N-O bonding in Figure 6.1 (b), the surface is likely disordered as a result of the incomplete oxidation at the 300 °C plasma pretreatment. In contrast, a sharp hexagonal pattern for sample D is observed in Figure 6.4 (d), which is the direct evidence of ordered oxide layer. Thus, the formation of the crystalline oxide is temperature dependent. Dong *et al.*⁶ also reported the same temperature dependent phenomenon for the *in situ* oxidization of GaN by molecular oxygen. However, it should be noted that the LEED pattern observed by Dong *et al.* corresponds to a (3√3×3√3-R30°) reconstruction and is likely due to the existence of a Ga bilayer on the starting surface.⁶ To summarize, the oxidation of AlGaN can be achieved by 300 °C and 550 °C plasma pretreatments, while the 550 °C plasma pretreatment contributes to an order crystalline oxides which is consistent with the proposed “2 ML EC” surface oxide structure proposed by Miao *et al.*⁴, which is expected to reduce the interface state density (D_{it}).

Punkkinen *et al.*²⁵ recently proposed that an ordered, well-defined crystalline oxide layer on InAs has the potential to provide defect-free interface enabling a new method for metal oxide semiconductor field-effect transistors (MOSFETs) and tunnel field-effect transistors (TFETs) applications. The stability of that crystalline oxide layer on InAs(100), prepared by *in situ* thermal anneal in O₂ atmosphere, upon exposure to ALD has also been investigated with *in situ* XPS and LEED.²⁶ Although the oxidation process produces an ordered (3×1)-O reconstruction,

this oxide layer could be reduced easily by even one pulse of TMA due to the “clean-up effect”. In contrast, the crystalline oxide on sample D is stable under such ALD exposures. Figure 6.6 (a) shows the *in situ* normalized Ga $2p_{3/2}$ and Al $2p$ spectra for sample D from the initial surface, after one pulse of TMA and 20 cycles of Al_2O_3 . The Ga $2p_{3/2}$ peaks from these ALD treatments overlap together fully, indicating that the Ga-oxide is not removed by the ALD precursor exposure and is likely enabled by the stability of the oxide formed on AlGaN, consistent with the high bond dissociation energy of Al-O (542 kJ/mol)²⁷ and Ga-O (349 ± 42 kJ/mol)²⁷. After one pulse of TMA, there is evidence of Al-O at 74.5 eV detected, suggesting the nucleation/reaction of TMA on the sample D surface.

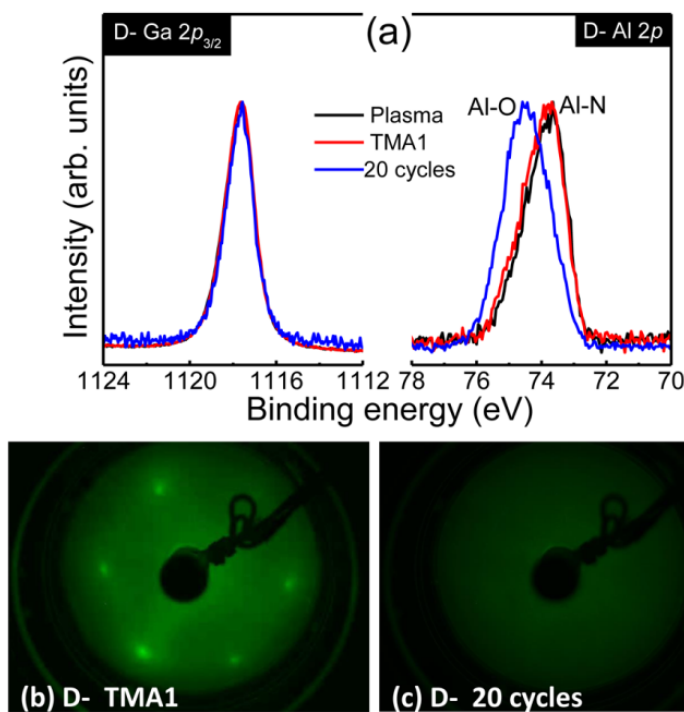


Figure 0.6. (a) *In situ* XPS spectra of the normalized Ga $2p_{3/2}$ and Al $2p$ for the sample D from initial surface, after one pulse of TMA and after 20 cycles of Al_2O_3 , and LEED pattern for the sample D taken at a beam energy of 113 eV (b) after one pulse of TMA and (c) after 20 cycles of Al_2O_3 .

With a further 20 ALD cycles of Al_2O_3 , an obvious increase of the Al-O peak is detected as a result of the successful growth of Al_2O_3 . The thickness of 20 cycles of Al_2O_3 on the sample D

is ~ 1.5 nm, thicker than the sample A (~ 1.1 nm¹⁵), suggesting a faster nucleation process is likely due to the removal of carbon contamination on the surface, which could passivate the nucleation reaction of precursors on AlGaIn.¹⁵ The faster nucleation has a potential to improve the interface quality. In contrast to an arsenide surface,²⁶ the LEED pattern in Figure 6.6 (b) can still be observed clearly after one pulse of TMA exposure, again demonstrating the stability of the crystalline oxide formed. As shown in Figure 6.6 (c), no LEED pattern is detected after 20 cycles of ALD Al₂O₃ as expected, and consistent with amorphous structure of a thick ALD Al₂O₃ film.

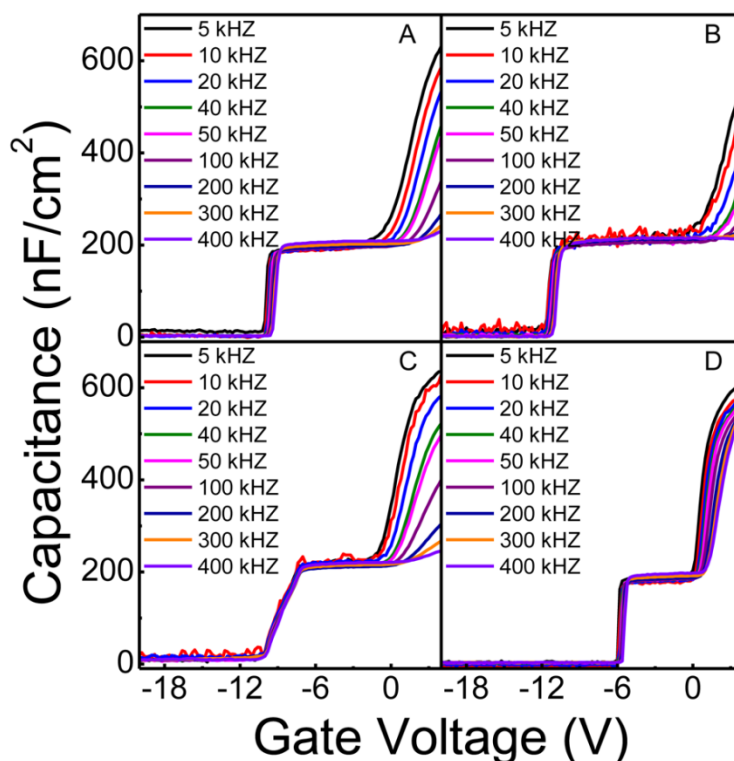


Figure 0.7. Frequency-dependent C-V curves from diodes for samples A, B, C and D.

In order to evaluate the D_{it} of Al₂O₃/AlGaIn/GaN interface for these pretreatments, the corresponding Al₂O₃ (~ 10 nm)/AlGaIn/GaN diodes were fabricated.²⁸ Figure 6.7 shows the C-V curves with the measurement frequency varied from 5 kHz to 400 kHz at room temperature for samples A, B, C and D, and the details of the C-V response in such device structures have been reported.^{1,2,28-31} The frequency dispersion originating from the Al₂O₃/AlGaIn interface traps response is visible in the second slope region ($V_{gate} > -3$ V) for the sample A. The 550 °C

annealing pretreatment does not reduce the dispersion and the 300 °C remote plasma exposure results in even worse frequency dispersion due to the amorphous oxide/oxy-nitride layer. The gradual C-V slope for the first step ($V_{\text{gate}} \sim -11\text{ V}$) from sample C indicates the high D_{it} as a result of low quality of oxide/oxy-nitride layer again.³² In contrast, the smallest amount of frequency dispersion is detected from the sample D, suggesting that the oxide layer on the sample D reduces the interface state density substantially.

The resulting benefits of the crystalline oxide interlayer are substantial. Firstly, the crystalline oxide saturates the Ga/Al dangling bonds for the Ga/Al-terminated AlGaN surface. The interfacial bonding between AlGaN and Al_2O_3 is one possible reason of high D_{it} .³³ The high quality of a crystalline oxide as a passivation layer between AlGaN and Al_2O_3 reduces the D_{it} . The observed threshold voltage (V_{TH}) values from the curves measured at 100 kHz for samples A, B, C and D in Figure 6.7 are shown in Table 6.1. It should be noted that the gradual/gentle C-V slope for sample makes the error of V_{TH} relatively high ($\sim \pm 1.5\text{ V}$). In particular, the crystalline oxide results in a 3.8 V positive shift. We speculate that the high fixed positive charge density at ALD- $\text{Al}_2\text{O}_3/\text{AlGaN}$ ³⁴ is reduced by the crystalline oxide passivation layer. In contrast, the positive V_{TH} shift effect is not obvious for samples B and C. This crystalline passivation layer also provides a potential for fabricating low D_{it} normally-off $\text{Al}_2\text{O}_3/\text{AlGaN}/\text{GaN}$ MOSHEMTs (see Table 6.1). The extraction of D_{it} refers to the method presented in ref.²⁸. Potential improvements in the extraction of D_{it} are also worthy of consideration, such as the effect of interface disorder or border traps,³⁵ but are beyond the scope of this study..

6.5 Conclusion

In conclusion, the oxidation behavior of AlGaN is investigated by *in situ* XPS and LEED and *ex situ* C-V characterization. Oxidation layers 2 ML could be achieved by 300 °C and 550 °C N_2+O_2 plasma pretreatments. In particular, the 550 °C remote plasma pretreatment contributes to a stable crystalline oxide layer and inhibits the formation of N-O and Ga-ON bonds, which likely contribute to interface defects. Additionally, AlGaN/GaN MOS diodes pretreated by the 550 °C plasma exhibits a good interface quality with the smallest frequency dispersion indicating a lower D_{it} . This crystalline oxide passivation will have potential for high quality of AlGaN/GaN MOSHEMTs.

6.6 References

- ¹ S. Huang, S. Yang, J. Roberts, and K.J. Chen, *Jpn. J. Appl. Phys.* **50**, 110202 (2011).
- ² C. Mizue, Y. Hori, M. Miczek, and T. Hashizume, *Jpn. J. Appl. Phys.* **50**, 021001 (2011).
- ³ T. Hung, M. Esposto, D.N. Nath, S. Krishnamoorthy, P.S. Park, and S. Rajan, in *Int. Conf. Compd. Semicond. Manuf. Technol.* (2013), pp. 191–194.
- ⁴ M.S. Miao, J.R. Weber, and C.G. Van de Walle, *J. Appl. Phys.* **107**, 123713 (2010).
- ⁵ M. Pashley, *Phys. Rev. B* **40**, 10481 (1989).
- ⁶ Y. Dong, R.M. Feenstra, and J.E. Northrup, *J. Vac. Sci. Technol. B* **24**, 2080 (2006).
- ⁷ O.I. Saadat, J.W. Chung, E.L. Piner, and T. Palacios, *IEEE Electron Device Lett.* **30**, 1254 (2009).
- ⁸ M. Tajima, J. Kotani, and T. Hashizume, *Jpn. J. Appl. Phys.* **48**, 020203 (2009).
- ⁹ R.M. Wallace, *ECS Trans.* **16**, 255 (2008).
- ¹⁰ S. Ruvimov, Z. Liliental-Weber, J. Washburn, K.J. Duxstad, E.E. Haller, Z.-F. Fan, S.N. Mohammad, W. Kim, A.E. Botchkarev, and H. Morkoç, *Appl. Phys. Lett.* **69**, 1556 (1996).
- ¹¹ B. Brennan and G. Hughes, *J. Appl. Phys.* **108**, 053516 (2010).
- ¹² E. Antonides, E.C. Janse, and G.A. Sawatzky, *Phys. Rev. B* **15**, 1669 (1977).
- ¹³ G. V. Soares, K.P. Bastos, R.P. Pezzi, L. Miotti, C. Driemeier, I.J.R. Baumvol, C. Hinkle, and G. Lucovsky, *Appl. Phys. Lett.* **84**, 4992 (2004).
- ¹⁴ Z.L. Fang, J.Y. Kang, and W.Z. Shen, *J. Phys. Chem. C* **112**, 17652 (2008).
- ¹⁵ X. Qin, H. Dong, B. Brennan, A. Azacatl, J. Kim, and R.M. Wallace, *Appl. Phys. Lett.* **103**, 221604 (2013).
- ¹⁶ X. Qin, B. Brennan, H. Dong, J. Kim, C.L. Hinkle, and R.M. Wallace, *J. Appl. Phys.* **113**, 244102 (2013).
- ¹⁷ B. Brennan, X. Qin, H. Dong, J. Kim, and R.M. Wallace, *Appl. Phys. Lett.* **101**, 211604 (2012).
- ¹⁸ Z.L. Fang, J.Y. Kang, and W.Z. Shen, *Nanotechnology* **20**, 045401 (2009).
- ¹⁹ J.A. Bardwell, S. Haffouz, W.R. McKinnon, C. Storey, H. Tang, G.I. Sproule, D. Roth, and R. Wang, *Electrochem. Solid-State Lett.* **10**, H46 (2007).

- ²⁰ A. Pirkle, J. Chan, A. Venugopal, D. Hinojos, C.W. Magnuson, S. McDonnell, L. Colombo, E.M. Vogel, R.S. Ruoff, and R.M. Wallace, *Appl. Phys. Lett.* **99**, 122108 (2011).
- ²¹ A. Azcatl, S. McDonnell, S. K. C., X. Peng, H. Dong, X. Qin, R. Addou, G.I. Mordi, N. Lu, J. Kim, M.J. Kim, K. Cho, and R.M. Wallace, *Appl. Phys. Lett.* **104**, 111601 (2014).
- ²² J.A. Wilson and A.D. Yoffe, *Adv. Phys.* **18**, 193 (1969).
- ²³ V.M. Bermudez, *J. Appl. Phys.* **80**, 1190 (1996).
- ²⁴ T.K. Zywiets, J. Neugebauer, and M. Scheffler, *Appl. Phys. Lett.* **74**, 1695 (1999).
- ²⁵ M.P.J. Punkkinen, P. Laukkanen, J. Lång, M. Kuzmin, M. Tuominen, V. Tuominen, J. Dahl, M. Pessa, M. Guina, K. Kokko, J. Sadowski, B. Johansson, I.J. Väyrynen, and L. Vitos, *Phys. Rev. B* **83**, 195329 (2011).
- ²⁶ D.M. Zhernokletov, P. Laukkanen, H. Dong, R. V. Galatage, B. Brennan, M. Yakimov, V. Tokranov, J. Kim, S. Oktyabrsky, and R.M. Wallace, *Appl. Phys. Lett.* **102**, 211601 (2013).
- ²⁷ Y. Luo, *Comprehensive Handbook of Chemical Bond Energies* (CRC Press, Boca Raton, FL, 2010).
- ²⁸ X. Qin, A. Lucero, A. Azcatl, J. Kim, and R.M. Wallace, *Appl. Phys. Lett.* In press (2014).
- ²⁹ S. Yang, Z. Tang, K. Wong, Y. Lin, C. Liu, Y. Lu, S. Huang, and K.J. Chen, *IEEE Electron Device Lett.* **34**, 1497 (2013).
- ³⁰ D.W. Johnson, R.T.P. Lee, R.J.W. Hill, M.H. Wong, G. Bersuker, E.L. Piner, P.D. Kirsch, and H.R. Harris, *IEEE Trans. Electron Devices* **60**, 3197 (2013).
- ³¹ M. Fagerlind, F. Allerstam, E.Ö. Sveinbjörnsson, N. Rorsman, A. Kakanakova-Georgieva, A. Lundskog, U. Forsberg, and E. Janzén, *J. Appl. Phys.* **108**, 014508 (2010).
- ³² T. Hashizume, S. Ootomo, T. Inagaki, and H. Hasegawa, *J. Vac. Sci. Technol. B* **21**, 1828 (2003).
- ³³ R. Gordon, X. Wang, L. Dong, J. Zhang, Y. Liu, and P. Ye, *Nano Lett.* **13**, 594 (2013).
- ³⁴ J. Son, V. Chobpattana, B.M. McSkimming, and S. Stemmer, *Appl. Phys. Lett.* **101**, 102905 (2012).
- ³⁵ R. V. Galatage, D.M. Zhernokletov, H. Dong, B. Brennan, C.L. Hinkle, R.M. Wallace, and E.M. Vogel, *J. Appl. Phys.* **116**, 014504 (2014).

CHAPTER 7

Very High I_{ON} and Low I_{OFF} Metal-Gate/High- κ /AlGaIn/GaN MOSFET with Excellent Reliability

7.1 Preface

The gate-recessed AlGaIn/GaN MOSFET on a Si substrate is demonstrated to achieve a record best normalized transistor current (μC_{ox}) of $335 \mu A/V^2$ (410 mA/mm at $L_G=5 \mu m$ and only $V_G=4 \text{ V}$), high breakdown voltage (V_{BD}) of 970 V , I_{ON}/I_{OFF} of $9\sim 10$ orders of magnitude, small 75 mV/dec sub-threshold slope (SS), low on-resistance (R_{on}) of $17.0 \Omega\text{-mm}$, excellent reliability of only $40 \text{ mV } \Delta V_T$ after $175^\circ\text{C } 1000 \text{ sec}$ stress at $I_{D,max}$, good V_T uniformity of $\pm 0.35 \text{ V}$, and a small $\Delta V_T/V_{BD}$ of only $<0.04\%$. Such excellent device integrities are due to the small EOT by using high- κ gate dielectric, p+-GaN buffer, and AlN etching stop layer. This joint work was submitted for consideration for the 2014 IEEE International Electron Devices Meeting.

7.2 Introduction

The ideal power device requires a high blocking voltage, high current at low voltage, fast switching speed, large safe-operation area (SOA), and good reliability robustness. The AlGaIn/GaN MOSFET or MISHEMT has positive V_T for better SOA than that of HEMT [1]-[5]. However, the reactive ion etching (RIE) process is challenging for AlGaIn/GaN MOSFET, where defects generated by the plasma damage, V_T shift during operation, and V_T variation are major issues.

Here we report record highest normalized I_D ($I_{ON,nor}$) of $335 \mu A/V^2$ at a low $V_G=4 \text{ V}$, a $970 \text{ V } V_{BD}$, low $17.0 \Omega\text{-mm } R_{on}$, $10^9\sim 4\times 10^{10} I_{ON}/I_{OFF}$, small 75 mV/dec SS, and $+V_T$ of 0.55 V for gate-recessed AlGaIn/GaN MOSFET on Si substrate. Excellent reliability of only $40 \text{ mV } \Delta V_T$ after $175^\circ\text{C } 1000 \text{ sec}$ stress, good V_T uniformity of $\pm 0.35 \text{ V}$, and a small $\Delta V_T/V_{BD} < 0.04\%$ were also achieved. The very high $I_{ON,nor}$ at only $V_G=4 \text{ V}$ is due to high- κ gate dielectric with a small

equivalent-oxide thickness (EOT) of 2.2 nm. Moreover, the gate-recessed AlGaIn/GaN MOSFET has $5\times$ higher I_{ON} than HEMT with the same structure, even though the mobility is lower for a MOSFET compared to a HEMT [3]-[4]. Such a low V_G can be controlled using a low-cost sub- μm IC operated at 5 V. The excellent small $\Delta V_T/V_{BD}$ is due to the inserted AlN etching stop layer- the key process toward manufacturing. The $10^9\sim 4\times 10^{10}$ I_{ON}/I_{OFF} is due to the extra p^+ buffer that is more efficient and simpler than using other buffer technology [2]. The small ΔV_T after 175°C stress is vitally better than reported $\Delta V_T=1$ V at 25°C of AlGaIn/GaN MISHEMT [4] and even better than SiC MOSFET stressed at lower current [6] due to better gate dielectric and MOS interface.

7.3 Device Fabrication

Fig. 7.1 is the schematic device structure of a 2.4- μm low- temperature AlGaIn buffer grown on 6-in Si(111) wafer, a GaN active layer, 30-nm AlGaIn barrier, and a 2-nm GaN cap (not shown). A thin AlN etching stop layer and a p^+ GaN layer were added during epitaxial growth. Then mesa isolation and gate region were recess etched by RIE. The gate dielectric of 1-nm SiO_2 and 5-nm high-k HfAlO were sputter deposited and annealed. The ohmic contacts were formed by Ti/Al/Ti/Au and RTA. The Pt/Au was used to form the gate electrode. An asymmetric drain and source was used for high power GaN devices [5].

7.4 Results and Discussion

7.4.1 Interface & Buffer Leakage Effects

Fig. 7.2-7.3 show the I_D-V_D and I_D-V_G data of RIE-etched MOSFET. Although a good I_D of 220 mA/mm is obtained, this device suffers from high I_{OFF} leakage of 10^{-4} mA/mm and poor SS of 372 mV/dec, due to poor high-k/GaN interface:

$$SS=kT/q*\ln 10*[1+(C_{dpl}+C_{it})/C_{ox}] \quad (7.1)$$

Here C_{dpl} , C_{it} , and C_{ox} are depletion, interface trap, and oxide capacitances. Then XPS was applied to analyze the oxide interface. From the normalized Ga $2p_{3/2}$ spectra in Fig. 7.4, the RIE

results in an increase of Ga-O. Because GaO_x has a weak bond strength, the GaO_x was etched before the gate dielectric deposition. As shown in Fig. 7.5-7.6, the I_{ON} , SS , and I_{OFF} leakage improve to 330 mA/mm, 87 mV/dec, and 5×10^{-6} mA/mm, respectively. We further applied RIE ion damage removal, GaO_x etching, and inserted a p⁺ buffer layer. In Fig. 7.7-7.8, very high 410 mA/mm at $L_G=5 \mu\text{m}$ & $V_G=4 \text{ V}$, or record highest $I_{ON,nor}$ of $335 \mu\text{A/V}^2$, is measured, which is due to >10x lower interface traps density ($D_{it}=C_{it}/q$). Here the $I_{ON,nor}$ is normalized by gate dimension (L_G and W_G) and gate overdrive (V_G-V_T):

$$I_{ON,nor} = I_D \cdot (2L_G/W_G) / (V_G-V_T)^2 = \mu C_{ox} \quad (7.2)$$

Such high transistor current can decrease the chip size and cost of power module. This device has a small SS of 75 mV/dec, large I_{ON}/I_{OFF} of 10^9 , and a low R_{on} of 17.0 $\Omega\text{-mm}$. Thus, the poorer interface not only lowers I_{ON} by increased carrier scattering, but also causes higher I_{OFF} . Fig. 7.9 shows the potential mechanism: the interface states allow ionizing trapped carriers leading to high I_{OFF} via trap-assistant conduction. The HEMT data with the same material structure were also shown in Fig. 7.8. The negative V_T , 120 mV/dec SS , and 10^{-4} mA/mm I_{OFF} are worse than those of the MOSFET. It is known that the high mobility is the merit for HEMT, but the AlGaIn/GaN MOSFET has 5x higher $I_{ON,nor}$ than the HEMT. Hence both high mobility (μ) and gate capacitance ($C_{ox}=\epsilon_0\kappa/t$) should be considered for high I_{ON} (see eq.(1)).

7.4.2 Uniformity, V_{BD} , & Reliability

V_T uniformity by RIE is a tough challenge. Good ΔV_T uniformity of $0.55 \pm 0.35 \text{ V}$ is shown in Fig. 7.10, due to selective AlN etching with a much slower rate (Fig. 7.11) and vital for manufacturability. The V_{BD} at V_G near turn-on is shown in Fig. 7.12. A high V_{BD} of 970 V was measured that gives a small $\Delta V_T\text{-uniformity}/V_{BD} < 0.04\%$. The reliability is the key factor for power device. As shown in Figs. 7.13-7.14, the AlGaIn/GaN MOSFET, stressed at 175°C, $I_{D,max}$, and $V_D=20 \text{ V}$, shows little I_{ON} degradation, and the I_{OFF} becomes better during stress. Very high I_{ON}/I_{OFF} of 4×10^{10} is measured during stress, which may be due to defect annihilation in

AlGaIn/GaN layer. The ΔV_T after 175°C stress is only 40 mV, which is much better than the reported $\Delta V_T=1$ V of a GaN MISHEMT at 25°C [4] and even better than a SiC MOSFET [5]. This result further supports the excellent gate dielectric and MOS interface, consistent with the small SS and low I_{OFF} . Table 7.1 compares the device performance [1]-[4]. This device has the highest $I_{ON,nor}$, high V_{BD} , low R_{on} , and the best reliability.

7.5 Conclusions

Excellent I_{ON} , I_{OFF} , V_{BD} , R_{ON} , SS , and reliability are obtained in AlGaIn/GaN MOSFET on Si substrate.

7.6 References

1. Z. Tang et al, IEDM Tech. Dig., pp. 156-159, 2013.
2. J.-H. Lee et al, IEEE EDL, vol. 34, pp. 975-977, 2013.
3. J. Kim et al, ISPSD Tech. Dig., pp. 315-318, 2013
4. Q. Zhou et al, IEDM Tech. Dig., pp. 777-780, 2011.
5. C. Y. Tsai et al, IEEE EDL, vol. 33, pp. 35-37, 2012.

Chapter 7 Figures

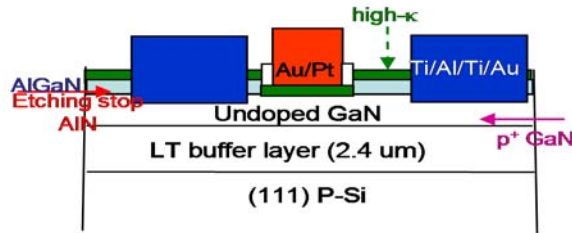


Fig. 1. Device structure of metal-gate/high-κ/AlGaIn/GaN MOSFET.

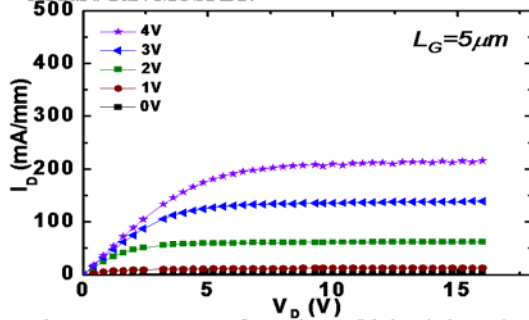


Fig. 3. I_D - V_G curves of metal-gate/high-κ/AlGaIn/GaN MOSFET formed after RIE w/o surface treatment.

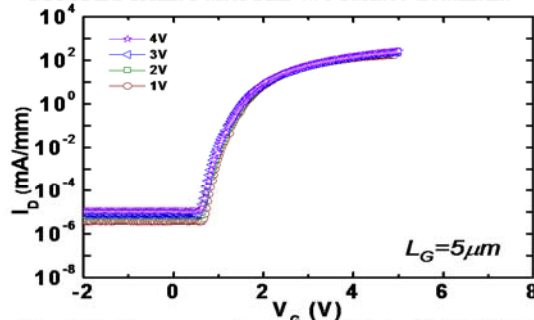


Fig. 5. I_D - V_G curves of metal-gate/high-κ/AlGaIn/GaN MOSFET formed after RIE & oxide etching

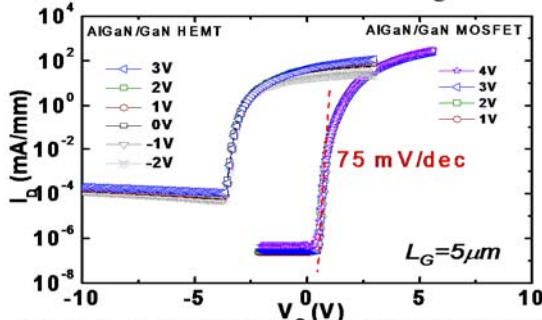


Fig. 7. I_D - V_G curves of metal-gate/high-κ/AlGaIn/GaN/p⁺-GaIn MOSFET, formed after RIE, damage removal, & oxide etching. AlGaIn/GaN HEMT data, with the same epitaxial structure, are added for comparison.

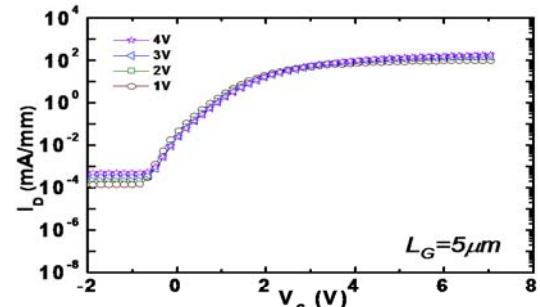


Fig. 2. I_D - V_G curves of metal-gate/high-κ/AlGaIn/GaN MOSFET formed after RIE w/o surface treatment.

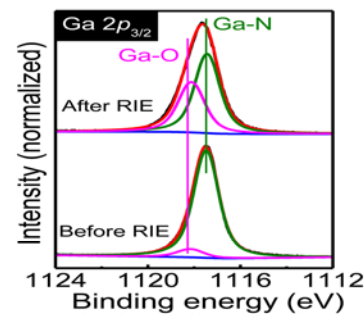


Fig. 4. XPS analysis of RIE effect on surface chemistry. Week GaO formation is found on GaN surface.

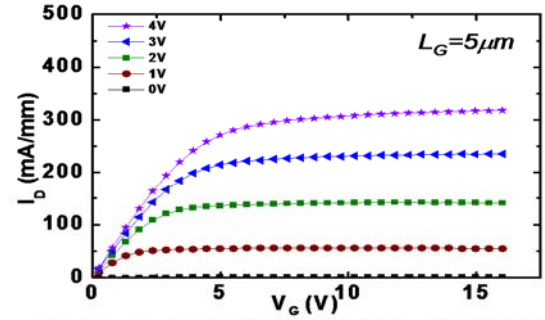


Fig. 6. I_D - V_G curves of metal-gate/high-κ/AlGaIn/GaN MOSFET formed after RIE & oxide etching.

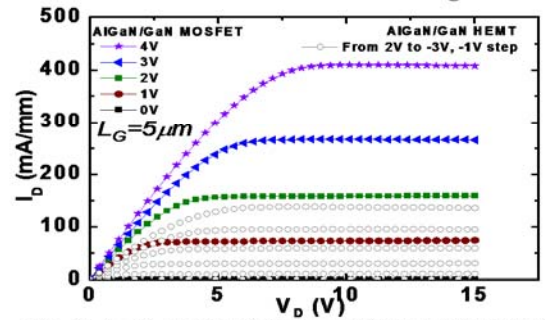


Fig. 8. I_D - V_G curves of metal-gate/high-κ/AlGaIn/GaN/p⁺-GaIn MOSFET, formed after RIE, damage removal, & oxide etching. AlGaIn/GaN HEMT data, with the same epitaxial structure, are added for comparison.

Chapter 7 Figures

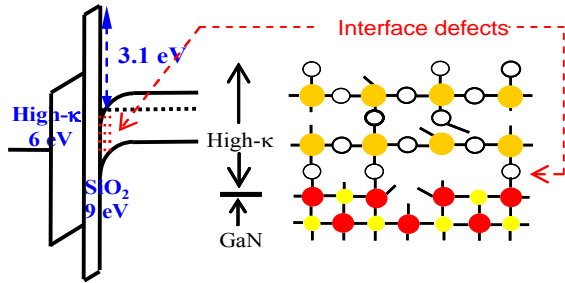


Fig. 9. The energy bandgap and potential mechanism of interface leakage by ionizing trapped carriers in interface states trap-assistant hopping conduction..

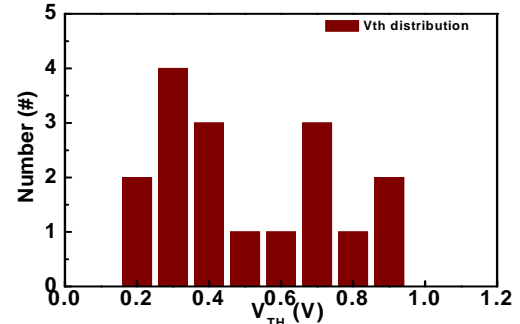


Fig. 10. V_{TH} distribution for devices with AlN etching stop layer.

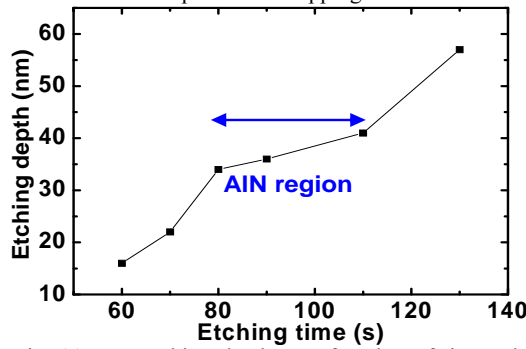


Fig. 11. RIE etching depth as a function of time. The much slower etching rate is due to AlN layer.

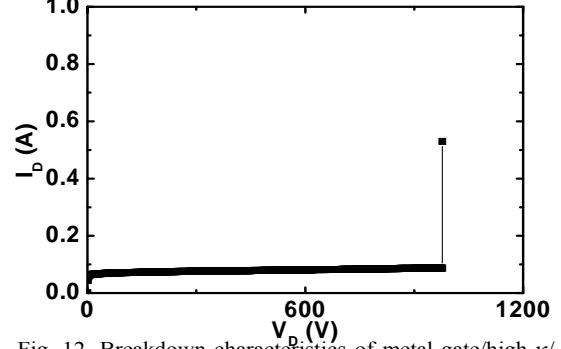


Fig. 12. Breakdown characteristics of metal-gate/high- κ /AlGaIn/GaN MOSFET biased near turn on at $V_G=0.5$ V.

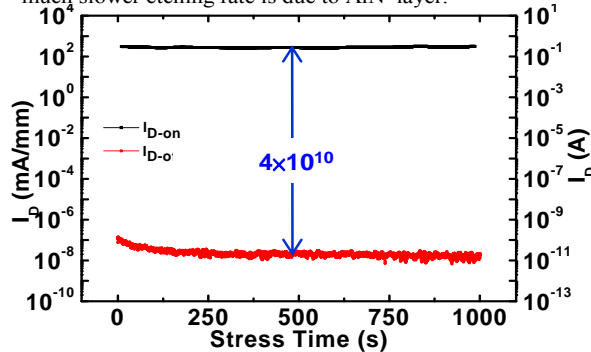


Fig. 13. I_{on} and I_{off} current at 175°C and $V_D=20$ V stress for 1000 sec.

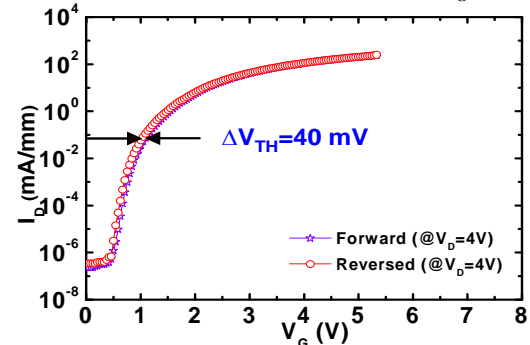


Fig. 14. Forward and reversed I_D - V_G sweep curves after 1000s stress at 175°C and $V_D=20$ V.

	I_{ON} (mA/mm)	$I_{ON, nor}$ ($\mu A/V^2$)	I_{ON}/I_{OFF}	V_{BD} (V)	R_{ON} (Ω -mm)	V_G (V)	V_{TH} (V)	S.S. (mV/dec)	Stress ΔV_{TH} (V)	Tech.
SiN/AlGaIn/GaN MISHEMT [1]	430 @ $L_G=1\mu m$	8 or 5.1	4×10^9	604	9.8	14	3.6 or 1.0	110	—	F-plasma ion implant
Al ₂ O ₃ /AlGaIn/GaN MOSFET Samsung [2]	120 @ $L_G=2\mu m$	3.3	10^8	600	—	19	7.2	80	—	AlSiC
p-GaN gate HEMT Samsung [3]	230 @ $L_G=2\mu m$	17	383 $V_G=10V$	670	20	10	2.8	—	—	p-GaN gate
Al ₂ O ₃ /InAlN/GaN MISHEMT [4]	416 @ $L_G=1\mu m$	33	$\sim 10^{10}$	—	—	3	~ -2	24 forward 74 reverse	1.0 (25°C) forward - reverse	Schottky Source/ Drain
This work	410 @ $L_G=5\mu m$	335	$10^9 \sim$ 4×10^{10}	970	17	4	0.55	75	0.04 (175°C 1000s)	Improved Interface p ⁺ GaN

Table I. Comparison of important device parameters among GaN-based MISHEMT and MOSFET.

List of Publications

1. X. Qin, , L. Cheng, S. McDonnell, A. Azcatl, H. Zhu, J. Kim, and R.M. Wallace, “ A comparative study of atomic layer deposition of Al₂O₃ and HfO₂ on AlGa_N/Ga_N”, *In preparation* (2014).
2. S. H. Yi, X. Qin, R. M. Wallace, J. B. Yeh, C. H. Kuan, and Albert Chin, “Very High I_{ON} and Low I_{OFF} Metal-Gate/High-κ/AlGa_N/Ga_N MOSFET with Excellent Reliability,” *submitted to the 2014 IEEE IEDM Conference* (2014).
3. X. Qin, H. Dong, J. Kim, and R.M. Wallace, “A crystalline oxide passivation for Al₂O₃/AlGa_N/ Ga_N ”Appl. Phys. Lett. **105**, 141604 (2014).
4. X. Qin, A. Lucero, A. Azcatl, J. Kim, and R.M. Wallace, “In situ x-ray photoelectron spectroscopy and capacitance voltage characterization of plasma treatments for Al₂O₃/AlGa_N/Ga_N stacks”Appl. Phys. Lett. **105**, 011602 (2014).
5. X. Qin, H. Dong, B. Brennan, A. Azcatl, J. Kim, and R.M. Wallace, “Impact of N₂ and forming gas plasma exposure on the growth and interfacial characteristics of Al₂O₃ on AlGa_N”Appl. Phys. Lett. **103**, 221604 (2013).
6. X. Qin, B. Brennan, H. Dong, J. Kim, C.L. Hinkle, and R.M. Wallace, “In situ atomic layer deposition study of HfO₂ growth on NH₄OH and atomic hydrogen treated Al_{0.25}Ga_{0.75}N” J. Appl. Phys. **113**, 244102 (2013).
7. B. Brennan, X. Qin, H. Dong, J. Kim, and R.M. Wallace, “In situ atomic layer deposition half cycle study of Al₂O₃ growth on AlGa_N” Appl. Phys. Lett. **101**, 211604 (2012).
8. P. Sivasubramani, T.J. Park, B. E. Coss, A. Lucero, J. Huang, B. Brennan, Y. Cao, D. Jena, H. Xing, R.M. Wallace, and J. Kim, “In-situ X-ray photoelectron spectroscopy of trimethyl aluminum and water half-cycle treatments on HF-treated and O₃-oxidized Ga_N substrates,” Phys. Stat. Sol. R R Lett. **6**, 22 (2012).

List of Presentations

1. "A Novel Crystalline Oxide Passivation for $\text{Al}_2\text{O}_3/\text{AlGaIn/GaN}$ " X. Qin, H. Dong, J. Kim, and R.M. Wallace, 45th IEEE Semiconductor Interface Specialists Conference, December 10-13, 2014 San Diego, California, USA, oral presentation.
2. "Characterization of $\text{Al}_2\text{O}_3/\text{AlGaIn/GaN}$ HEMT Structure Using Capacitance-Voltage and In Situ XPS" X. Qin, A. Lucero, A. Azcatl, J. Kim and R. M. Wallace, 2014 Fall Materials Research Society Meeting, November 30-December 5, 2014, Boston, Massachusetts, USA, oral presentation.
3. "Interfacial and Electrical Study of Crystalline Oxidation Passivation for AlGaIn/GaN HEMTs" X. Qin, H. Dong, J. Kim, and R.M. Wallace, AVS 61st International Symposium and Exhibition, November 9-14, 2014, Baltimore, Maryland, oral presentation.
4. "Interfacial and Electrical Study of Crystalline Oxidation in $\text{Al}_{0.25}\text{Ga}_{0.75}\text{N}$ " X. Qin, R. Addou, H. Dong, J. Kim and R.M. Wallace, 2014 Spring Materials Research Society Meeting, San Francisco, California, USA, oral presentation.
5. "Impact of N_2 and Forming Gas Plasma Exposure on the Growth and Interfacial Characteristics of Al_2O_3 ON $\text{Al}_{0.25}\text{Ga}_{0.75}\text{N}$ " X. Qin, B. Brennan, H. Dong, A. Azcatl, and R.M. Wallace, AVS 60th International Symposium and Exhibition, October 27-November 1, 2013, Long Beach, California, oral presentation.
6. "A comparative in situ study of HfO_2 growth on $\text{Al}_{0.25}\text{Ga}_{0.75}\text{N}$ by atomic layer deposition, electron beam evaporation and RF sputtering", X. Qin, B. Brennan, H. Dong and R.M. Wallace, 2013 Spring Materials Research Society Meeting, April 1-5, 2013, San Francisco, California, USA, oral presentation.
7. "Impact of atomic hydrogen exposure on the growth, interfacial, and electrical characteristics of HfO_2 on $\text{Al}_{0.25}\text{Ga}_{0.75}\text{N}$ " X. Qin, S. Anwar, B. Brennan, C.L. Hinkle and R.M. Wallace, 40th Conference on the Physics and Chemistry of Surfaces and Interfaces, January 20-24, 2013,

Waikoloa, Hawaii, USA, oral presentation.

8. "Interface Study of the Atomic Layer Deposited Al_2O_3 on $\text{Al}_{0.25}\text{Ga}_{0.75}\text{N}$ " X. Qin, B. Brennan, H. Dong, and R.M. Wallace, AVS 59th International Symposium and Exhibition, October 28-November 2, 2012, Tampa, Florida, USA, oral presentation.